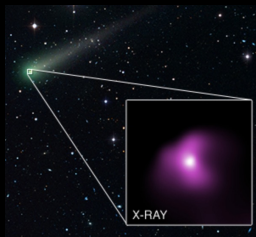


Radiative Processes in Astrophysics

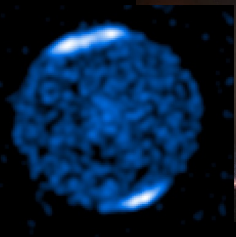
Observation

Up to cosmic size scale

C/2012S1
(comet)



Jupiter
(planet)



Sun
(star)



Cas A
(SNR)



M82
(galaxy)



Phoenix
(gal. cluster)



Cosmic web filament

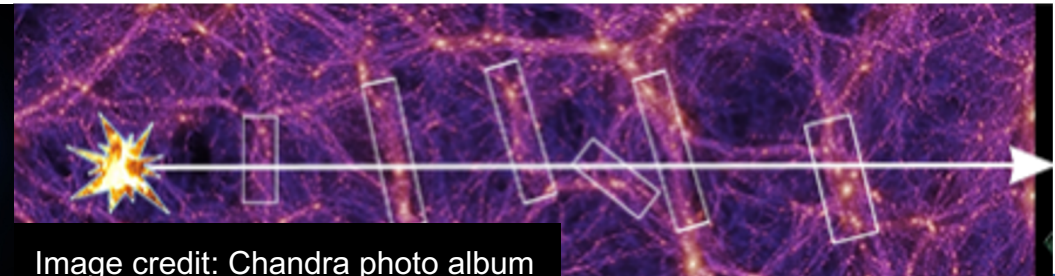


Image credit: [Chandra photo album](#)

Chpt.5 Atomic processes

5.1 Atomic data for astrophysics

5.2 Two-level system

5.3 Bremsstrahlung

5.4 Recombination and photoionization

5.5 Collisional excitation and de-excitation

Image credit: Junjie Mao

5.6 Other atomic processes

5.6.1 Collisional ionization

5.6.2 Fluorescence and autoionization

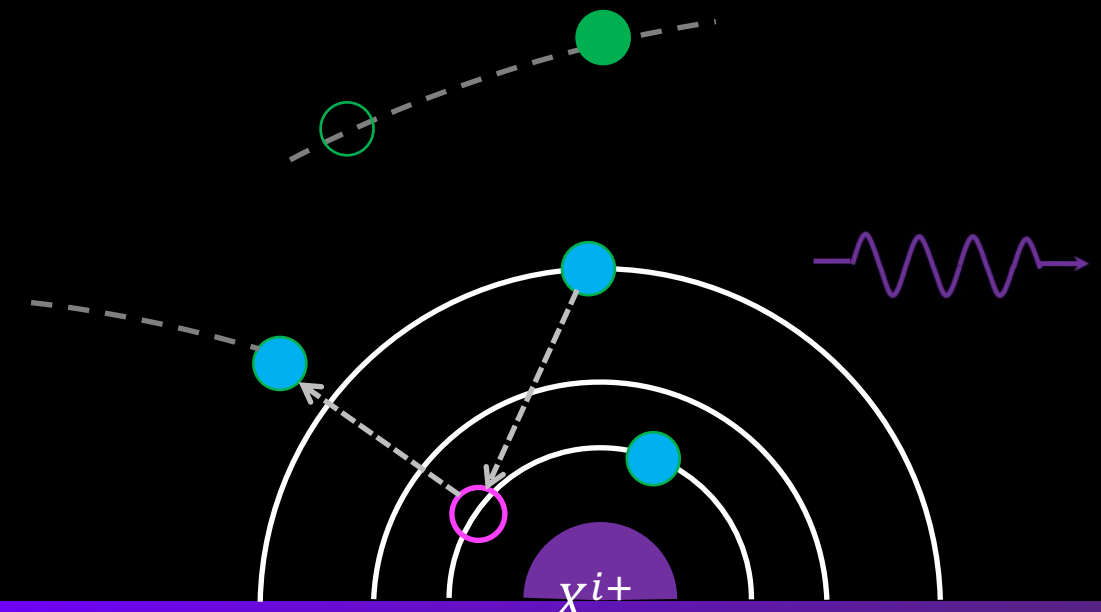
5.6.3 Line broadening

5.6.4 Resonant scattering

5.6.5 Charge exchange

5.6.6 Two-photon process

5.7 Astrophysical plasma models



Electron-impact ionization process

During the EII process, the free electron transfers part of its kinetic energy to ionize a bound electron (at any state) of an ion.

- ✓ EII is a **cooling** process for the electrons

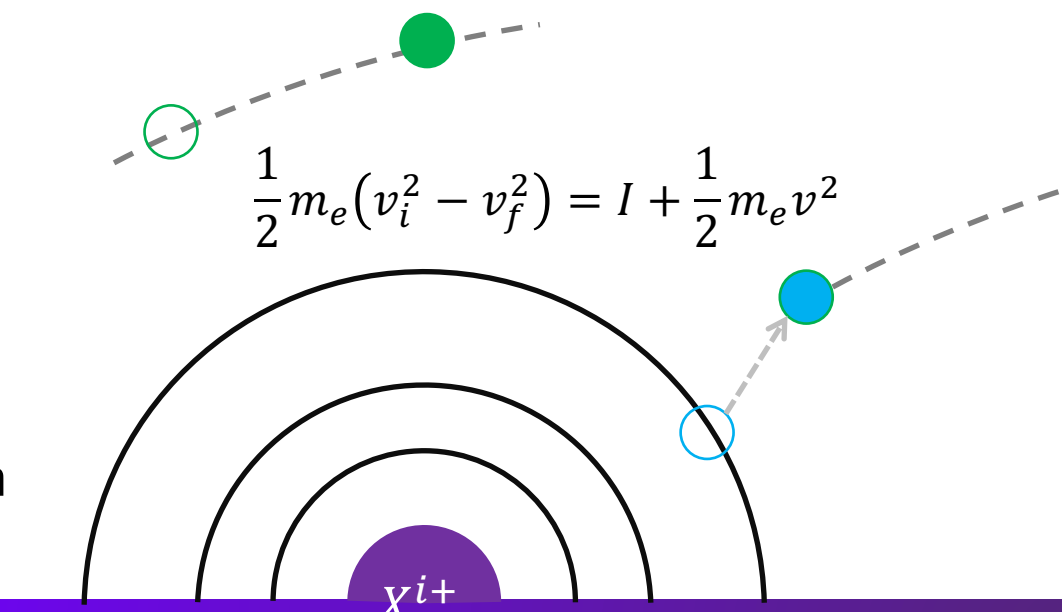
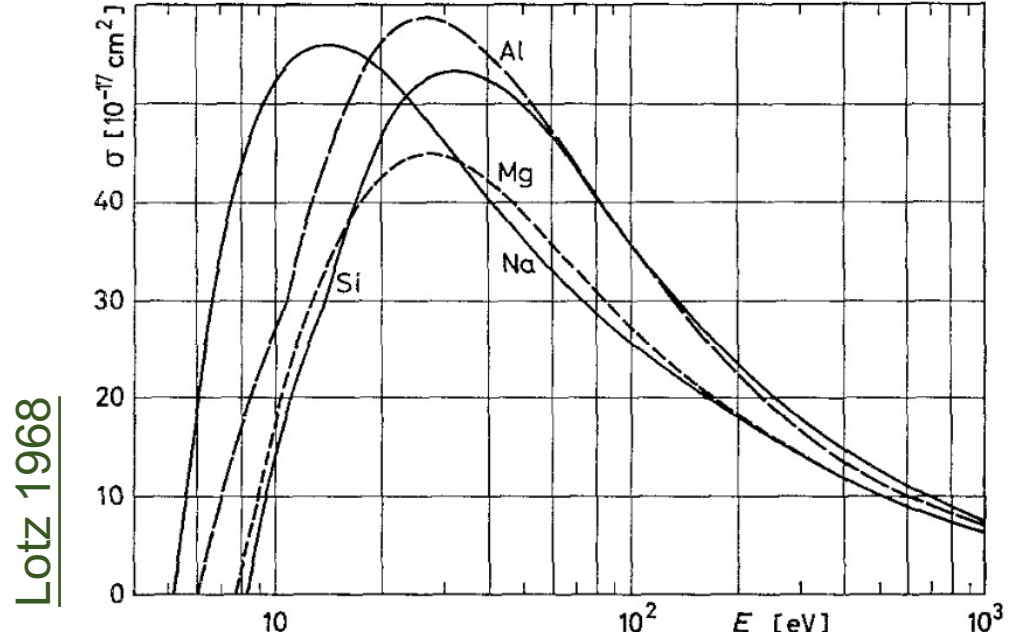
EII cross section for $E = \frac{1}{2}m_e v^2 \gg I$ ([Lotz 1968](#))

$$\sigma^{\text{EII}} \propto \frac{\ln(E)}{E}$$

↑
ionization energy of
an atomic state

$$E = \frac{1}{2}m_e v_i^2 \geq I + \frac{1}{2}m_e v^2$$

In this case, the **larger** the initial kinetic energy of the free electron, the **smaller** the collisional ionization cross section



EII rate coefficient

prev. sl.

$$q = \int_{v_0}^{\infty} v f(v) \sigma^{\text{EIE}}(v) dv$$

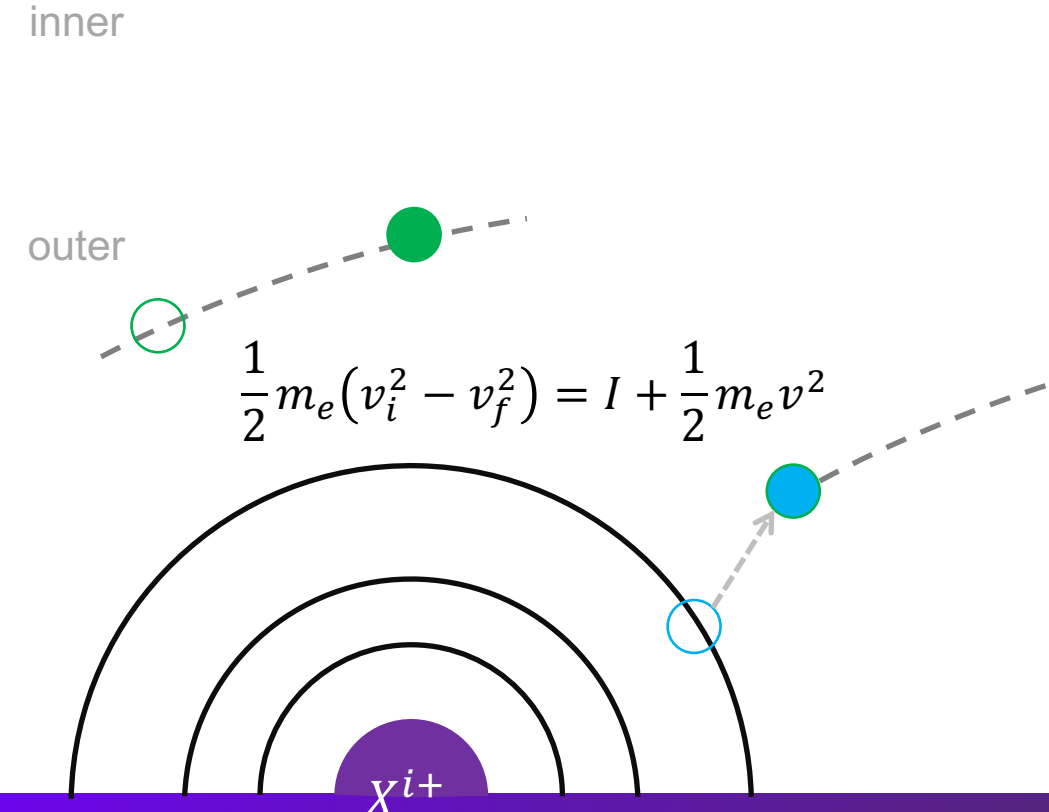
$$d = \int_{v_0}^{\infty} v f(v) \sigma^{\text{EII}}(v) dv$$

$$\frac{1}{2} m_e v_0^2 = I$$

Kaastra et al. 2008

$$d \propto \begin{cases} \frac{\exp(-I/kT_e)}{I^2}, & \text{for } kT_e \ll I \\ \ln\left(\frac{kT_e}{I}\right) \\ \frac{I}{I \sqrt{kT_e}}, & \text{for } kT_e \gg I \end{cases}$$

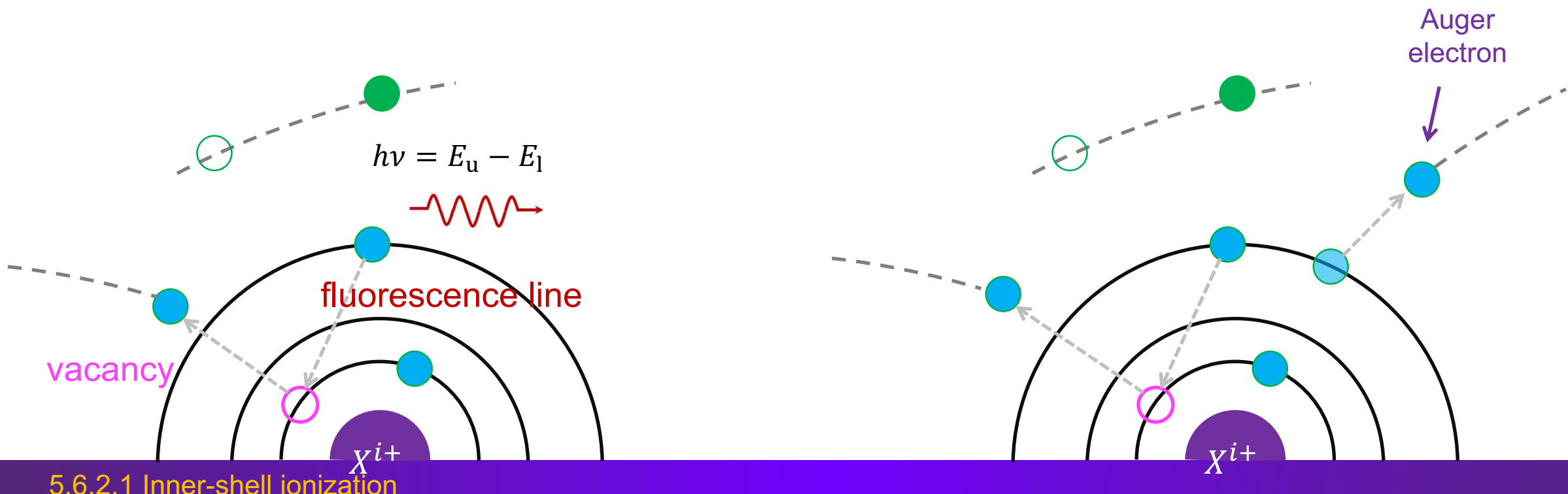
- At both low and high temperatures, the EII rate coefficients approaches zero.
- EII of electrons in the outermost atomic states is more probable ($d \propto I^{-1}$ or I^{-2}) than inner atomic states.



Inner-shell ionization

Inner-shell ionization can also occur, leading to an unstable atomic structure. Subsequently, one of the two processes will follow:

- an electron in the outer atomic state fill the vacancy by emitting a **fluorescence line**
- an electron in the outer atomic state fill the vacancy and ionize another electron in the outer atomic state (autoionization, viz. Auger process)

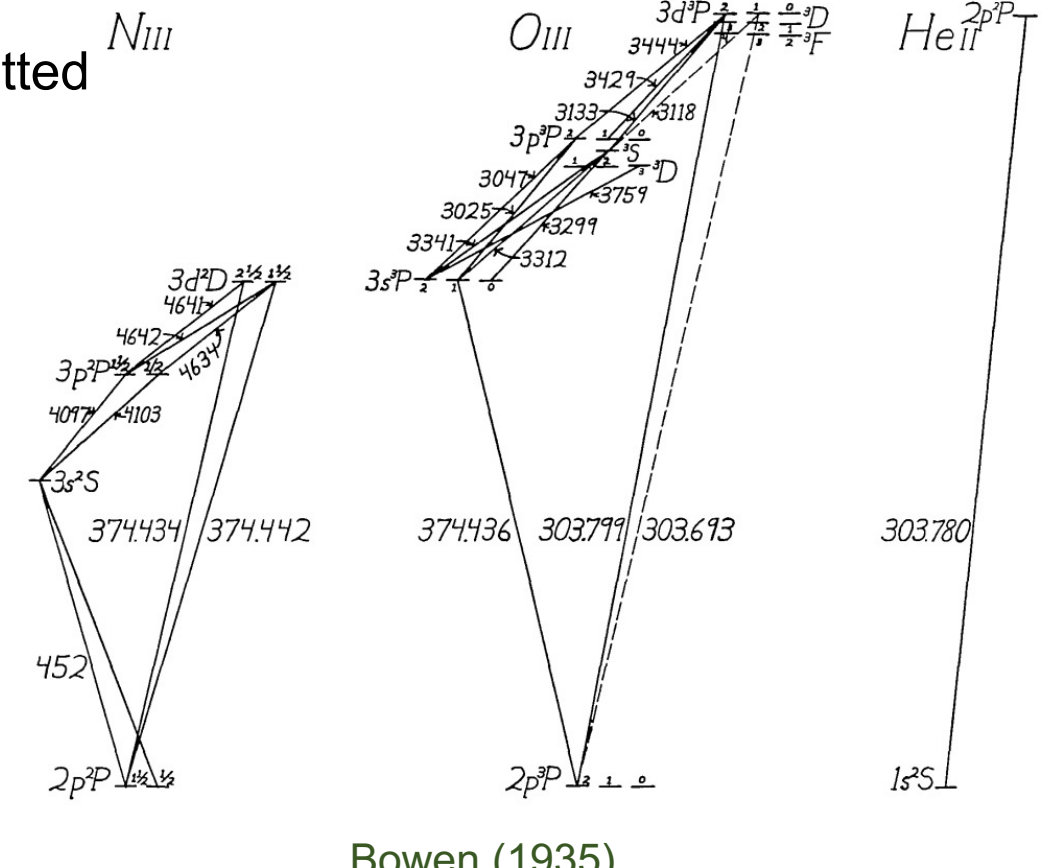
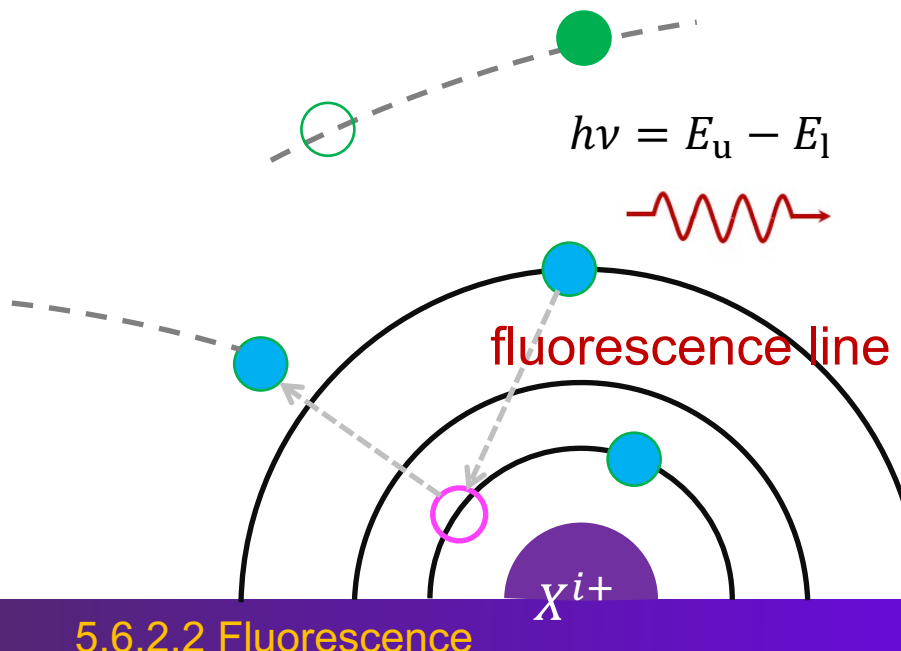


Fluorescence

The absorption of radiation at one wavelength followed by nearly immediate re-radiation usually at a different wavelength

- ✓ fluorescence ceases almost at once when the incident radiation stops
- ❑ resonance fluorescence: if the wavelength of the re-emitted photon is similar to that of the incident radiation

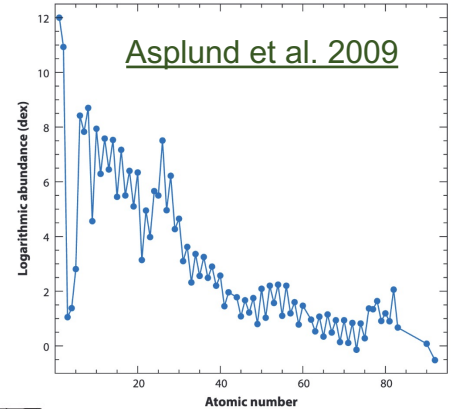
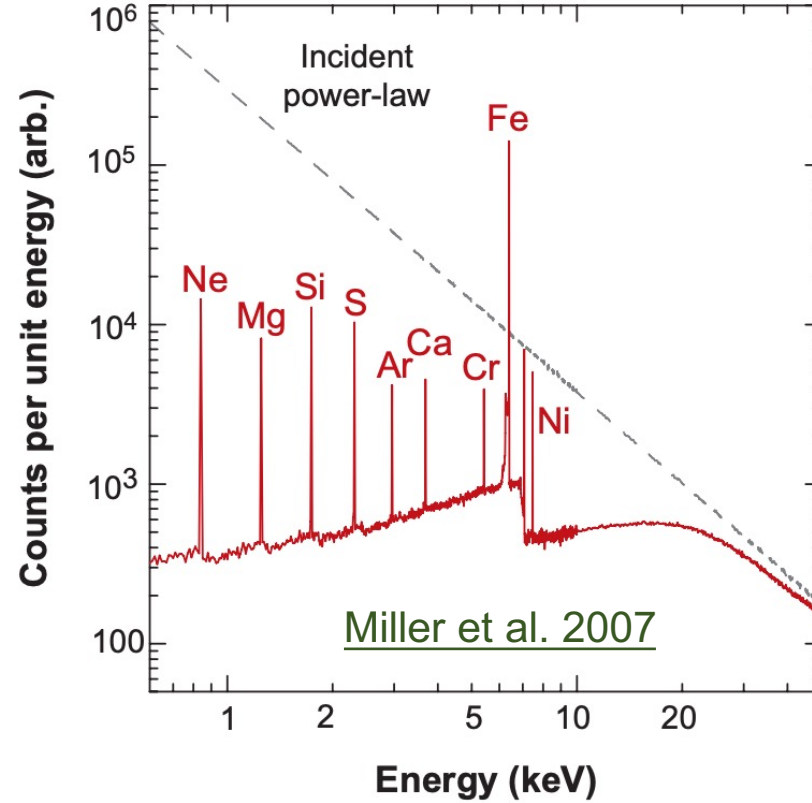
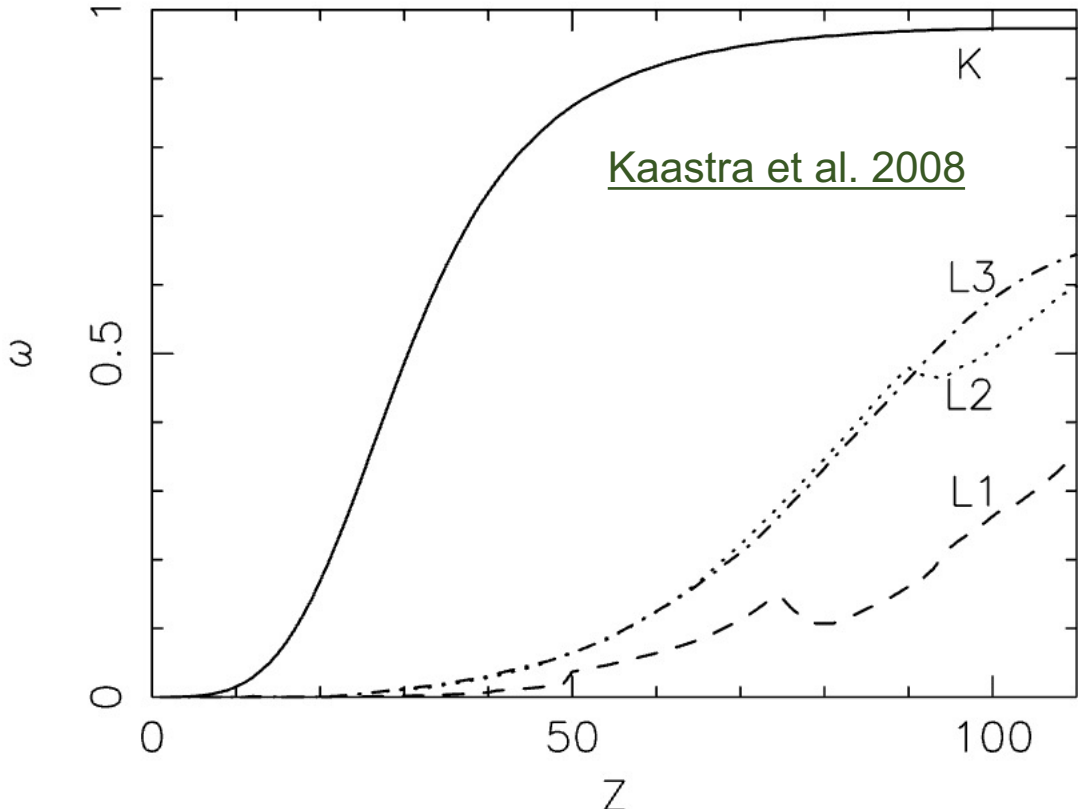
Bowen resonance fluorescence mechanism



Fluorescence line

Fluorescence yield ω indicates the probability of fluorescence line emission.

The **larger** the atomic number, the **stronger** the fluorescence line.

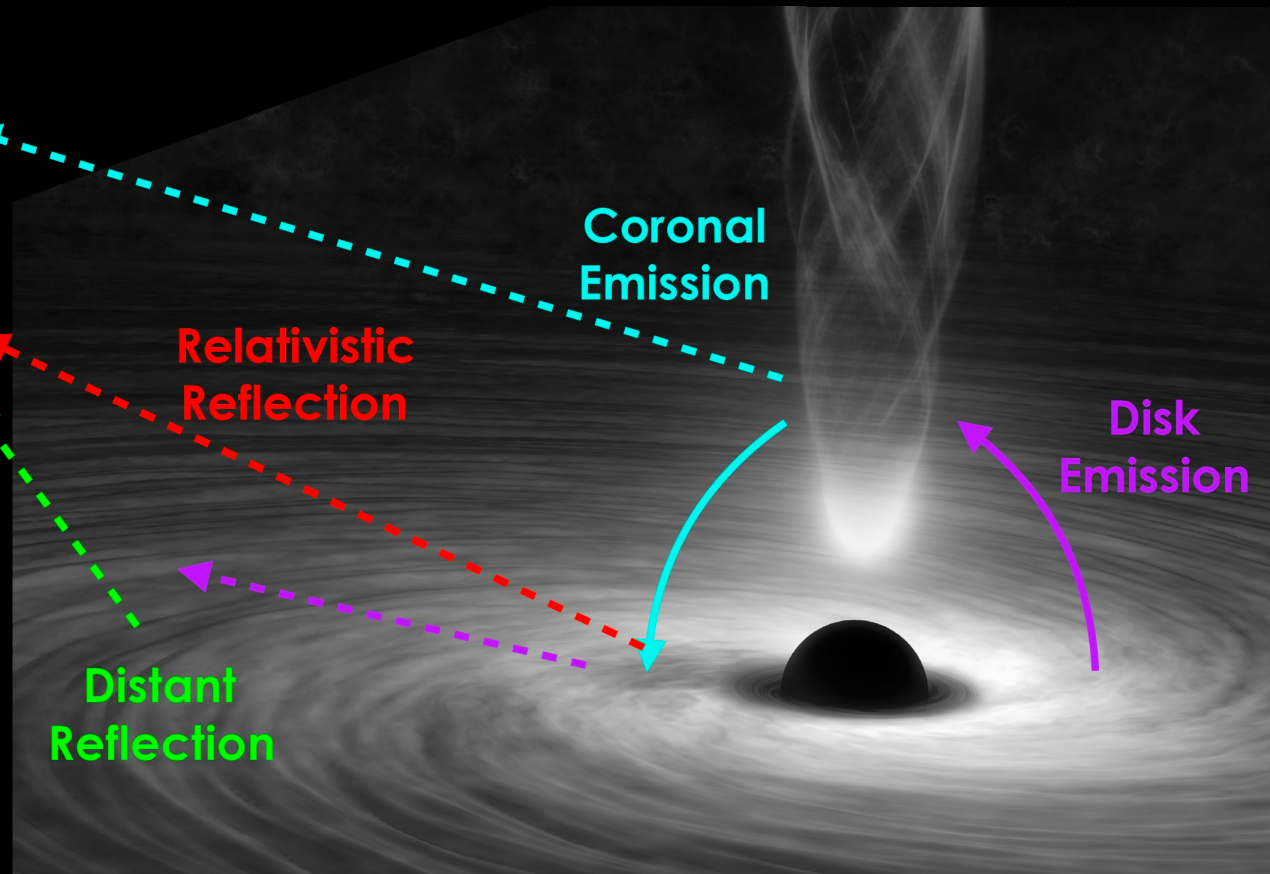
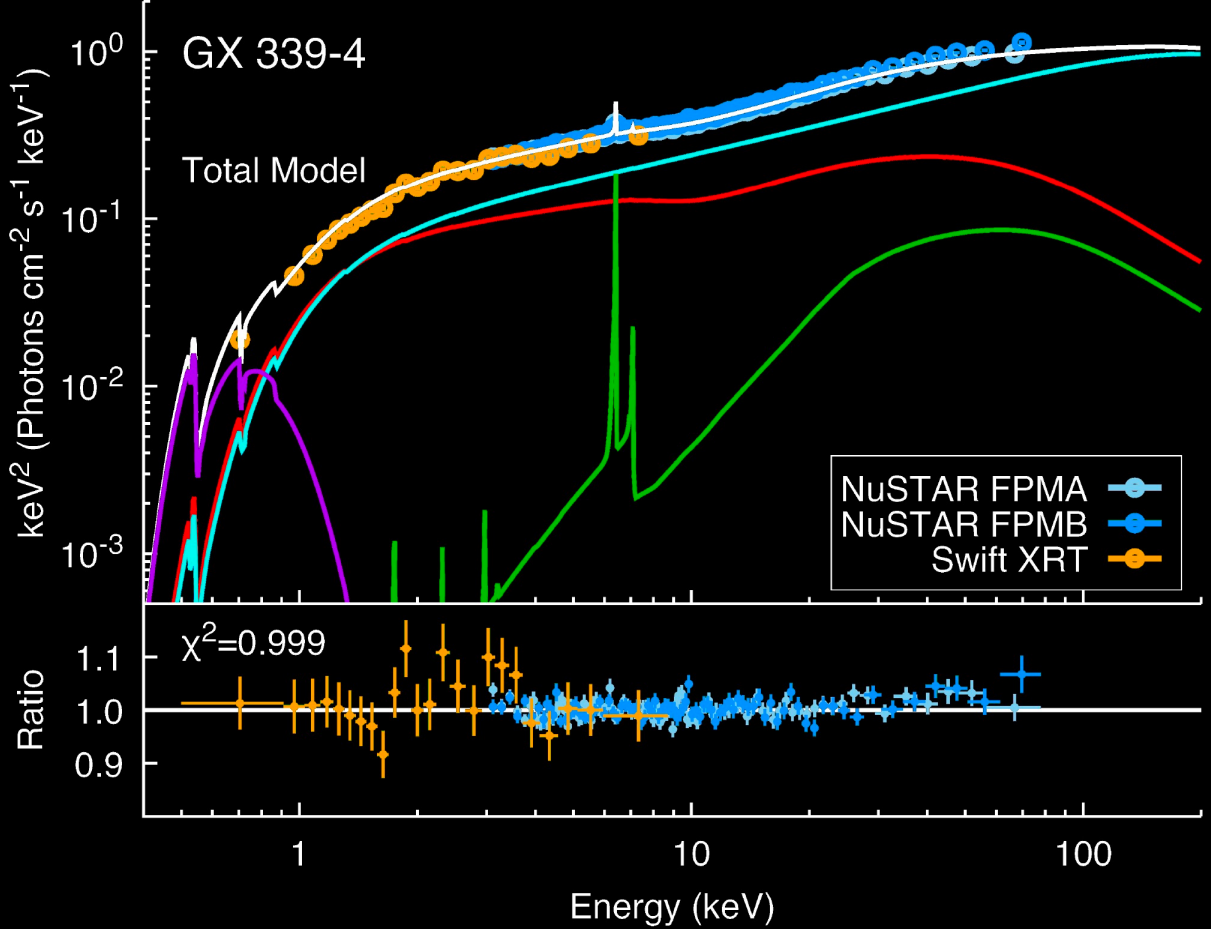


Combined with cosmic elemental abundance, Fe fluorescence lines are commonly observed.

XRB reflection spectrum

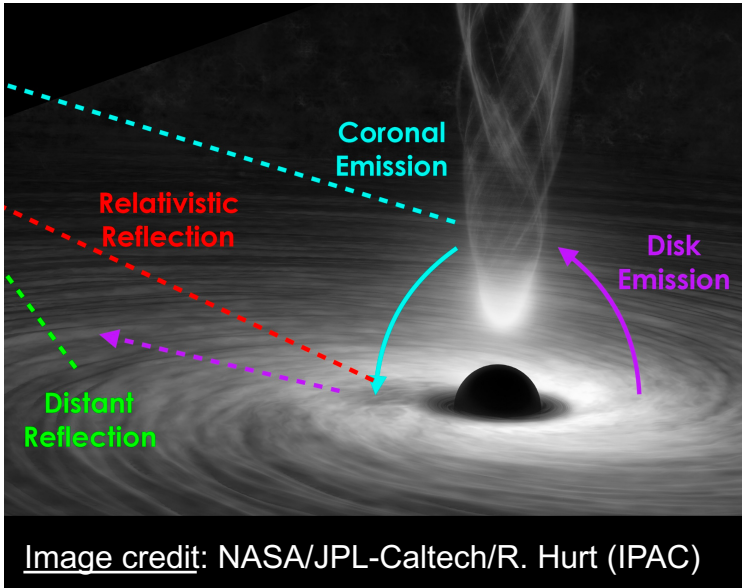
Image credit: NASA/JPL-Caltech/R. Hurt (IPAC)

Image credit: ESA, NASA
and Felix Mirabel

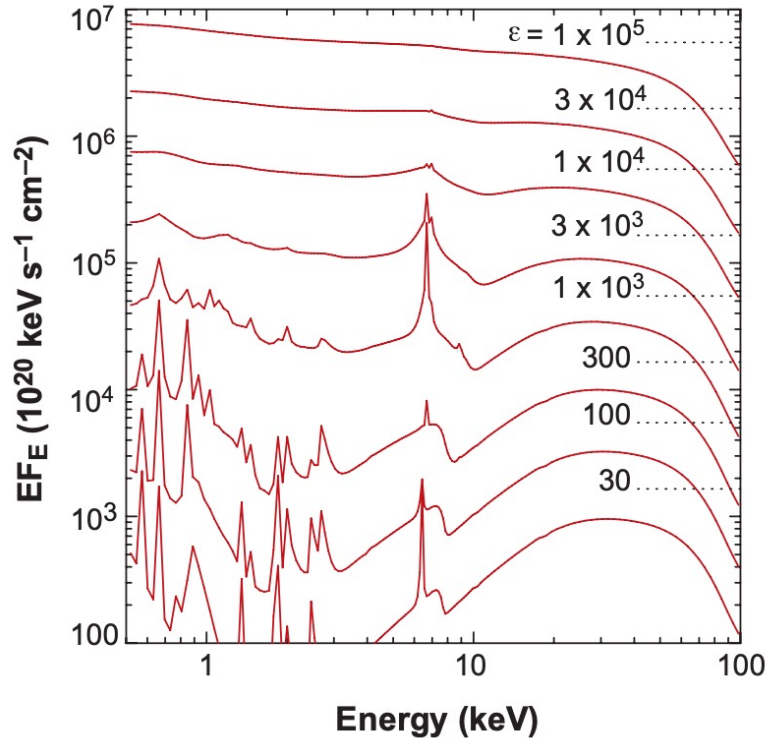


Fluorescence Fe lines

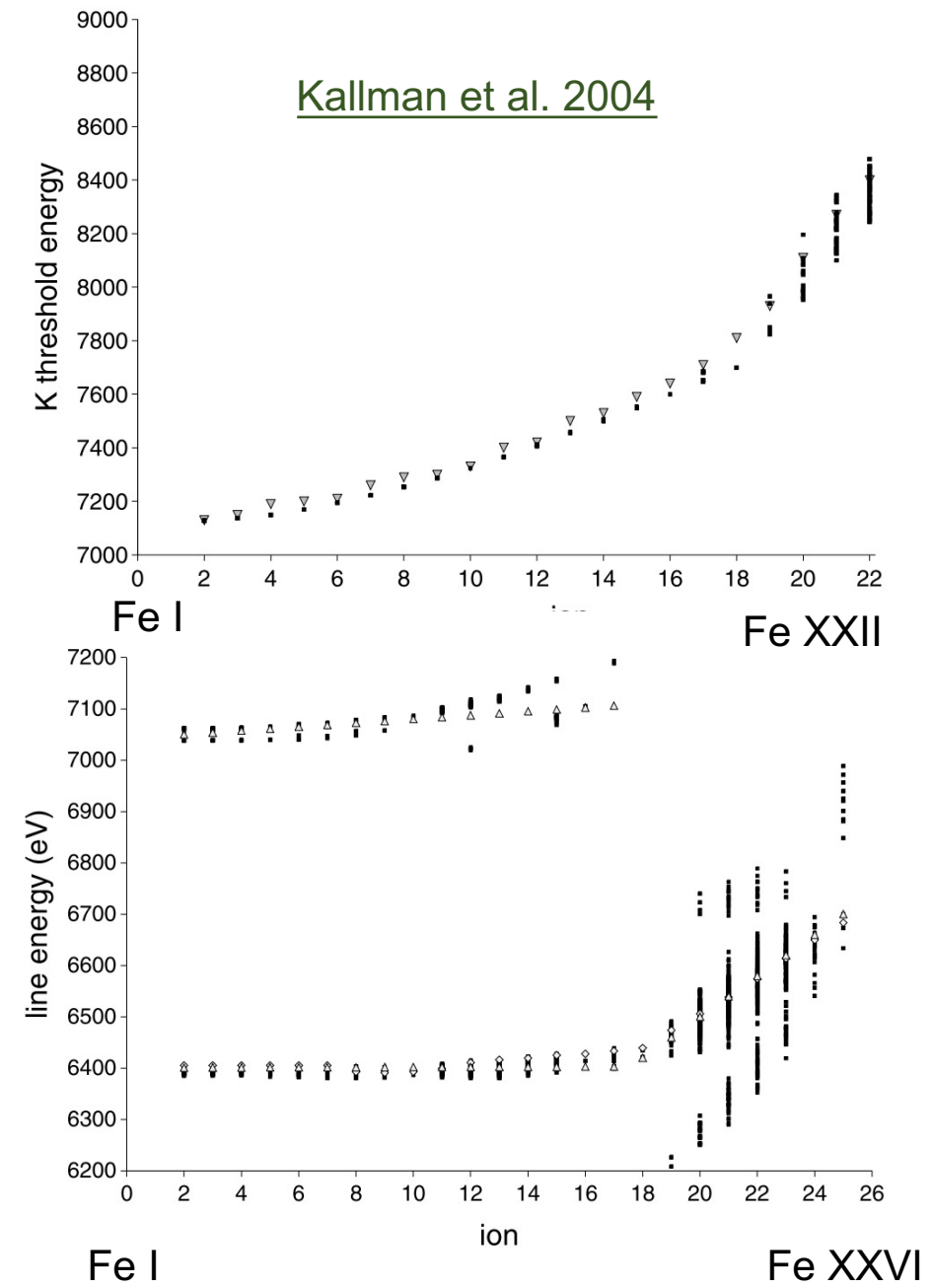
Image credit: NASA/JPL-Caltech/R. Hurt (IPAC)



Miller et al. 2007



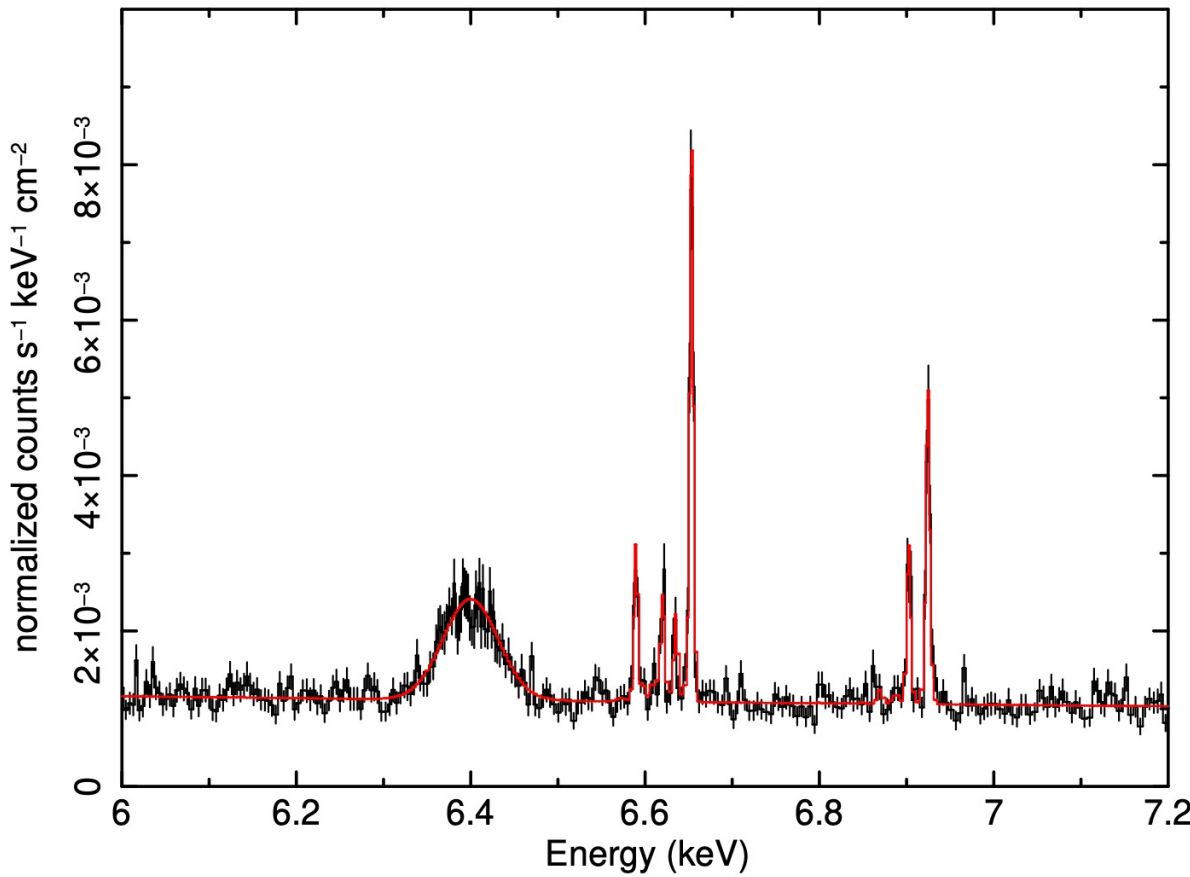
Kallman et al. 2004



Distance to the BH	Center	Width
far	6.4 keV (small ξ)	narrow
close	~ 7 keV (large ξ)	broad

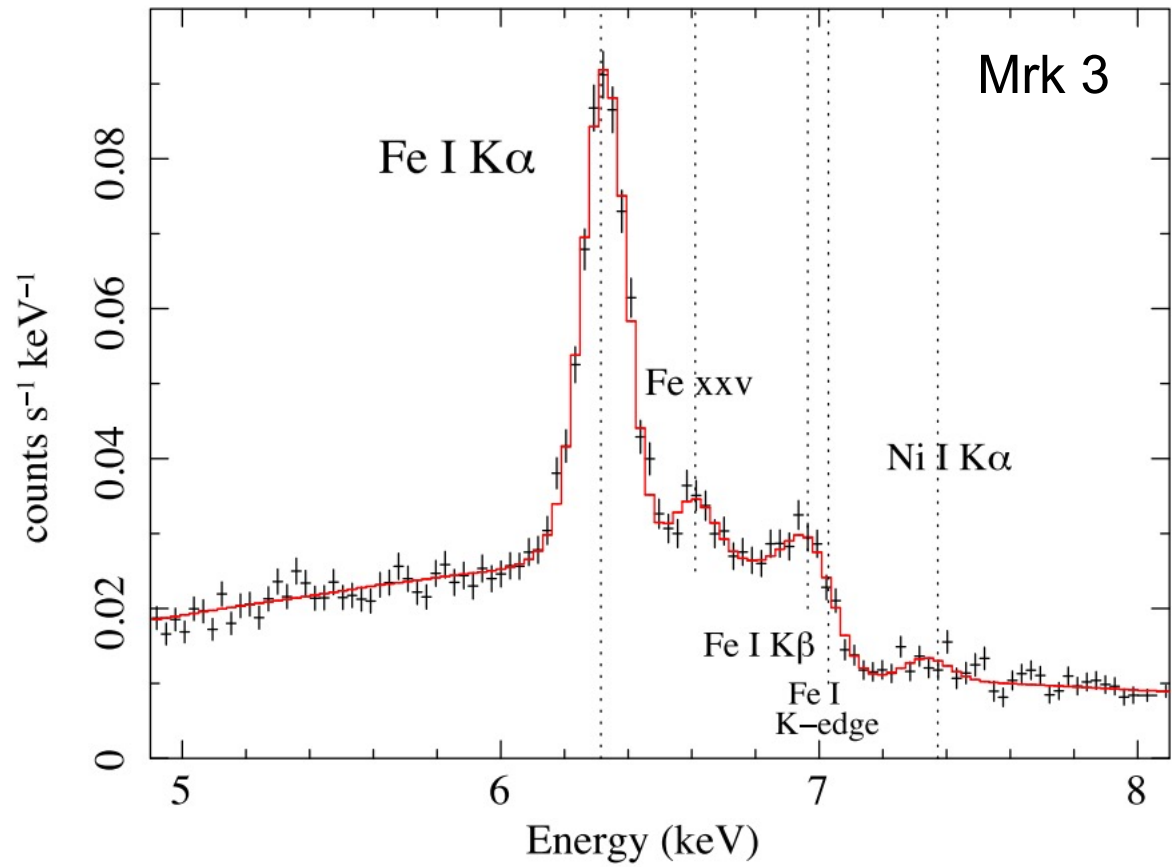
Distant reflection spectrum

simulated XRISM spectrum of LMC X-4



XRISM Science team 2020

Yaqoob et al. 2015



Relativistic reflection

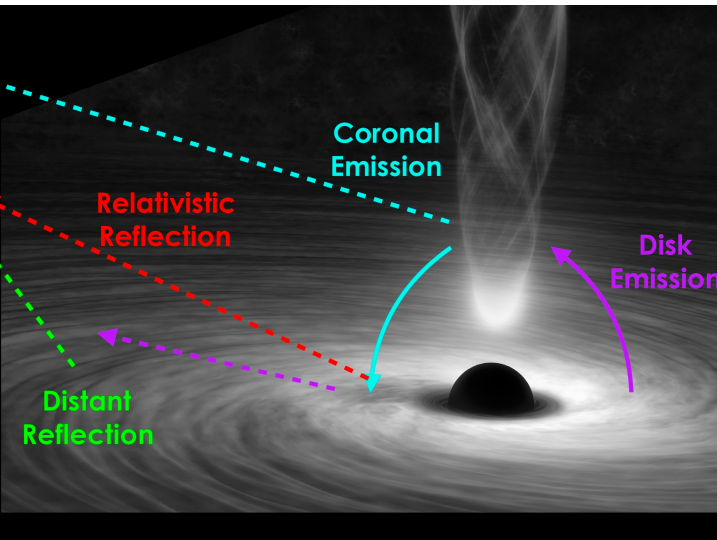
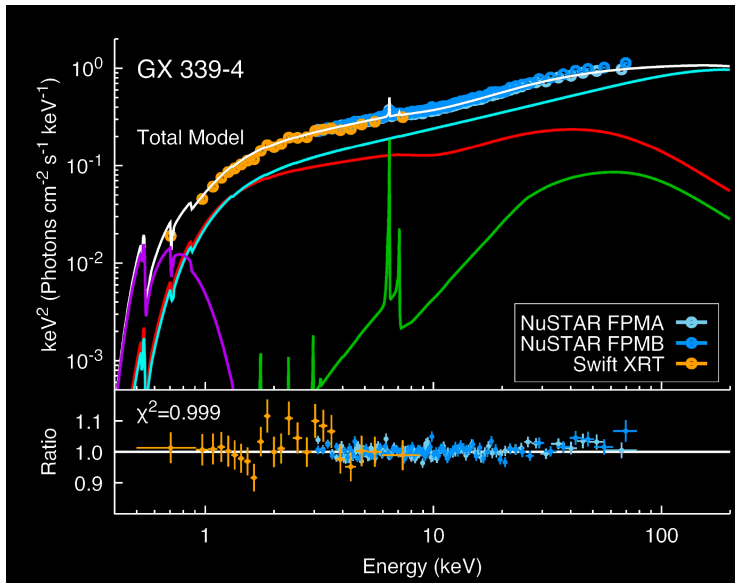
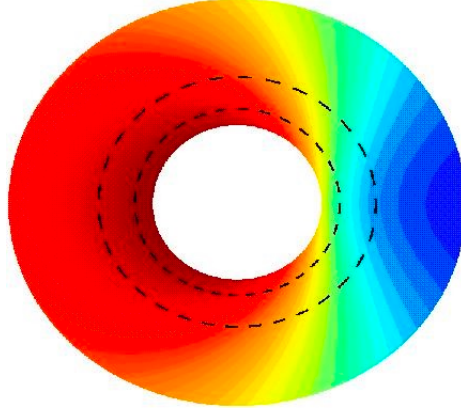
Close to the BH, special and general relativity determine the line profile.

Bardeen et al. 1972

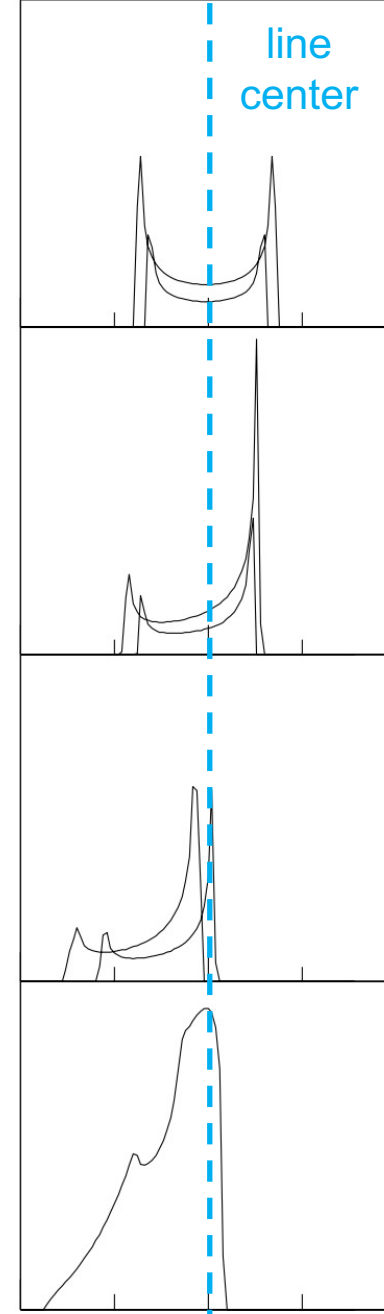
angular momentum of the BH

$$a = \frac{Jc}{GM_{\text{BH}}^2}$$

spin parameter of the BH (dimensionless)



Fabian et al. 2000



Innermost Stable Circular Orbit

ISCO varies with BH spin

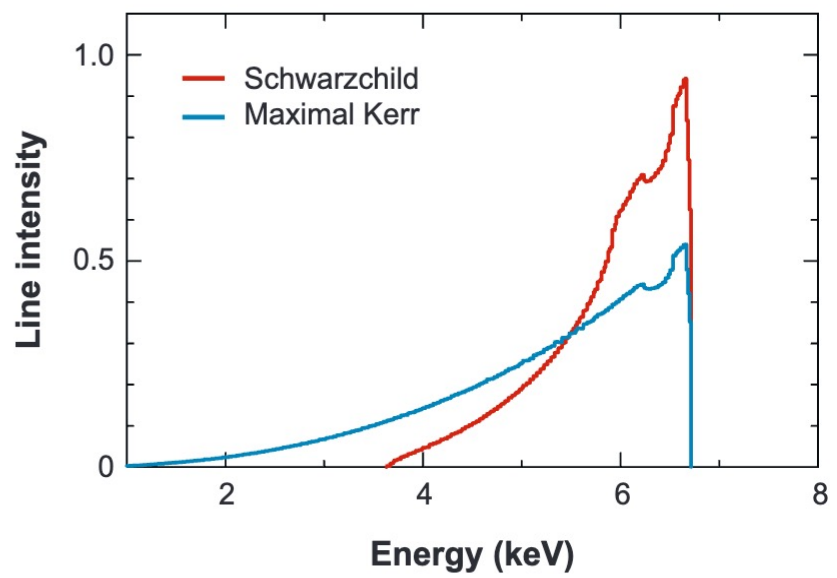
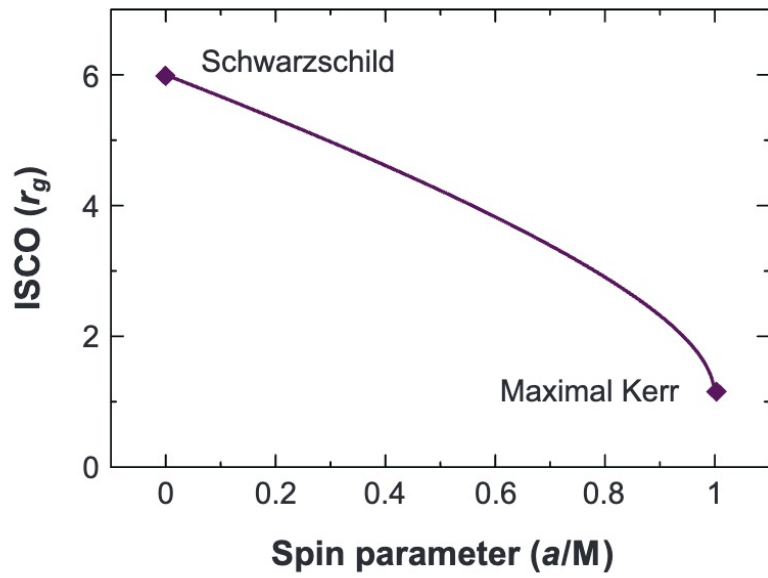
- Schwarzschild BH ($a = 0, r_{\text{ISCO}} = 6 r_g$)
- Kerr BH ($a = 0.998, r_{\text{ISCO}} \sim 1.2 r_g$)

Gravitational radius

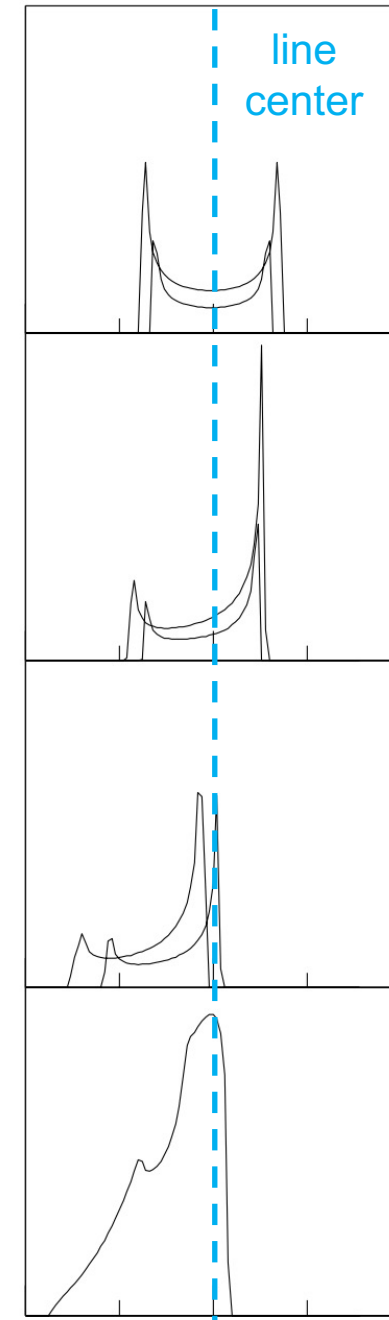
$$r_g = \frac{GM_{\text{BH}}}{c^2}$$

Schwarzschild radius

$$r_s = \frac{2GM_{\text{BH}}}{c^2}$$

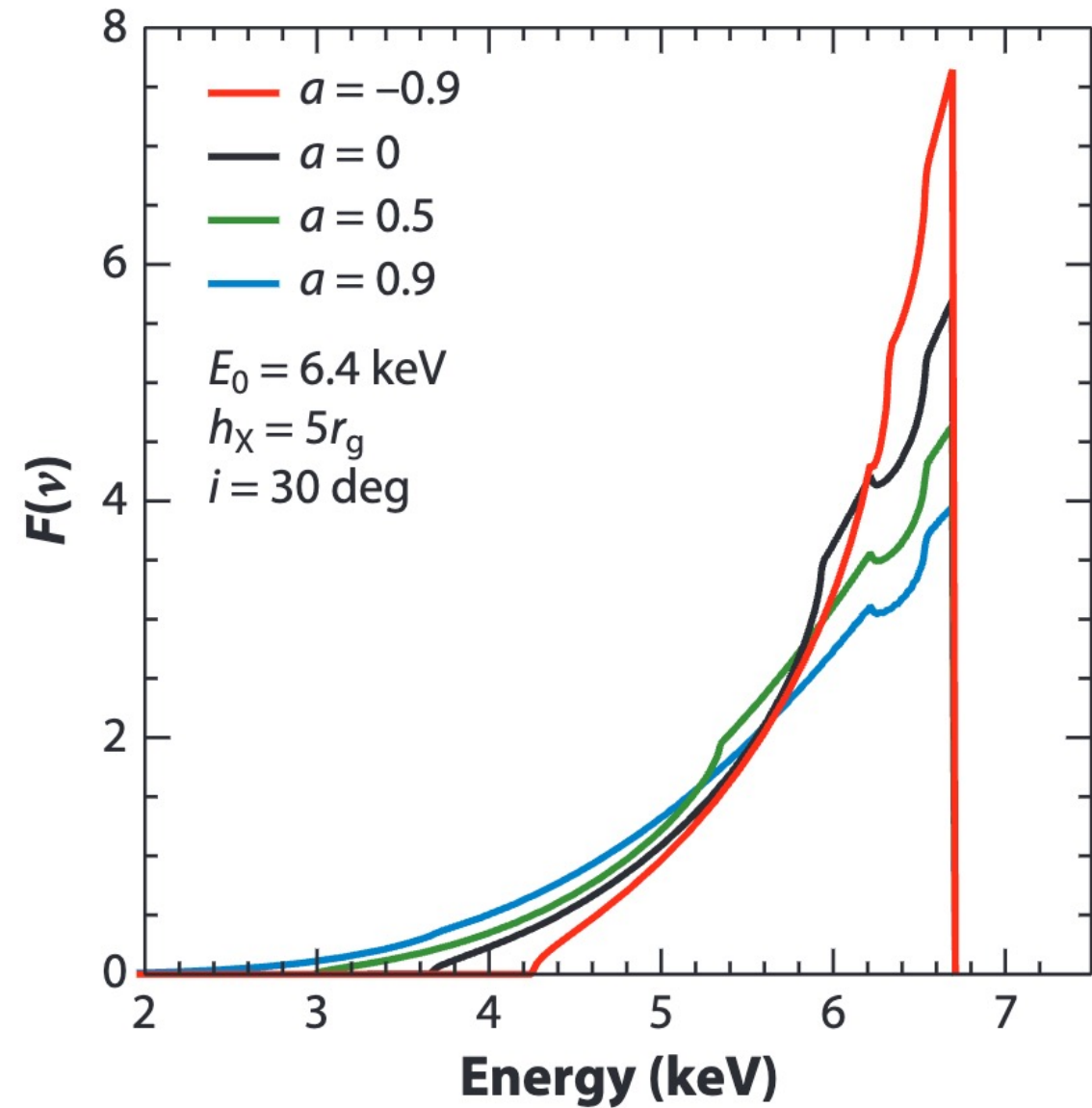
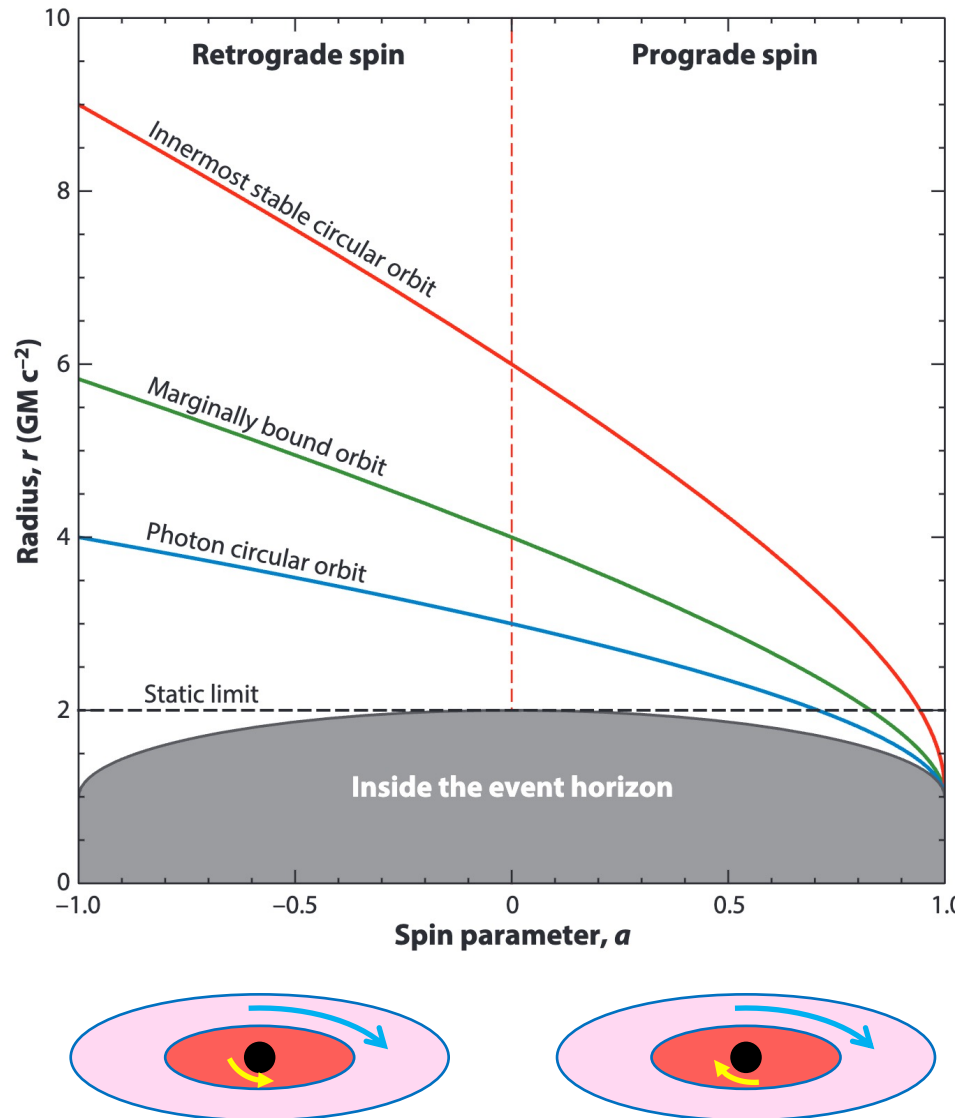


Fabian et al. 2000



Relativistic reflection: prograde and retrograde

[Reynolds \(2021\)](#)

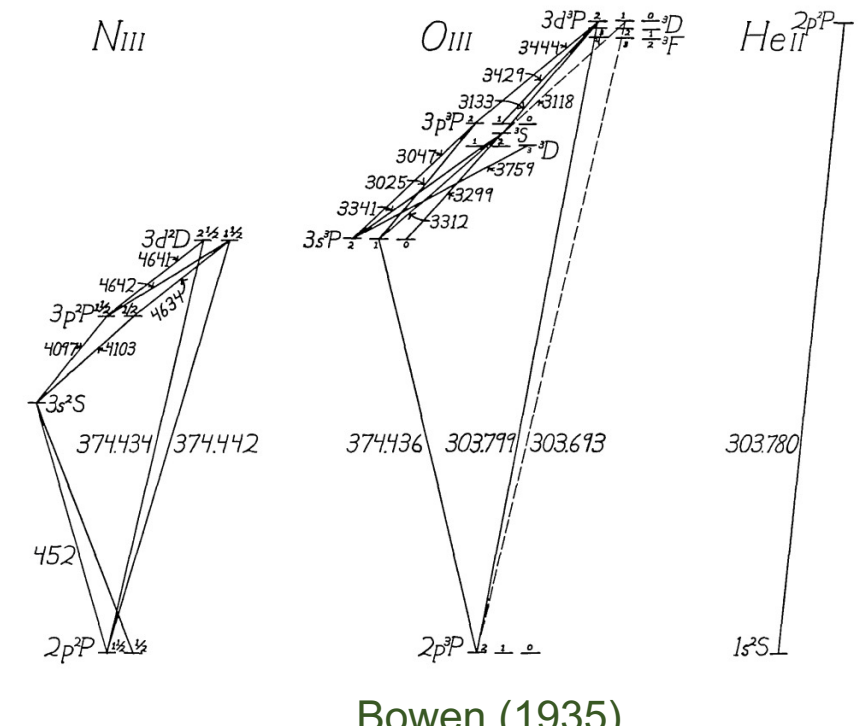
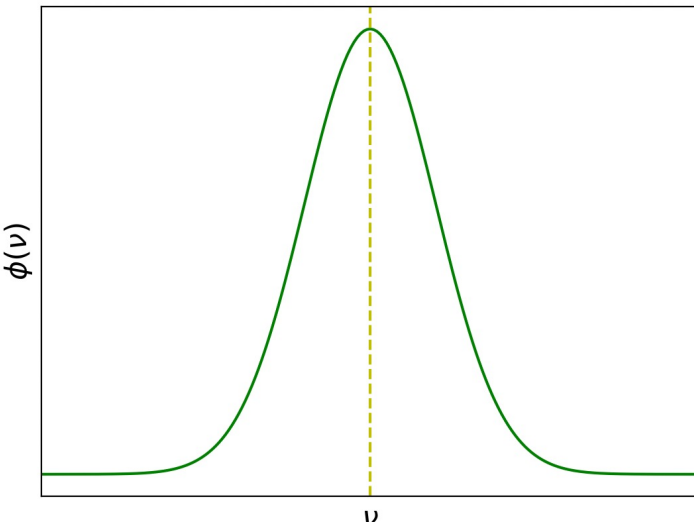


Line broadening

Line broadening $\phi(\nu)$ plays a role in the Bowen resonance-fluorescence mechanism

Ion	Transition	$\lambda (\text{\AA})$	$A (\text{s}^{-1})$
He II	$2\text{p } ^2\text{P}_{3/2,1/2} - 1\text{s } ^2\text{S}_{1/2}$	303.78	1.0×10^{10}
O III	$2\text{s}^2 2\text{p}^2 ^3\text{P}_2 - 2\text{s}^2 2\text{p } 3\text{d } ^3\text{P}_2$	303.80	9.6×10^9
O III	$2\text{s}^2 2\text{p}^2 ^3\text{P}_2 - 2\text{s}^2 2\text{p } 3\text{d } ^3\text{P}_1$	303.70	5.3×10^9

Ion	Transition	$\lambda (\text{\AA})$	$A (\text{s}^{-1})$
O III	$2\text{s}^2 2\text{p } ^2\text{P}_1 - 2\text{s}^2 2\text{p } 3\text{s } ^3\text{P}_0$	374.33	3.8×10^9
N III	$2\text{s}^2 2\text{p } ^2\text{P}_{3/2} - 2\text{s}^2 3\text{d } ^2\text{D}_{5/2}$	374.43	1.2×10^{10}
N III	$2\text{s}^2 2\text{p } ^2\text{P}_{3/2} - 2\text{s}^2 3\text{d } ^2\text{D}_{3/2}$	374.44	2.0×10^9



Gaussian profile

Thermal random motion will lead to a Gaussian line profile

Doppler shift

$$\nu = \nu_0 \left(1 + \frac{v}{c}\right) \rightarrow v = \frac{c(\nu - \nu_0)}{\nu_0}$$

Sect. 10.6 of the REF by Rybicki & Lightman (p288)

$$\Delta\nu_D \equiv \frac{\nu_0}{c} \sqrt{\frac{2kT}{m}}$$

$$\phi_D(v) = \frac{c}{\nu_0} \left(\frac{m}{2\pi kT} \right)^{1/2} \exp \left(-\frac{mc^2}{2kT} \frac{(v - \nu_0)^2}{\nu_0^2} \right)$$

$$\phi_D(v) = \frac{1}{\Delta\nu_D \sqrt{\pi}} \exp \left(-\frac{(v - \nu_0)^2}{\Delta\nu_D^2} \right)$$

$$\int_0^\infty \phi(v) dv = 1$$

$$\phi_D(v = \nu_0) = \frac{1}{\Delta\nu_D \sqrt{\pi}} \quad \Delta\nu_{\text{FWHM}} = 2\sqrt{\ln 2} \Delta\nu_D \sim 1.665 \Delta\nu_D$$

FWHM = Full Width Half Maximum

Gaussian profile (cont.)

[prev. sl.](#)

$$\phi_D(\nu) = \frac{1}{\Delta\nu_D \sqrt{\pi}} \exp\left(-\frac{(\nu - \nu_0)^2}{\Delta\nu_D^2}\right) \quad \Delta\nu_D = \frac{\nu_0}{c} \sqrt{\frac{2kT}{m}} \quad \Delta\nu_{\text{FWHM}} = 2\sqrt{\ln 2} \Delta\nu_D \sim 1.665 \Delta\nu_D$$

Microscopic turbulent motion will also lead to a Gaussian line profile

$$\phi(\nu) = \frac{1}{\sqrt{2\pi} \sigma_\nu} \exp\left(-\frac{(\nu - \nu_0)^2}{2\sigma_\nu^2}\right)$$

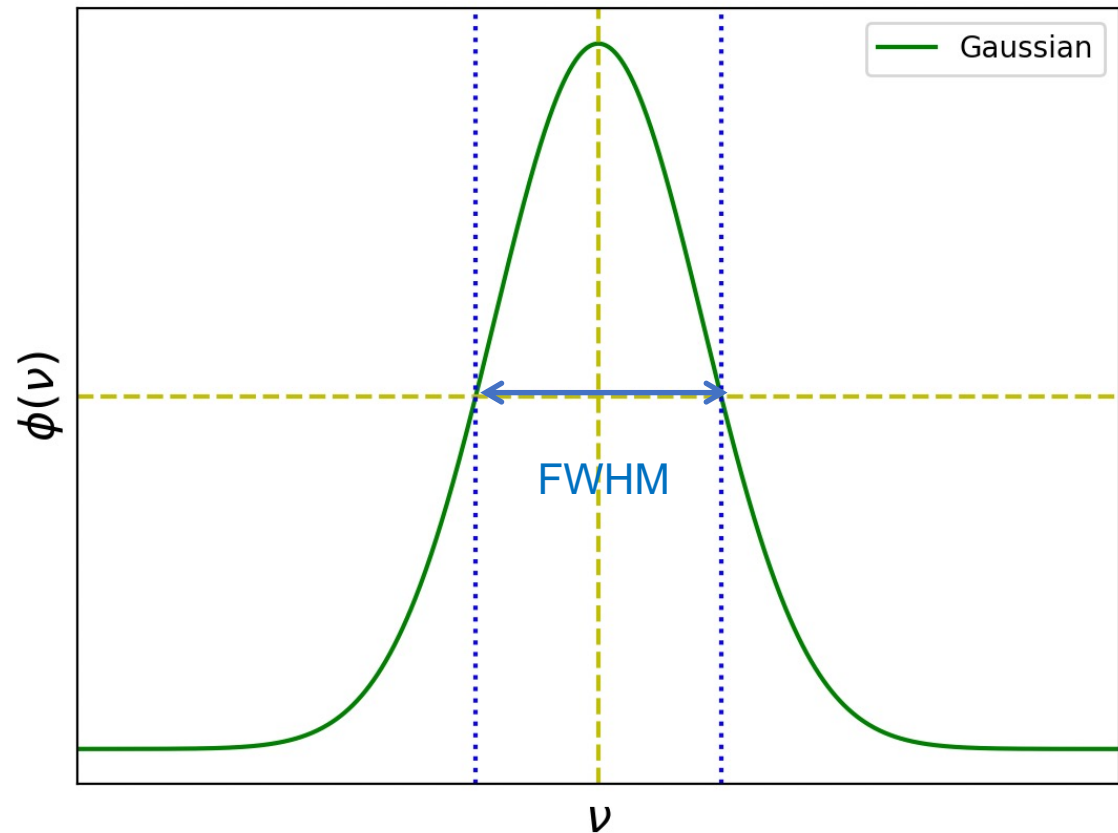
$$\sigma_\nu = \frac{\nu_0}{c} \sqrt{\sigma_{\text{th}}^2 + \sigma_{\text{tu}}^2}$$

↑ ↑
 thermal velocity dispersion turbulent velocity dispersion

$$\sigma_{\text{th}} = \sqrt{\frac{kT_e}{A m_p}}$$

↑
 atomic weight

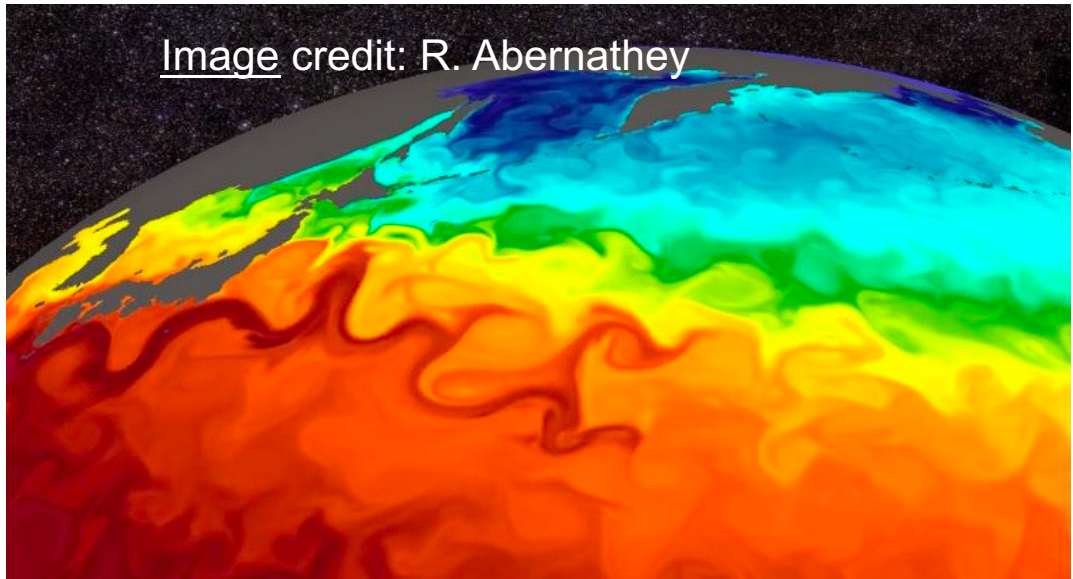
$$\Delta\nu_{\text{FWHM}} = 2\sqrt{2\ln 2} \sigma_\nu \sim 2.355 \sigma_\nu$$



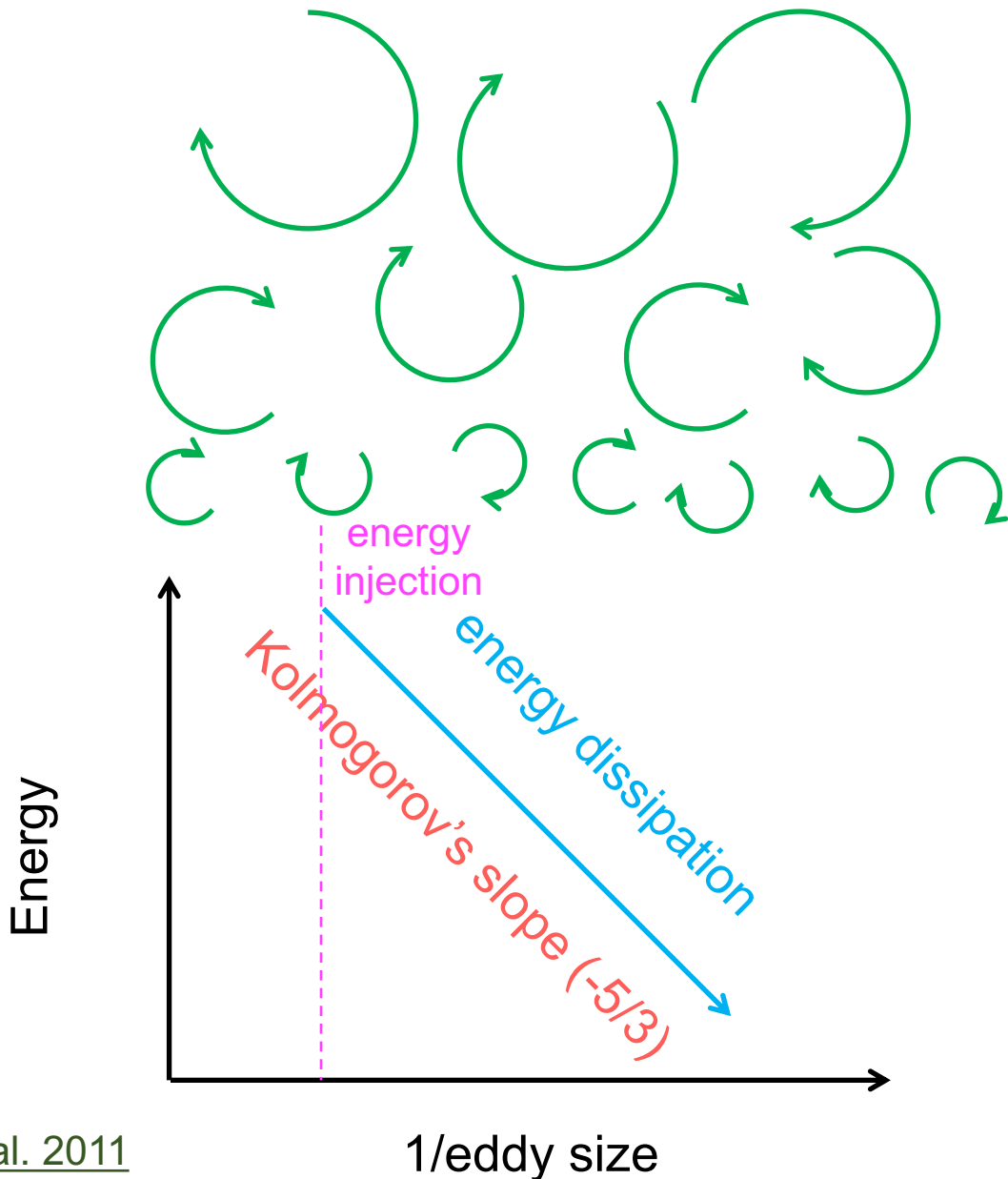
Turbulence length scale

To use the expression below, the microscopic turbulence length scale needs to be smaller than the mean free path of the collision

$$\sigma_v = \sqrt{\sigma_{th}^2 + \sigma_{tu}^2}$$



Zhuravleva et al. 2011
for more discussions



Lorentzian profile

Natural broadening

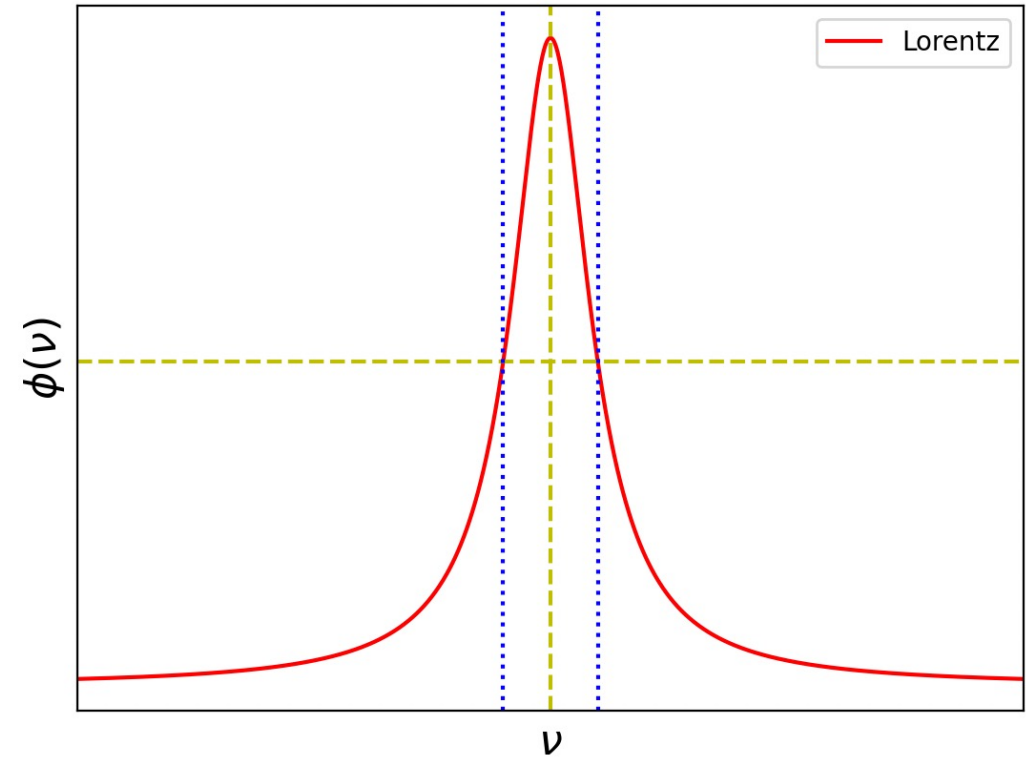
$$\Gamma \sim \frac{1}{\Delta t} \sim \frac{\Delta\nu_{\text{nat}}}{2\pi}$$

width of the energy level
lifetime of the energy level

$$\phi_{\text{nat}}(\nu) = \frac{\Gamma/2\pi}{(\nu - \nu_0)^2 + (\Gamma/2)^2}$$

$$\Delta\nu_{\text{FWHM}} = \Gamma$$

- ❖ Hard to observe, usually dominated by other line broadening mechanisms



Lorentzian profile (cont.)

Collisional broadening

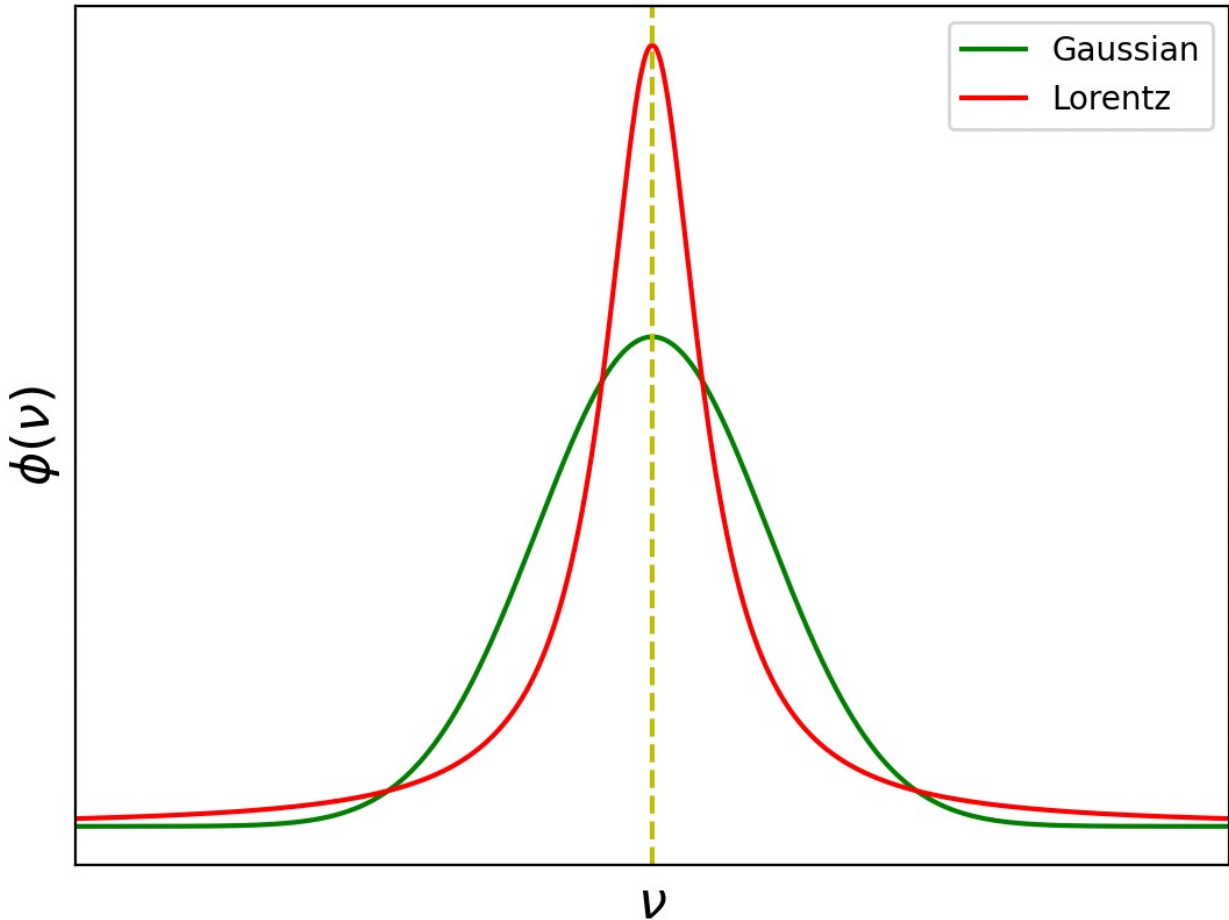
$$\Delta\nu_{\text{col}} \sim \frac{1}{\Delta t} \quad \leftarrow \text{mean collisional time}$$

Natural + collisional broadening

$$\Gamma \sim \Delta\nu_{\text{col}} + \Delta\nu_{\text{nat}}$$

$$\phi(\nu) = \frac{\Gamma/2\pi}{(\nu - \nu_0)^2 + (\Gamma/2)^2}$$

$$\Delta\nu_{\text{FWHM}} = \Gamma$$



- ❖ Collisional broadening dominates the natural broadening for high-density plasmas (shorten the lifetime via collisional de-excitation)
- ❖ Away from the line center, the Lorentzian profile declines slower than the Gaussian profile

Voigt profile

Convolving the Lorentz profile with the Doppler profile

$$\phi(\mu) = \frac{\Gamma/2\pi}{(\nu - \nu_0 - \mu)^2 + (\Gamma/2)^2} \frac{1}{\sqrt{2\pi} \sigma_\nu} \exp\left(-\frac{\mu^2}{2\sigma_\nu^2}\right)$$

$$a = \frac{\Gamma}{2\sqrt{2} \sigma_\nu}$$

$$x = \frac{\nu - \nu_0}{\sqrt{2} \sigma_\nu}$$

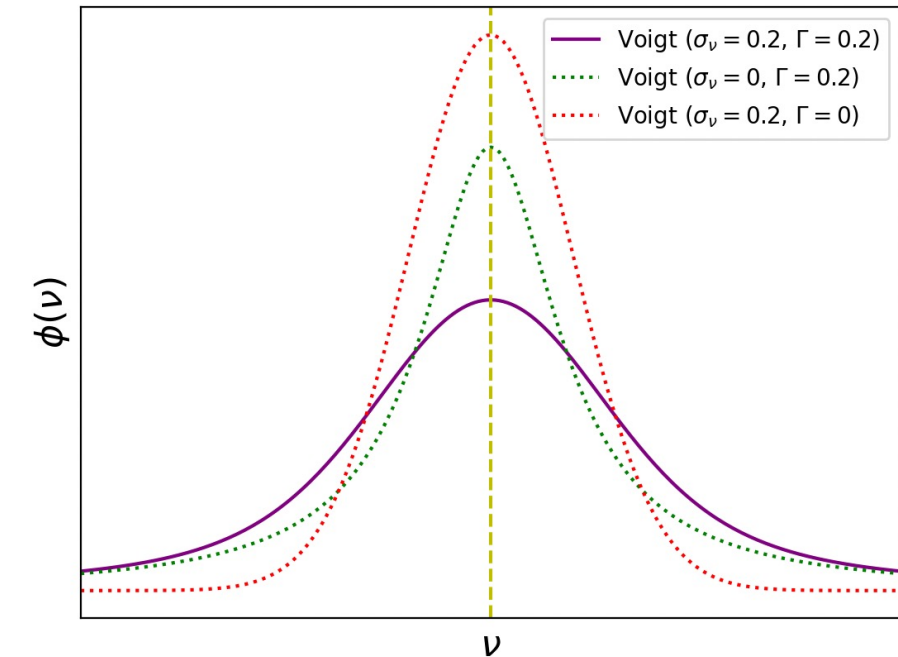
$$u = \frac{\mu}{\sqrt{2} \sigma_\nu}$$

$$\int_{-\infty}^{\infty} \phi(\mu) d\mu = \frac{1}{\sqrt{2\pi} \sigma_\nu} \int_{-\infty}^{\infty} \frac{a}{\pi} \frac{\exp(-u^2)}{(x - u)^2 + a^2} du$$



Voigt function $H(a, x)$

Schreier (2011)

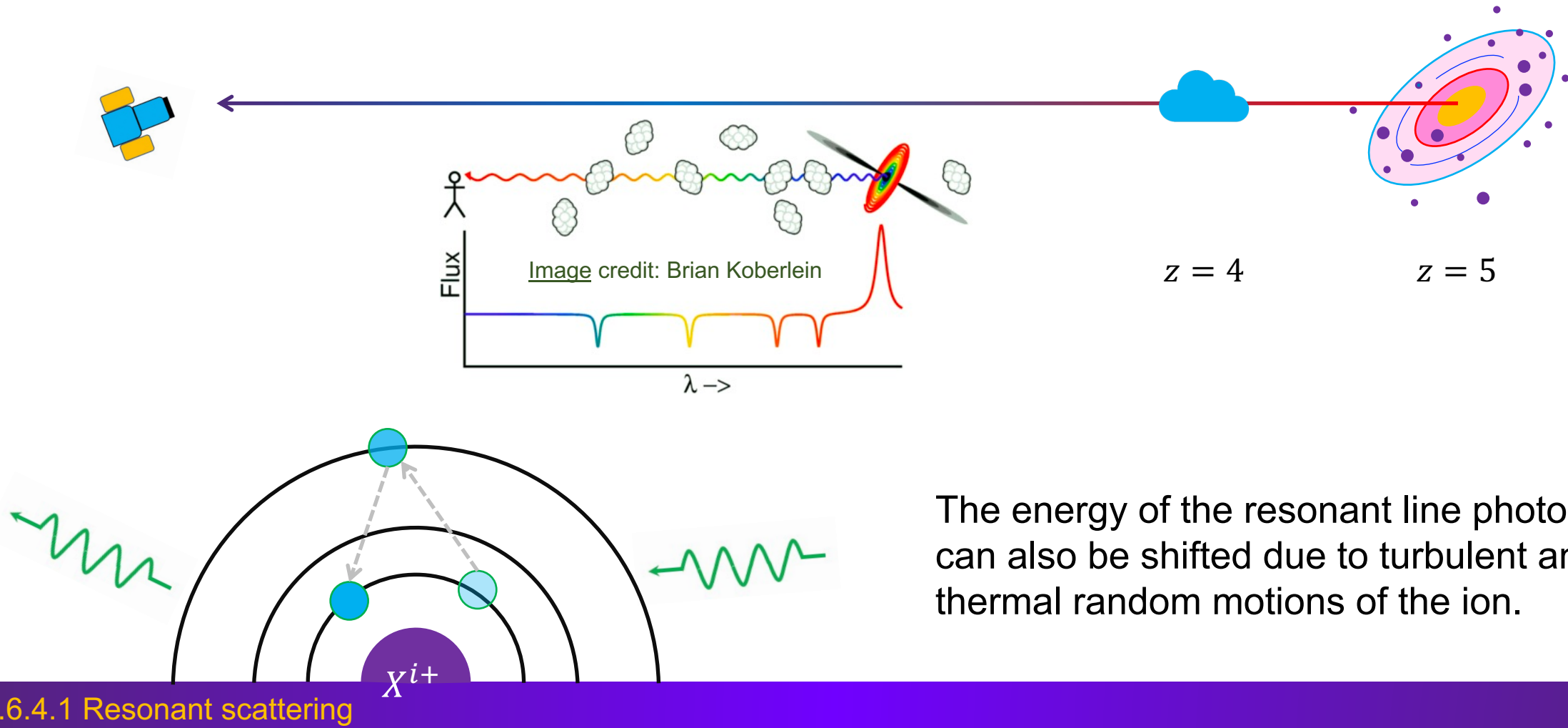


`scipy.special.voigt_profile`

$$\frac{1}{\sqrt{2\pi} \sigma_\nu} \int_{-\infty}^{\infty} \frac{a}{\pi} \frac{\exp(-u^2)}{(x - u)^2 + a^2} du$$

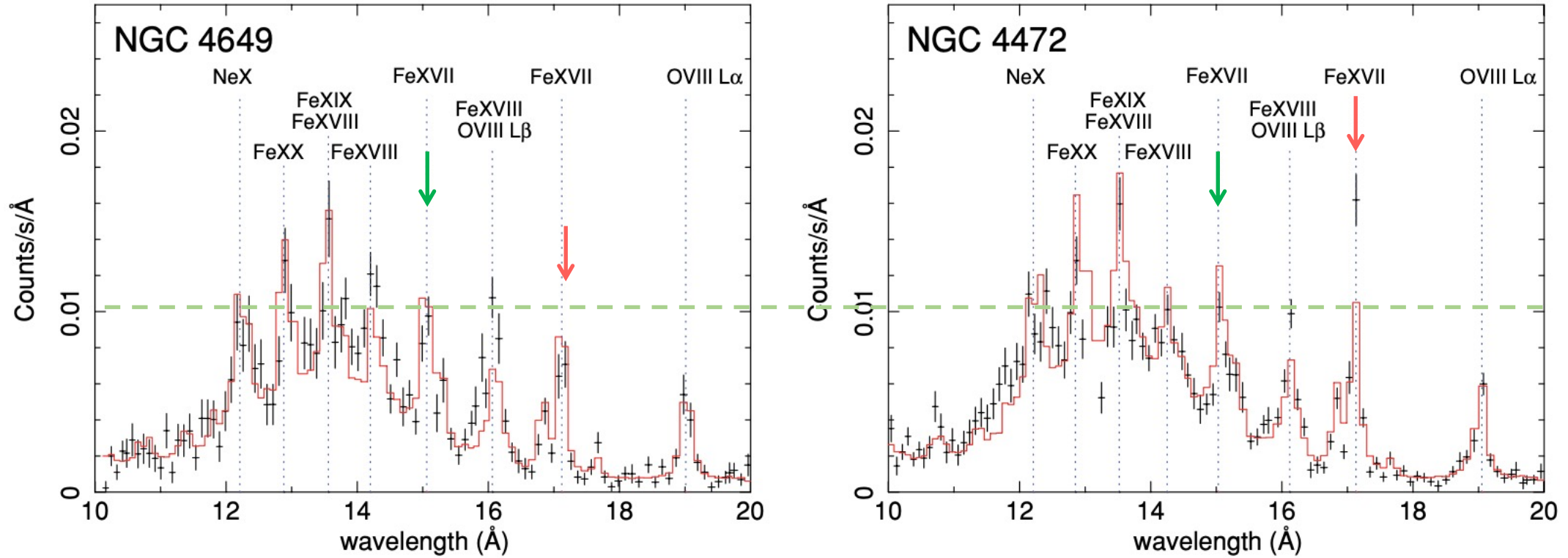
Resonant scattering

A resonance transition photon (with sufficient large A-values) can be absorbed and re-emitted in different directions. This results in the reduction of the resonance lines (e.g., H-like Ly α).



Resonant scattering of Fe XVII

Werner et al. 2009



Line ratios from Fe XVII 15 Å /17 Å appear differently in the hot plasmas of two elliptical galaxies
 Same temperature ($kT_e \sim 0.78$ keV for both targets)

Resonant scattering optical depth

The optical depth of resonant scattering of a line from the level l in ion X^{i+} is

$$\tau = \int n_{i,l} \sigma_{\text{RS}} dl$$

(absorption) oscillator strength

$$\sigma_{\text{RS}} = \frac{\sqrt{\pi} e^2}{m_e c} \frac{f_{\text{lu}}}{\sqrt{2} \sigma_\nu} H(a, x)$$

Among lines from the same ion in the same target, the **larger** the f-value, the **stronger** the resonant scattering

prev. sl.

$$H(a, x) = \int_{-\infty}^{\infty} \frac{a}{\pi} \frac{\exp(-u^2)}{(x - u)^2 + a^2} du$$

$$a = \frac{\Gamma}{2\sqrt{2} \sigma_\nu}$$

$$x = \frac{\nu - \nu_0}{\sqrt{2} \sigma_\nu}$$

prev. sl.

$$\sigma_\nu = \sqrt{\sigma_{\text{th}}^2 + \sigma_{\text{tu}}^2}$$

$$\sigma_{\text{th}} = \sqrt{\frac{kT_e}{A m_p}}$$

(absorption) oscillator strength

$$f_{\text{lu}} = \frac{m_e c}{8 \pi^2 e^2} \frac{g_u}{g_l} \lambda^2 A_{\text{ul}} = 1.499 \times 10^{-16} \frac{g_u}{g_l} \left(\frac{\lambda}{\text{\AA}}\right)^2 \left(\frac{A_{\text{ul}}}{\text{s}^{-1}}\right)$$

NIST f-values

NIST Atomic Spectra Database Lines Form

Best viewed with the latest versions of Web browsers and JavaScript enabled

Main Parameters

Spectrum: Fe XVII e.g., Fe I or Na;Mg; Al or mg i-iii or 198Hg I

Limits for Wavelengths: Lower: _____
Upper: _____

Wavelength Units: Å

Reset input **Retrieve Data** **Show Graphical Options** **Show Advanced Settings** 

Can you please provide some [feedback](#) to improve our database?

Transition strength: A_{ki} $g_k A_{ki}$ in units of 10^8 s^{-1}

f_{ik} S_{ik} $\log(gf)$

Relative Intensity

Transition Type: Allowed (E1) Forbidden (M1,E2,...)

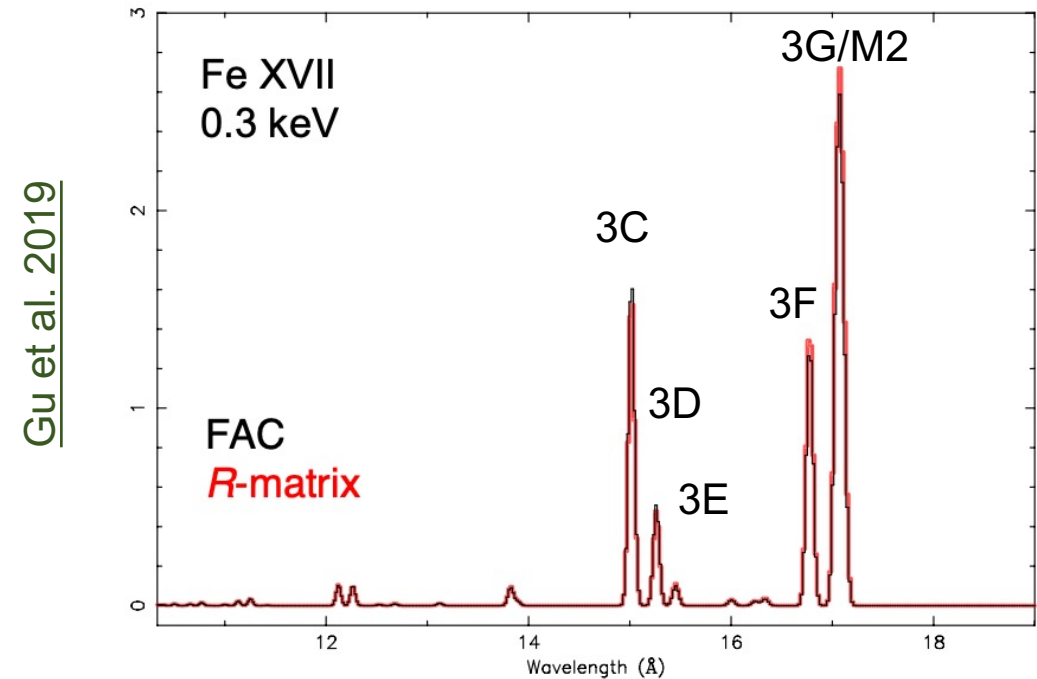
Level information: Configurations Terms Energies J g

NIST provides f-values
(if available)

Fe XVII lines: f-values



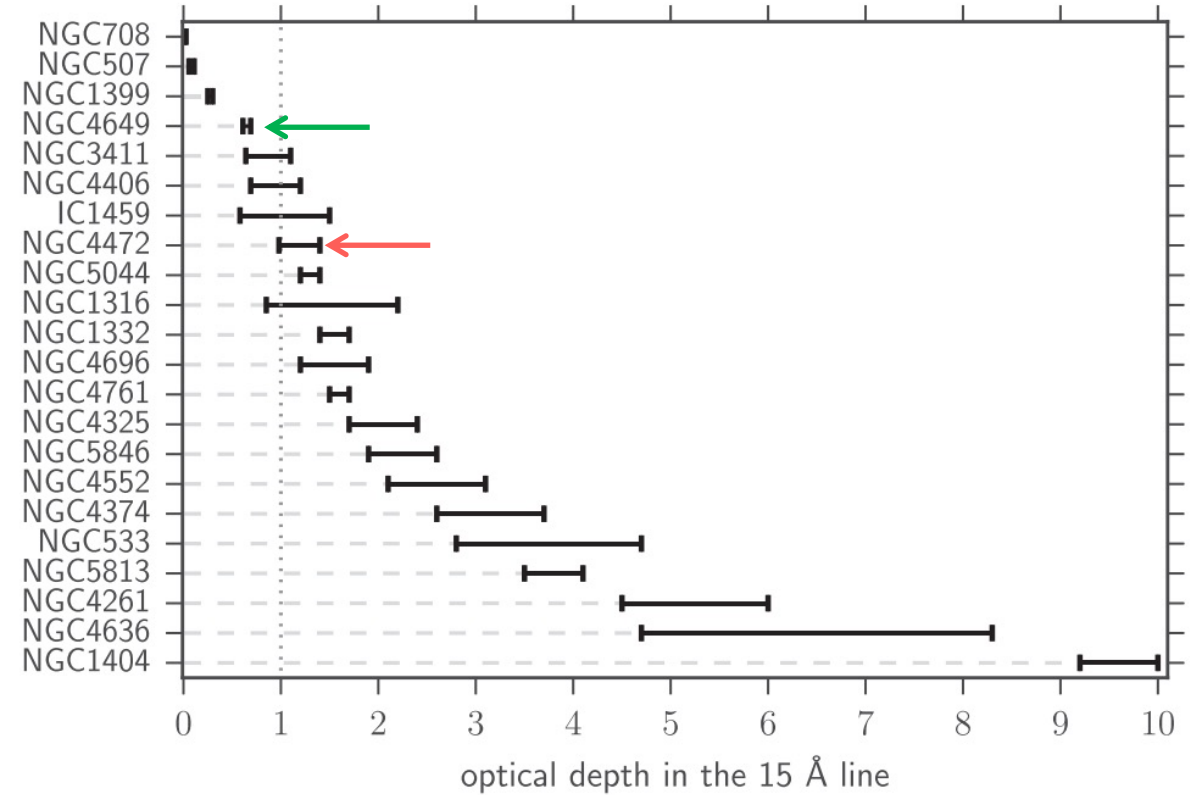
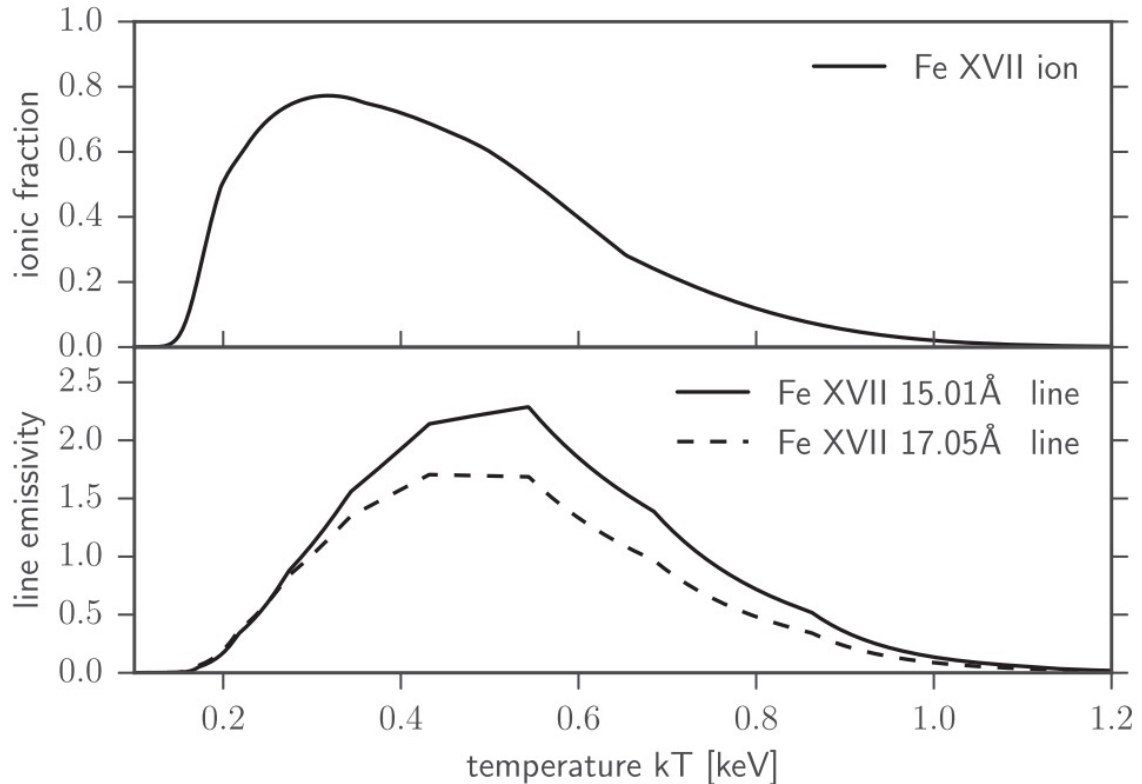
Fe XVII: 99 Lines of Data Found
Z = 26, Ne isoelectronic sequence



Ion	Label	Transition	λ (\u00c5)	A (s ⁻¹)	f
Fe XVII	3C	$2p^6 \ ^1S_0 - 2p^5 \ 3d \ ^1P_1$	15.02	2.3×10^{13}	2.31
Fe XVII	3D	$2p^6 \ ^1S_0 - 2p^5 \ 3d \ ^3D_1$	15.26	6.0×10^{12}	0.63
Fe XVII	3E	$2p^6 \ ^1S_0 - 2p^5 \ 3d \ ^3P_1$	15.45	9.0×10^{10}	9.7×10^{-3}
Fe XVII	3F	$2p^6 \ ^1S_0 - 2p^5 \ 3s \ ^3P_1$	16.78	8.3×10^{11}	0.11
Fe XVII	3G	$2p^6 \ ^1S_0 - 2p^5 \ 3s \ ^1P_1$	17.05	9.3×10^{11}	0.12
Fe XVII	M2	$2p^6 \ ^1S_0 - 2p^5 \ 3s \ ^3P_2$	17.10	2.0×10^5	5.5×10^{-8}

Resonant scattering (thermal broadening only)

Ogorzalek et al. 2017



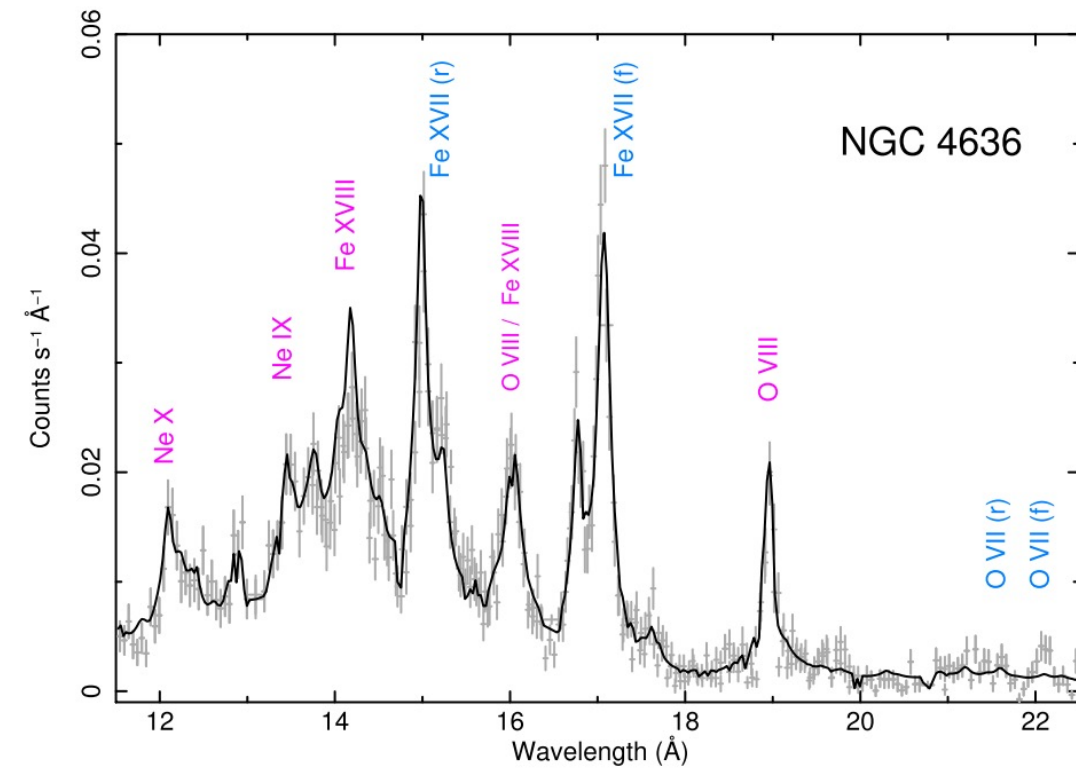
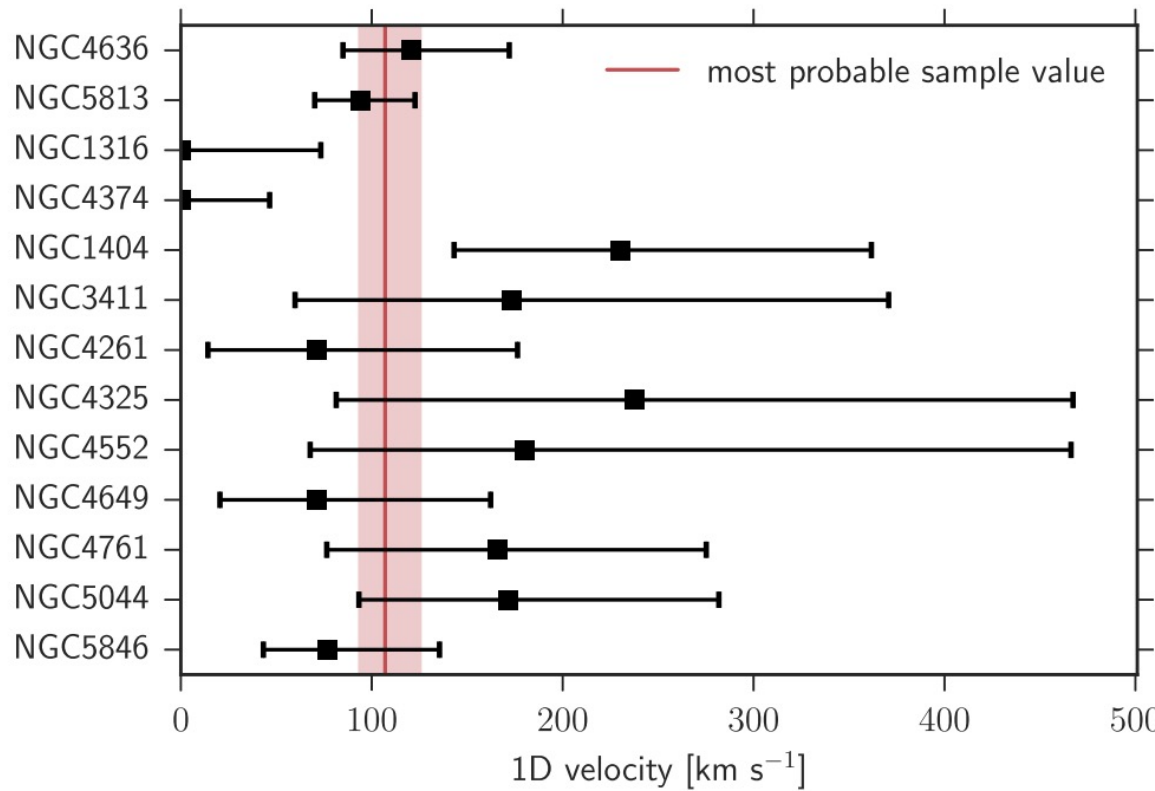
prev. sl.

$$\tau = \int n_{i,l} \sigma_{RS} dl \quad \sigma_{RS} = \frac{\sqrt{\pi} e^2}{m_e c} \frac{f_{lu}}{\sqrt{2} \sigma_v} H(a, x)$$

Considering only the thermal broadening, most of the targets have $\tau(\text{Fe XVII}, 15.04 \text{ \AA})$ larger than unity.

Resonant scattering (with turbulence broadening)

Ogorzalek et al. 2017



Comparing the observed spectra with theoretical prediction (taking into account the turbulence broadening), one can constrain the turbulence velocity

prev. sl.

$$\sigma_\nu = \sqrt{\sigma_{\text{th}}^2 + \sigma_{\text{tu}}^2} \quad \sigma_{\text{th}} = \sqrt{\frac{kT_e}{A m_p}}$$

Resonant scattering: He α – w lines

Ion	Label	Transition	λ (Å)	A (s $^{-1}$)	f
H I	Ly α	$1s\ ^2S_{1/2} - 2p\ ^2P_{3/2,1/2}^0$	1215.7	6.3×10^8	0.27, 0.14
H I	Ly β	$1s\ ^2S_{1/2} - 3p\ ^2P_{3/2,1/2}^0$	1025.7	1.7×10^8	0.053, 0.026
He II	Ly α	$1s\ ^2S_{1/2} - 2p\ ^2P_{3/2,1/2}^0$	303.78	1.0×10^{10}	0.27, 0.14
O VII	He α – w	$1s^2\ ^1S_0 - 1s\ 2p\ ^1P_1^0$	21.60	3.3×10^{12}	0.69
O VIII	Ly α	$1s\ ^2S_{1/2} - 2p\ ^2P_{3/2,1/2}^0$	18.97	2.6×10^{12}	0.27, 0.14
O VIII	Ly β	$1s\ ^2S_{1/2} - 3p\ ^2P_{3/2,1/2}^0$	16.01	6.9×10^{11}	0.053, 0.026
Fe XVII	3C	$2p^6\ ^1S_0 - 2p^5\ 3d\ ^1P_1$	15.02	2.3×10^{13}	2.31
Fe XXV	He α – w	$1s^2\ ^1S_0 - 1s\ 2p\ ^1P_1^0$	1.85	4.6×10^{14}	0.70
Fe XXVI	Ly α	$1s\ ^2S_{1/2} - 2p\ ^2P_{3/2,1/2}^0$	1.78	2.8×10^{14}	0.27, 0.14

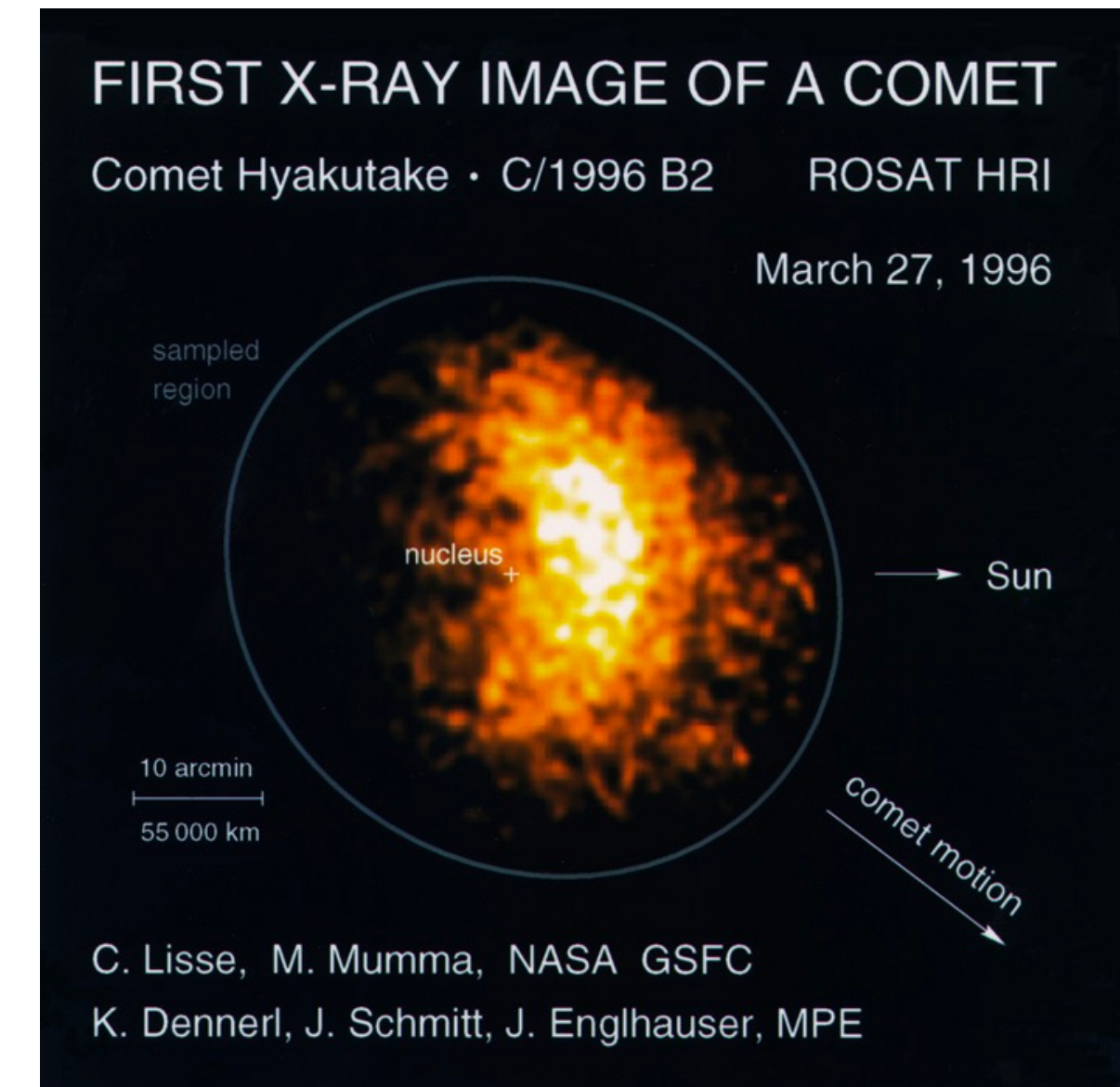


NIST Atomic Spectra Database Lines Data

X-ray emission from Comet

Unexpected X-ray emission from Comet C/1996 B2 (Hyakutake), observed by the High Resolution Imager on the ROSAT X-ray observatory ([Lisse et al. 1996](#)). Comet is cold, why do we expect to see hot X-ray emission?

- [Cravens 1997](#): Charge exchange of solar wind heavy ions
- [Freyberg 1998](#): an X-ray emitting region around the Earth
- [Cox 1998](#): Charge exchange around heliosphere

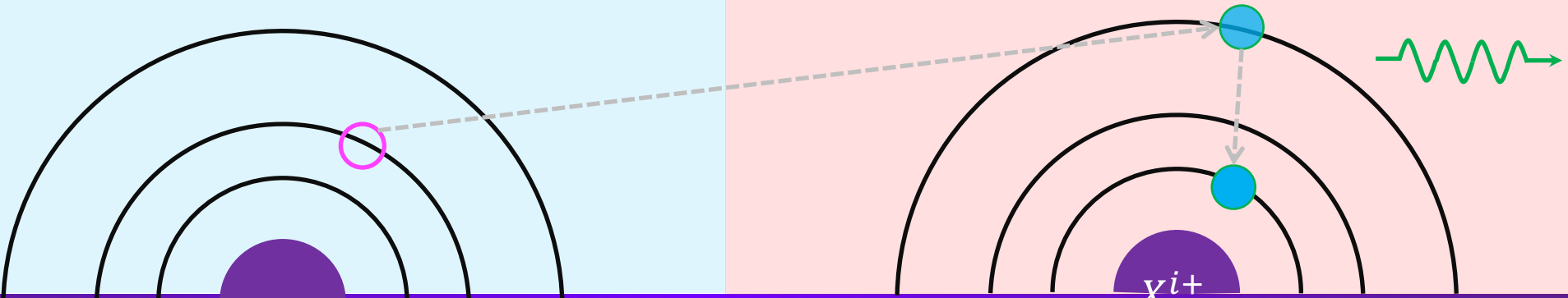


Charge exchange

Charge eXchange (CX) is also known as charge transfer

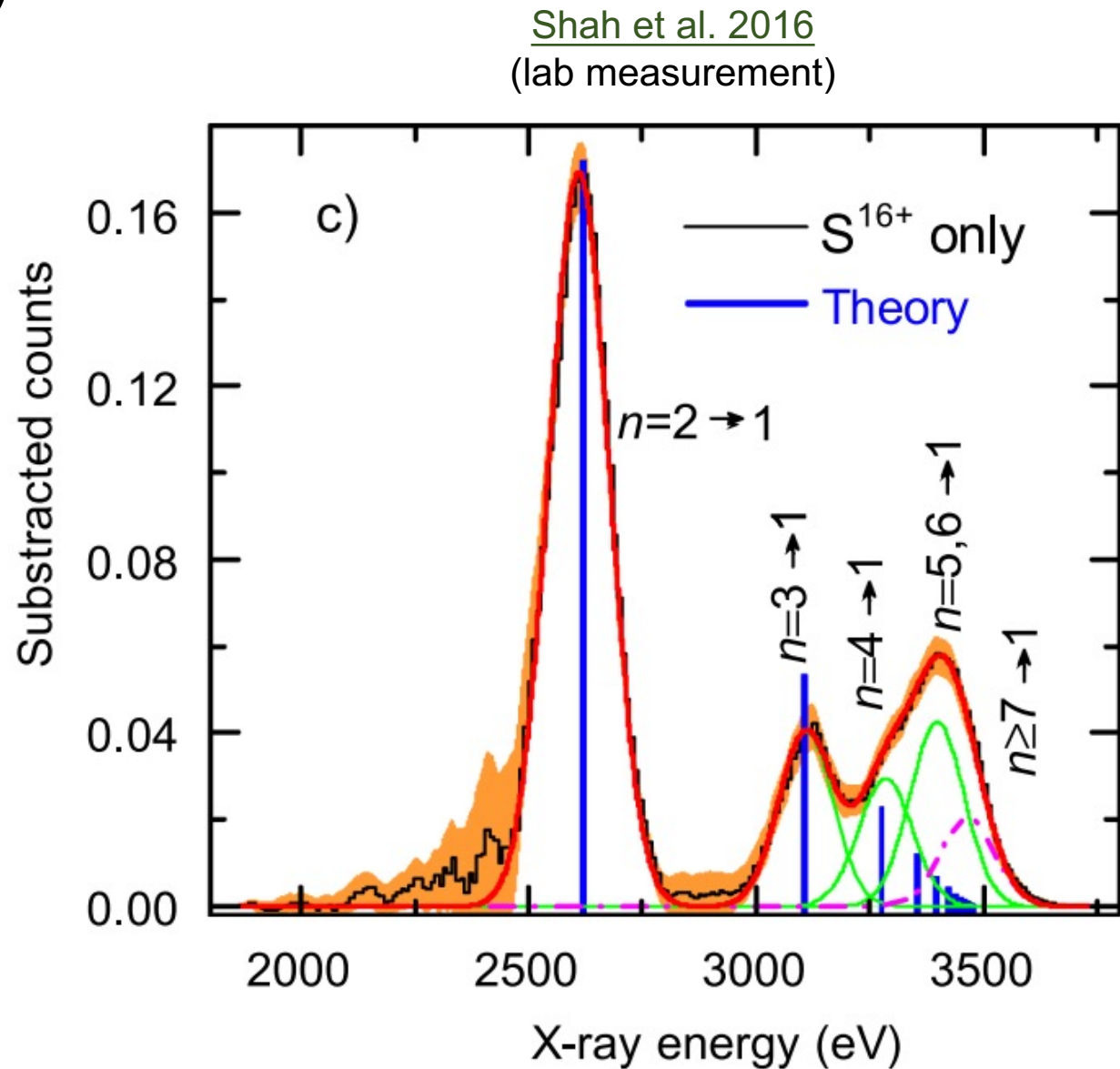
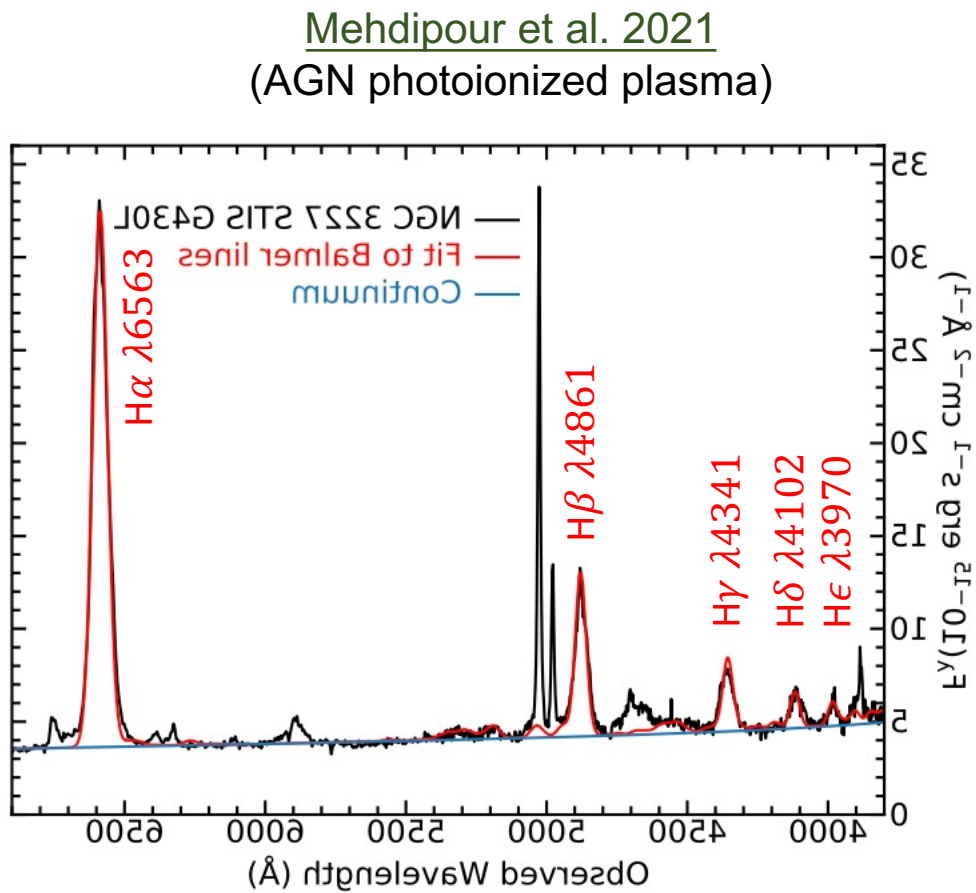
At the interface between **ionized** and **neutral** media, during the ion and atom interaction, one electron can be transferred from the atom to ion:

- The originally neutral atom (typically, H) is ionized, i.e., $H I \rightarrow H II$
- The originally ion gets recombined, $X^{(i+1)+} \rightarrow X^{i+}$
- CX produce characteristic **line emission**
- Multi-electron capture can occur between hot ions and He atoms and molecules



CX line features (Lyman series)

During the CX process, the high- n Lyman lines will be enhanced.

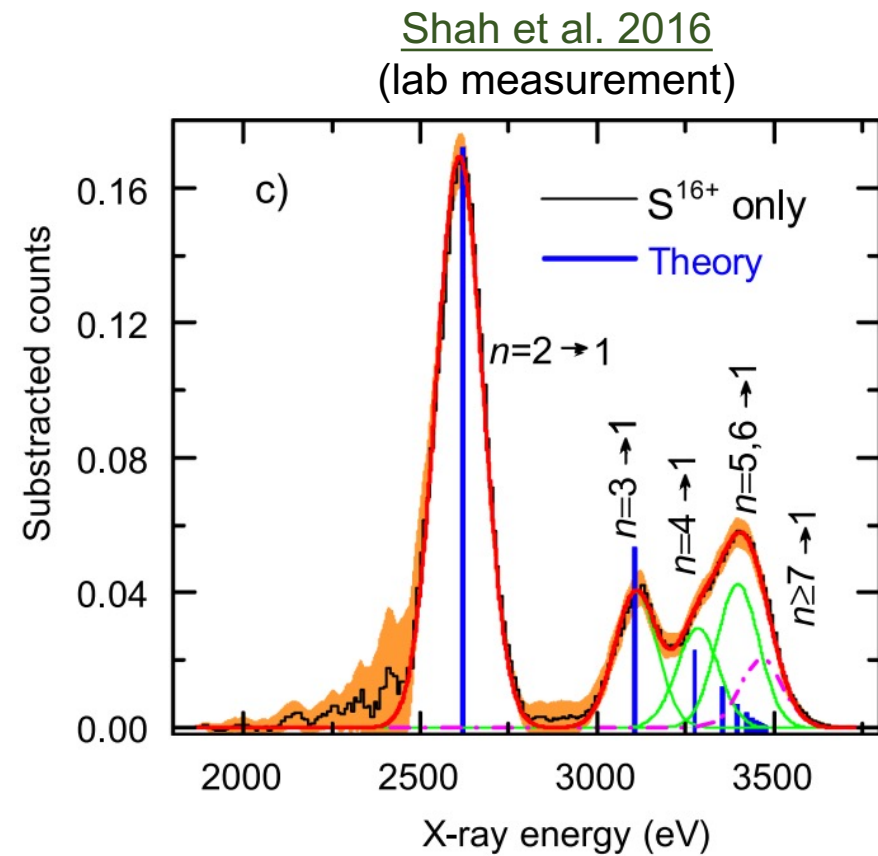


CX line features (Lyman series, cont.)

During the CX process, the high- n Lyman lines will be enhanced.

cf. CX vs. RS

- Resonant scattering can reduce the Ly α line intensity, boosting the $\frac{\text{Ly}\beta}{\text{Ly}\alpha}$, $\frac{\text{Ly}\gamma}{\text{Ly}\alpha}$, ... ratios, but it is less likely to enhance the $\frac{\text{Ly}\gamma}{\text{Ly}\beta}$, $\frac{\text{Ly}\delta}{\text{Ly}\gamma}$, ... ratios



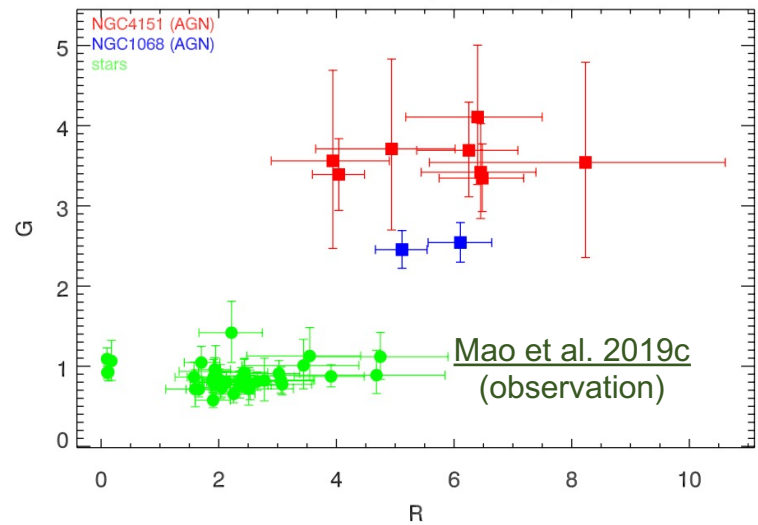
Ion	Label	Transition	λ (Å)	A (s^{-1})	f
H I	Ly α	$1s^2S_{1/2} - 2p^2P_{3/2,1/2}^0$	1215.7	6.3×10^8	0.27, 0.14
H I	Ly β	$1s^2S_{1/2} - 3p^2P_{3/2,1/2}^0$	1025.7	1.7×10^8	0.053, 0.026
O VIII	Ly α	$1s^2S_{1/2} - 2p^2P_{3/2,1/2}^0$	18.97	2.6×10^{12}	0.27, 0.14
O VIII	Ly β	$1s^2S_{1/2} - 3p^2P_{3/2,1/2}^0$	16.01	6.9×10^{11}	0.053, 0.026

CX line features (He-like triplet)

During the CX process, the forbidden line of the He-like triplet will be enhanced.

cf. CX vs. PE vs. RS

- Photoexcitation can boost the forbidden to resonance line ratio (in photoionized plasmas)
- Resonant scattering can boost the forbidden to resonance line ratio as well

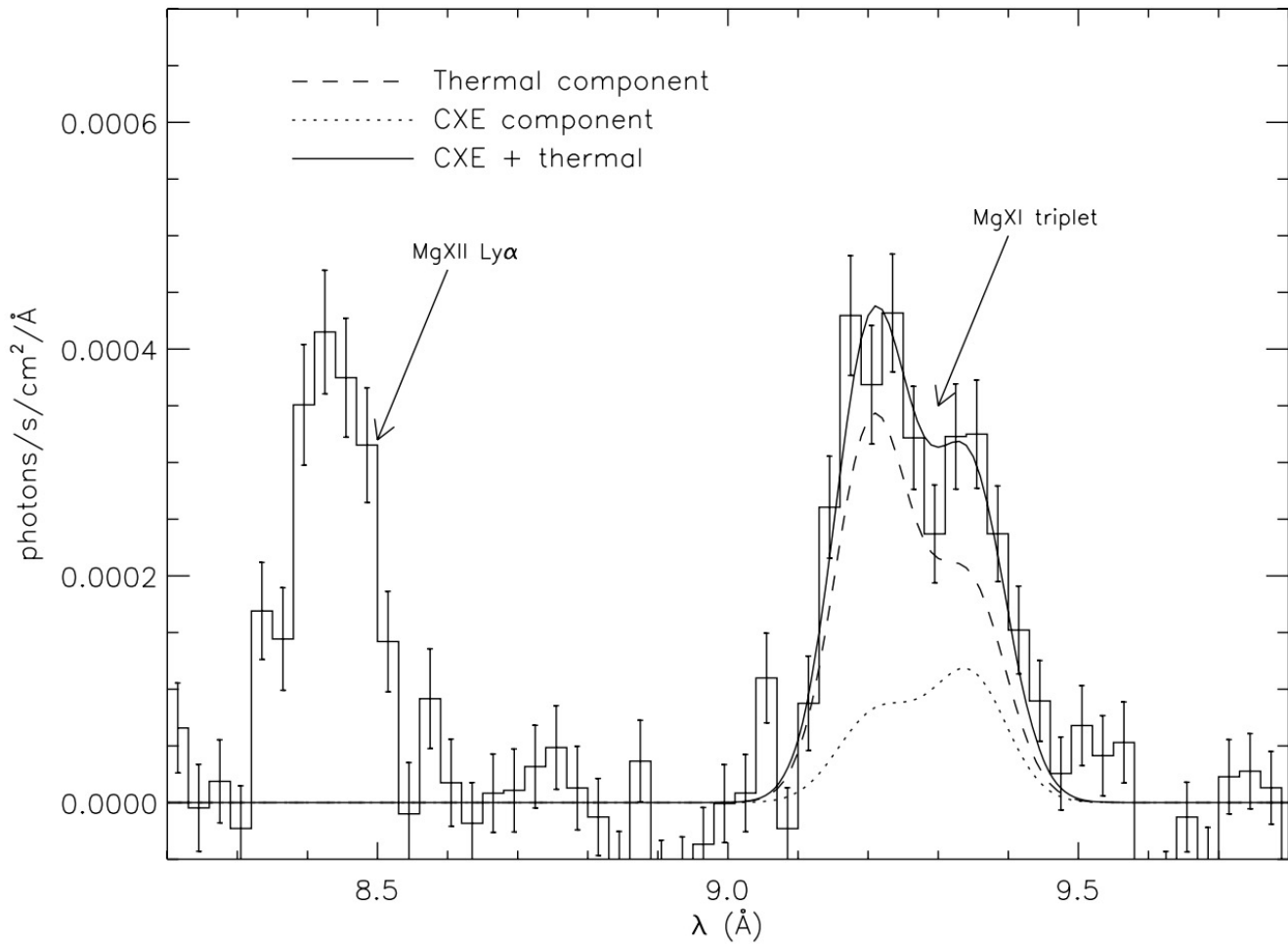


M82 (starburst galaxy)

Image credit: Chandra photo album



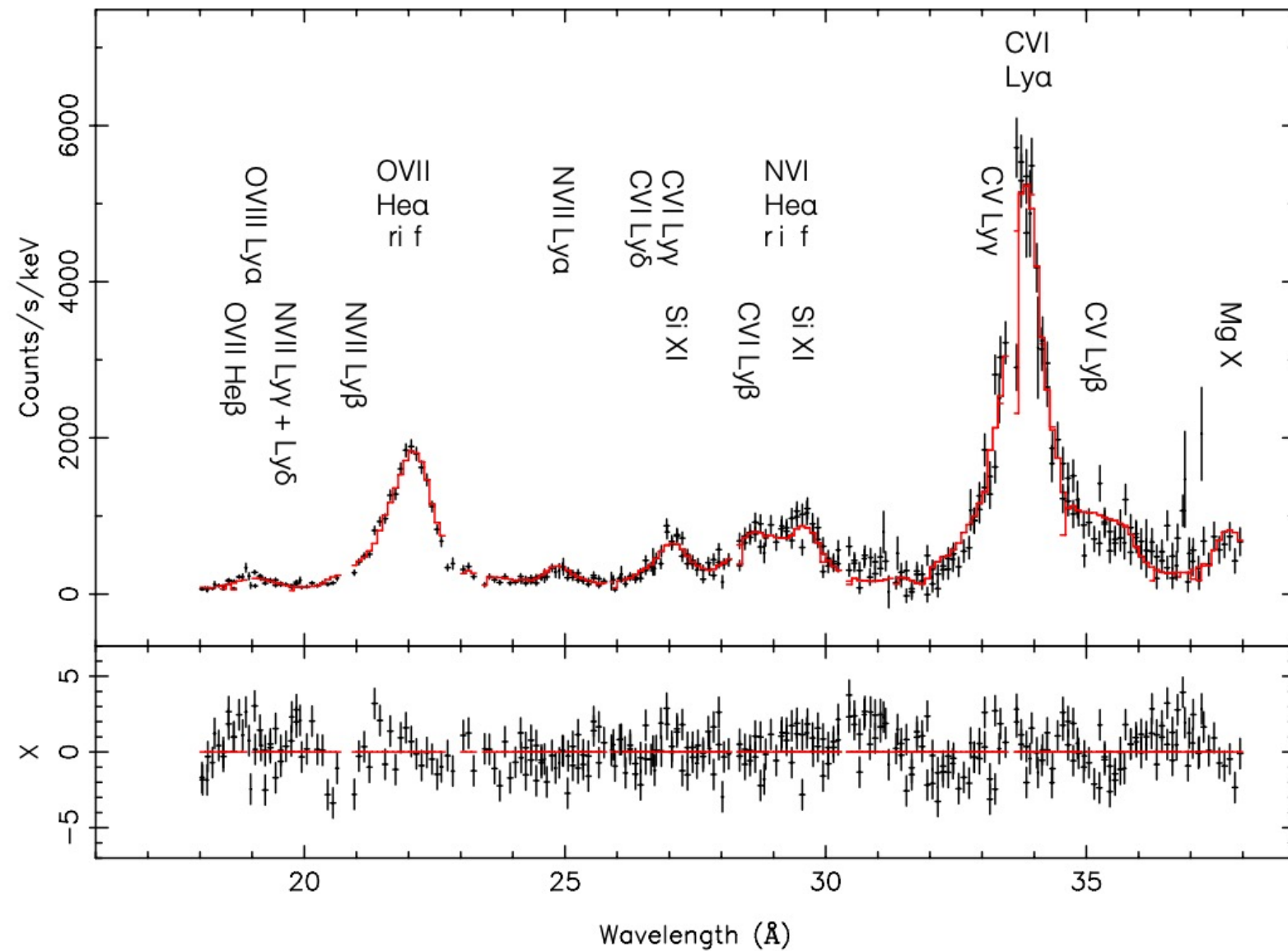
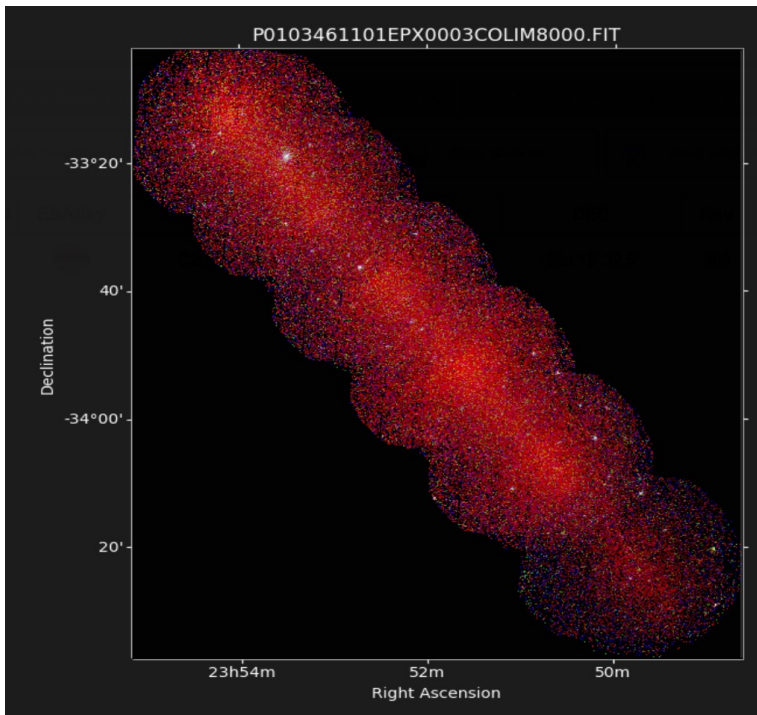
Liu, Mao & Wang (2011)



Comet CX emission

Gu et al. 2016

The X-ray emission from Comet C/2000 WM1 (LINEAR) is dominated by charge exchange between hot solar wind ions and cometary neutrals (H and H₂O)

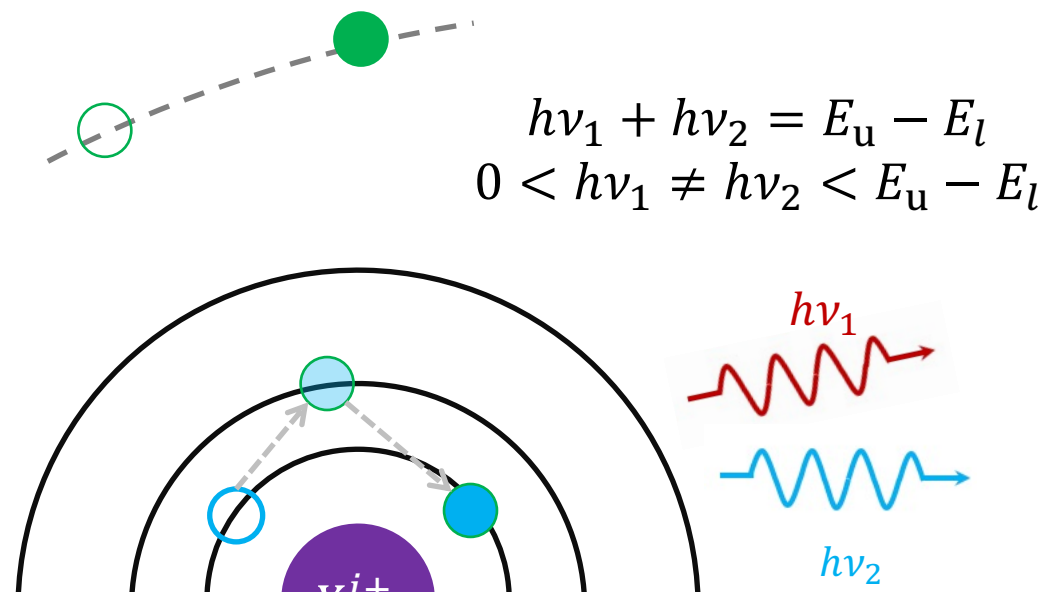


Two-photon process

The two-photon process is particularly important for H- and He-like ions.

After electron-impact excitation from $1s \rightarrow 2s$ (H-like) or $1s^2 \rightarrow 1s\ 2s$ (He-like), the excited level cannot decay back to ground level by emitting one photon.

- ❖ In a high density plasma, electron-impact excitation can further promote to those levels that can cascade down to the ground level; alternatively, electron-impact de-excitation can occur
- ❖ In a low density plasma, the excited level will decay back to the ground $2s \rightarrow 1s$ (H-like) or $1s\ 2s \rightarrow 1s^2$ (He-like) by emitting two photons, giving rise to **continuum emission**



Empirical critical TP density for H- and He-like ions by Mewe et al. 1986:

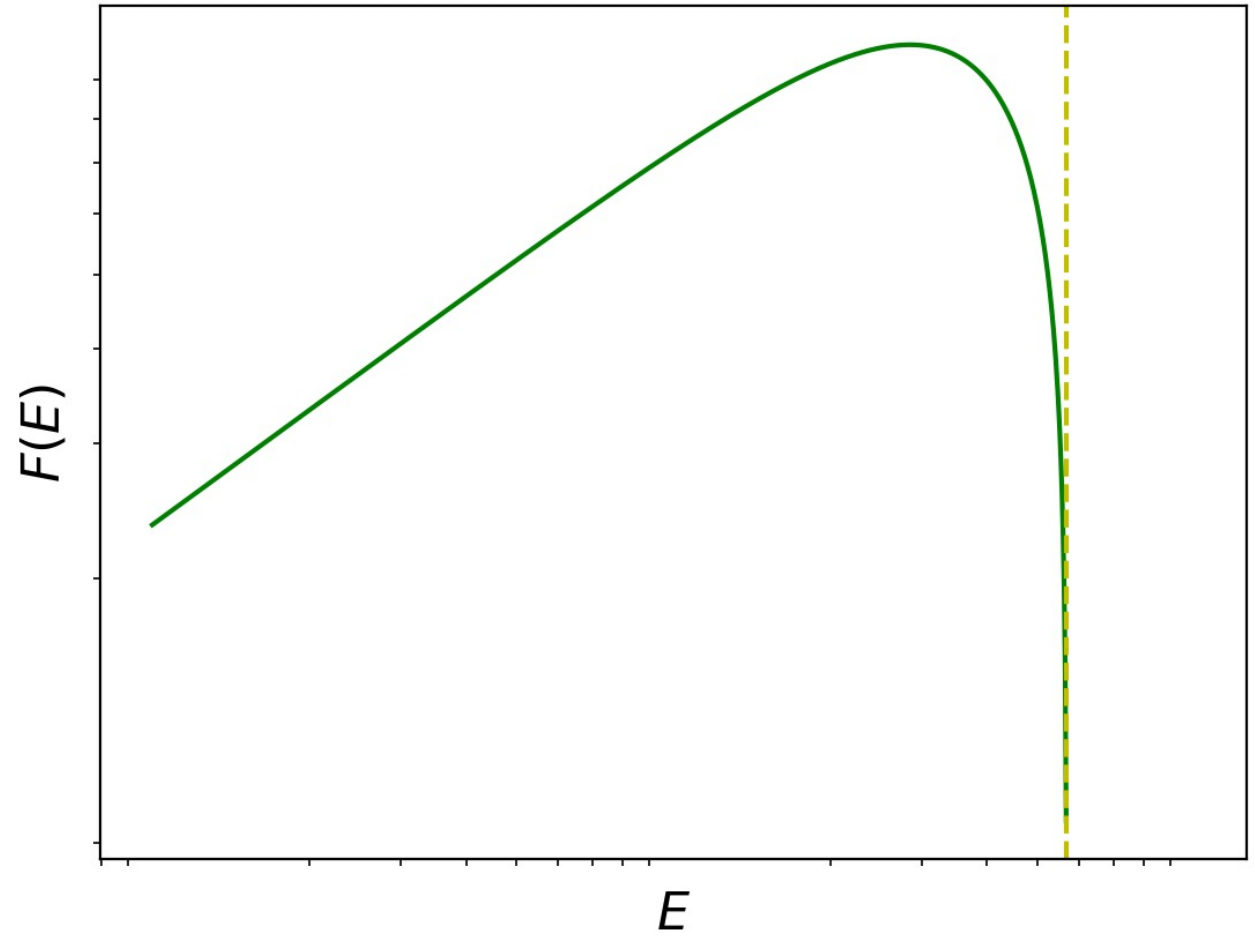
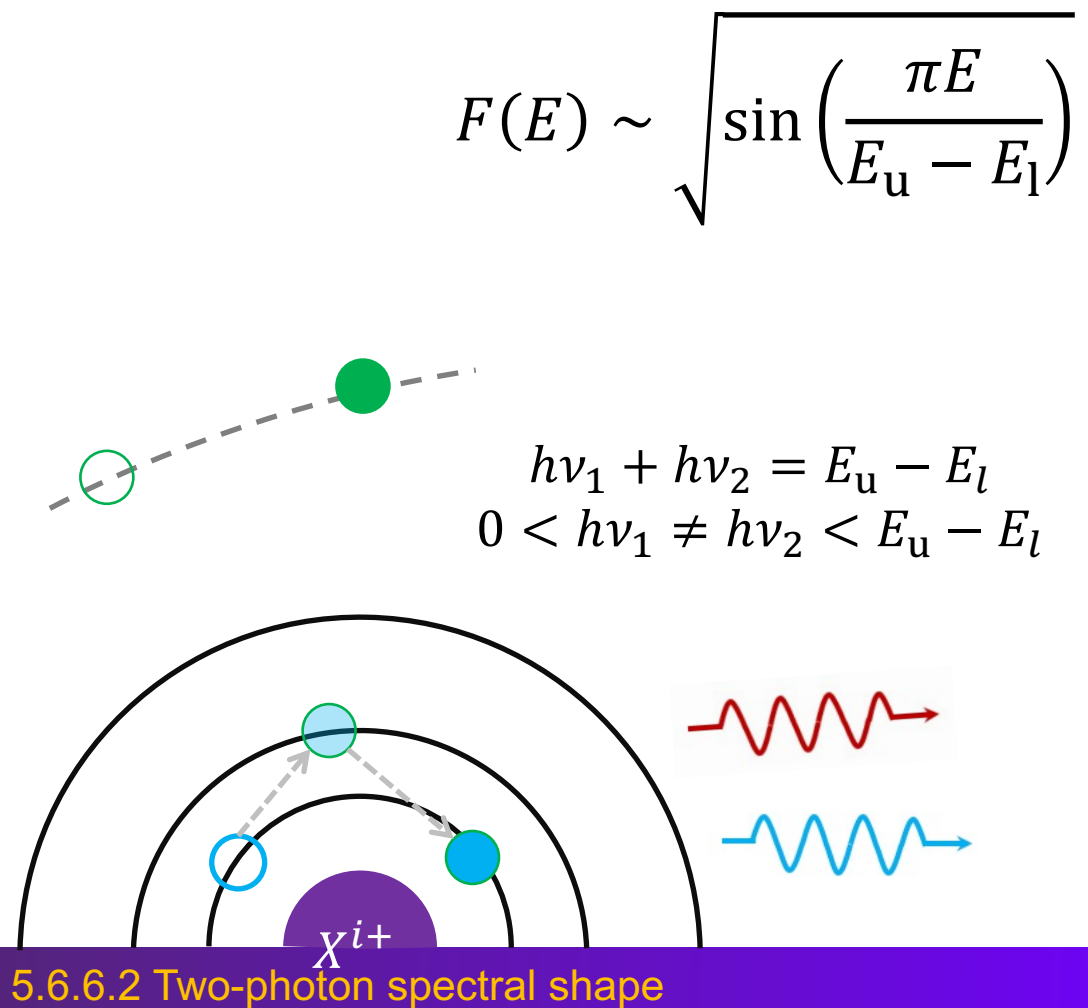
$$n_{\text{crit}}^{\text{TP}}(\text{H-like}) = 7 \times 10^3 Z^{9.5} \text{ cm}^{-3}$$

$$n_{\text{crit}}^{\text{TP}}(\text{He-like}) = 2 \times 10^5 (Z - 1)^{9.5} \text{ cm}^{-3}$$

atomic number

Two-photon spectral shape

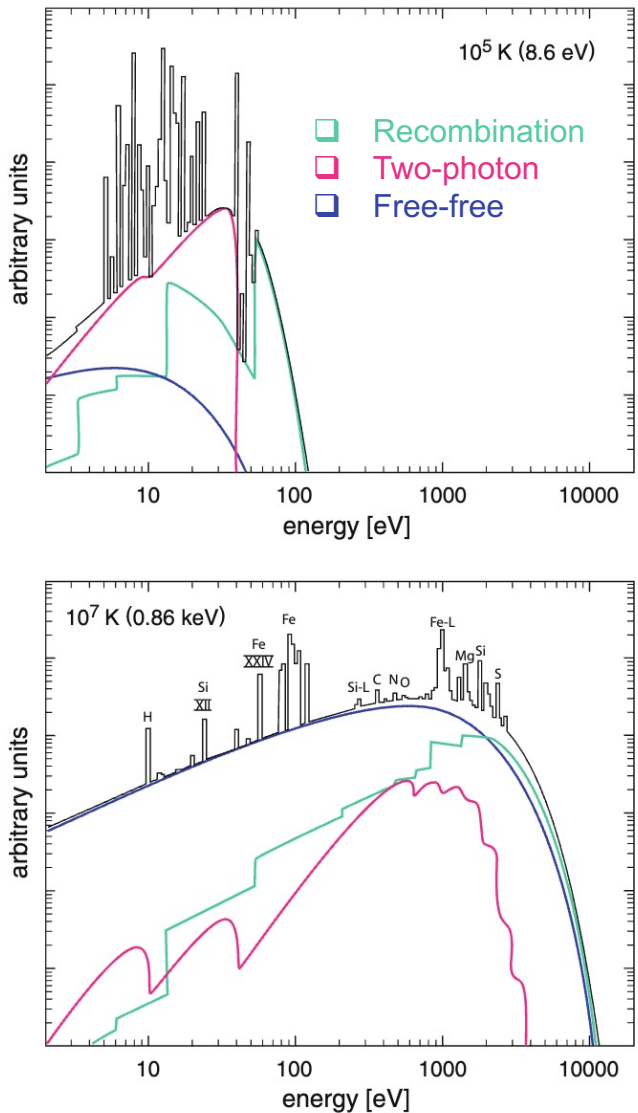
The spectral shape of the two-photon process can be approximated via the following empirical function ([Kaastra et al. 2008](#))



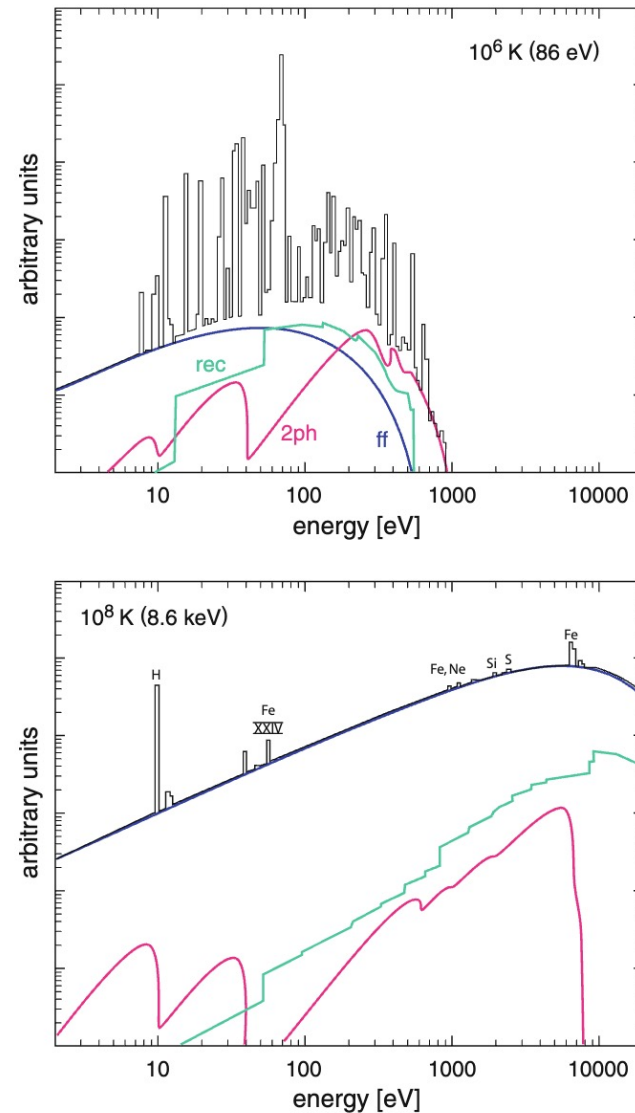
Two-photon continuum

Two-photon emissions from H- and He-like ions (especially H, He, C, N, and O) for a broad-band continuum

Ion	Transition	E (eV)
H I	$1s\ ^2S_{1/2} - 2s\ ^2S_{1/2}$	10.2
He II	$1s^2\ ^1S_0 - 1s\ 2s\ ^1S_0$	40.8
C V	$1s^2\ ^1S_0 - 1s\ 2s\ ^1S_0$	304.4
C VI	$1s\ ^2S_{1/2} - 2s\ ^2S_{1/2}$	367.5
N VI	$1s^2\ ^1S_0 - 1s\ 2s\ ^1S_0$	426.4
N VII	$1s\ ^2S_{1/2} - 2s\ ^2S_{1/2}$	500.3
O VII	$1s^2\ ^1S_0 - 1s\ 2s\ ^1S_0$	568.9
O VIII	$1s\ ^2S_{1/2} - 2s\ ^2S_{1/2}$	653.5



Böhringer & Werner (2010)



Chpt.5 Atomic processes

5.1 Atomic data for astrophysics

5.2 Two-level system

5.3 Bremsstrahlung

5.4 Recombination and photoionization

5.5 Collisional excitation and de-excitation

5.6 Other atomic processes

5.7 Astrophysical plasma models

5.7.1 Collisional ionization equilibrium

5.7.2 Non-equilibrium ionization

5.7.3 Photoionization equilibrium

Ionization

- collisional ionization
- (excitation-)autoionization
- photoionization

Recombination

- radiative recombination
- dielectronic recombination

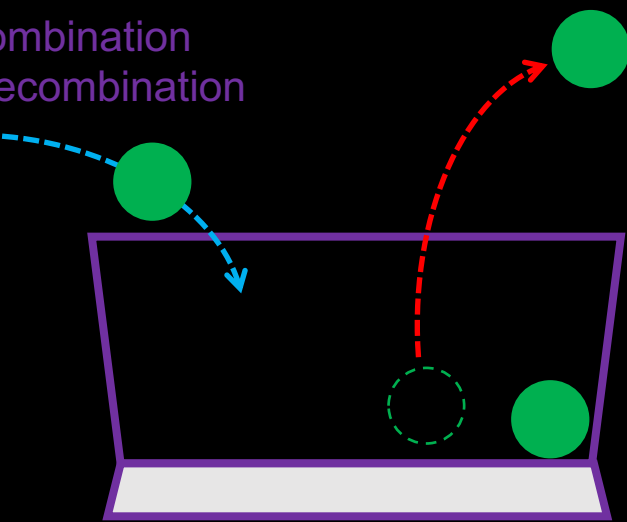
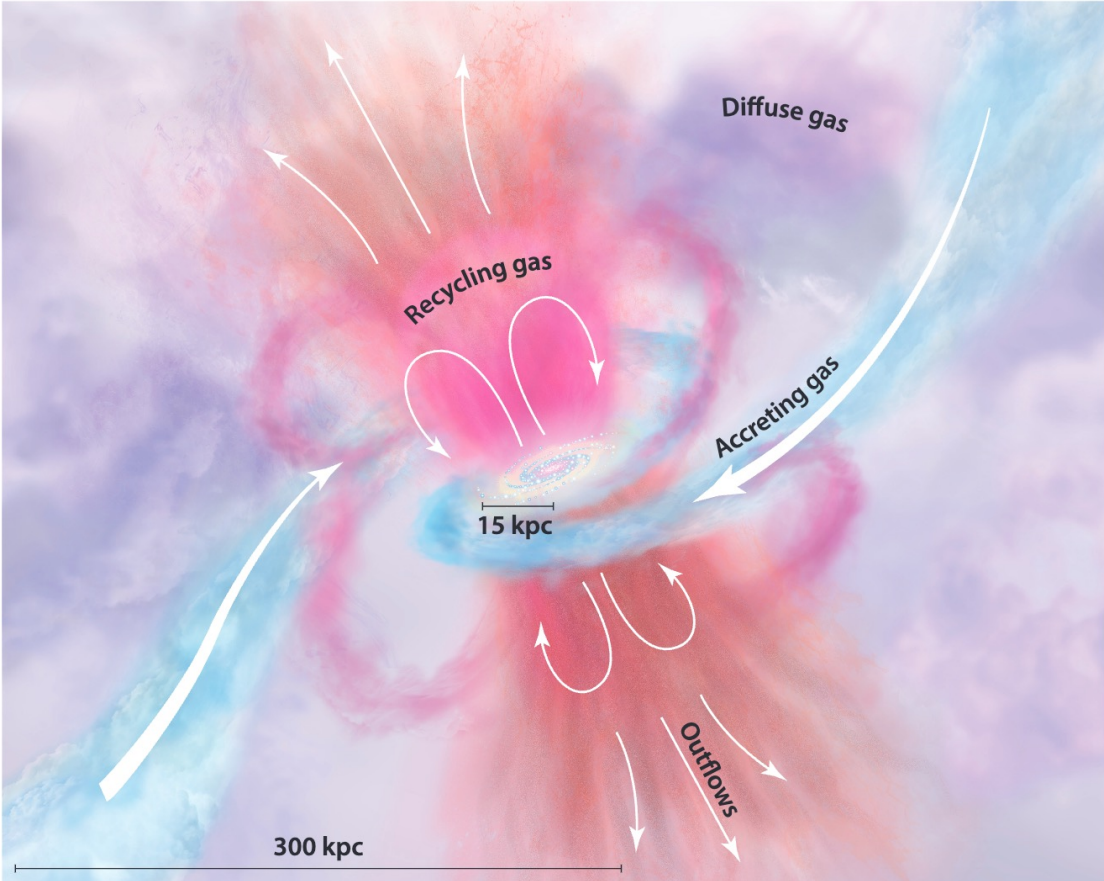


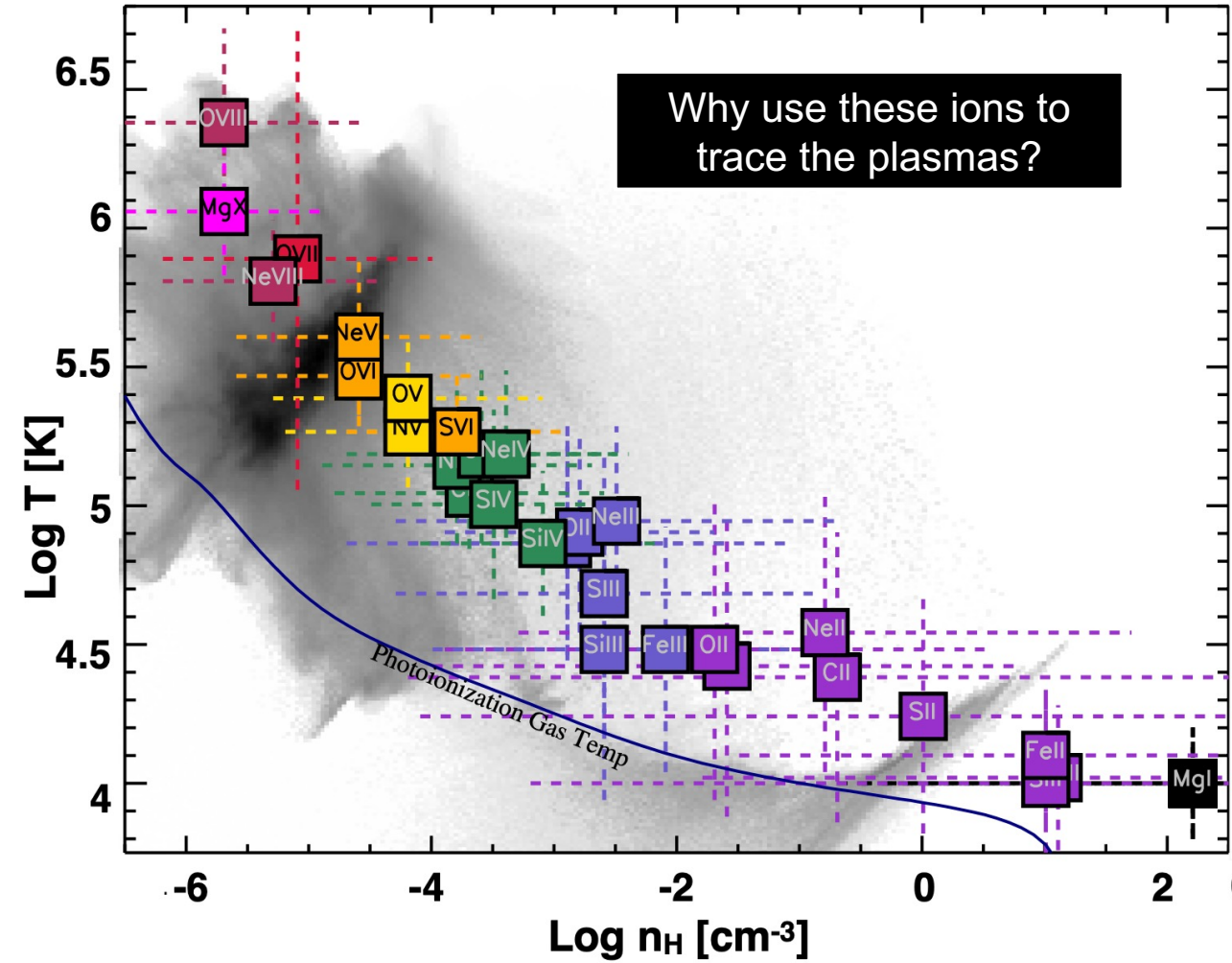
Image credit: Junjie Mao

Multi-phase plasmas in the galactic ecosystem



Multi-phase plasmas in the galactic ecosystem with a wide range of temperature, density, abundances ...

Tumlinson et al. 2017



Tumlinson et al. 2019

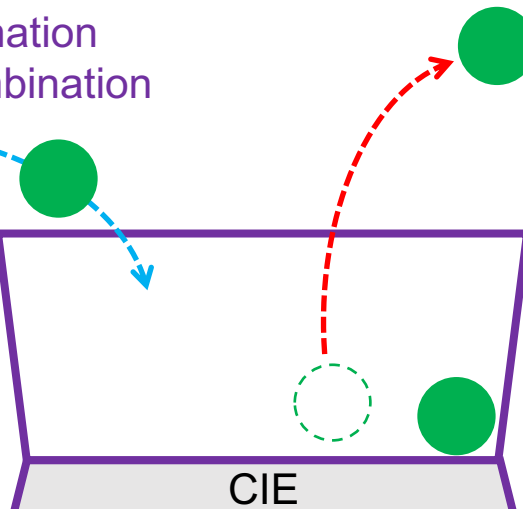
Collisional ionization equilibrium

CIE is the simplest plasma

- no external radiation field
- typically, **low-density** and **high-temperature**
- collisional processes dominates the **charge state distribution (CSD)**
- **temperature** is the key parameter for CSD
- plasma properties do not vary over time
- examples: stellar coronae, ICM

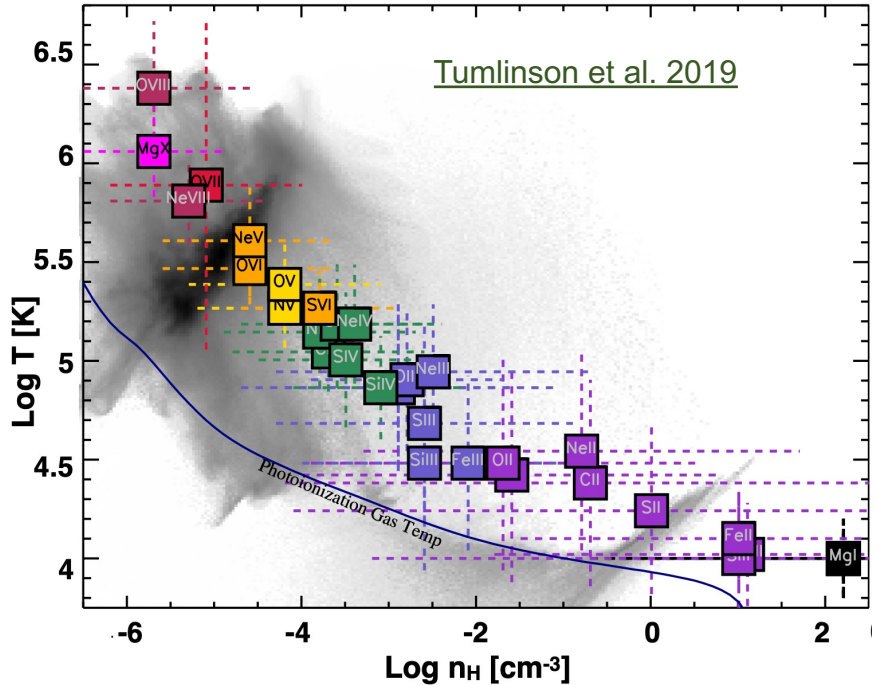
Recombination

- radiative recombination
- dielectronic recombination



Ionization

- collisional ionization
- (excitation-)autoionization



CIE: ionization balance

the net change of ion fraction X^{i+} is zero

$$\frac{dn_i}{dt} = n_e(n_{i-1}I_{i-1} - n_iI_i - n_iR_i + n_{i+1}R_{i+1}) = 0$$

total ionization rate (per ion)
for $X^{i-1+} \rightarrow X^{i+}$

$i \rightarrow i + 1$

$i + 1 \rightarrow i$

total recombination rate (per ion)
for $X^{i+} \rightarrow X^{i-1+}$

for neutral atom (n_0)

$$n_0I_0 = n_1R_1$$

for bare ion (n_{Z+})

$$n_{Z-1}I_{Z-1} = n_ZR_Z$$

Examples:

Neutral hydrogen ($Z = 1$): H I = H

Isoelectronic sequence: H-like (i.e., one bounded electron)

Ionic charge (used by the atomic physics community): 0

Triply ionized carbon ($Z = 6$): C IV = C³⁺

Isoelectronic sequence: Li-like (i.e., three bounded electrons)

Ionic charge (used by the atomic physics community): 3

Triply ionized iron ($Z = 26$): Fe XVII = Fe¹⁶⁺

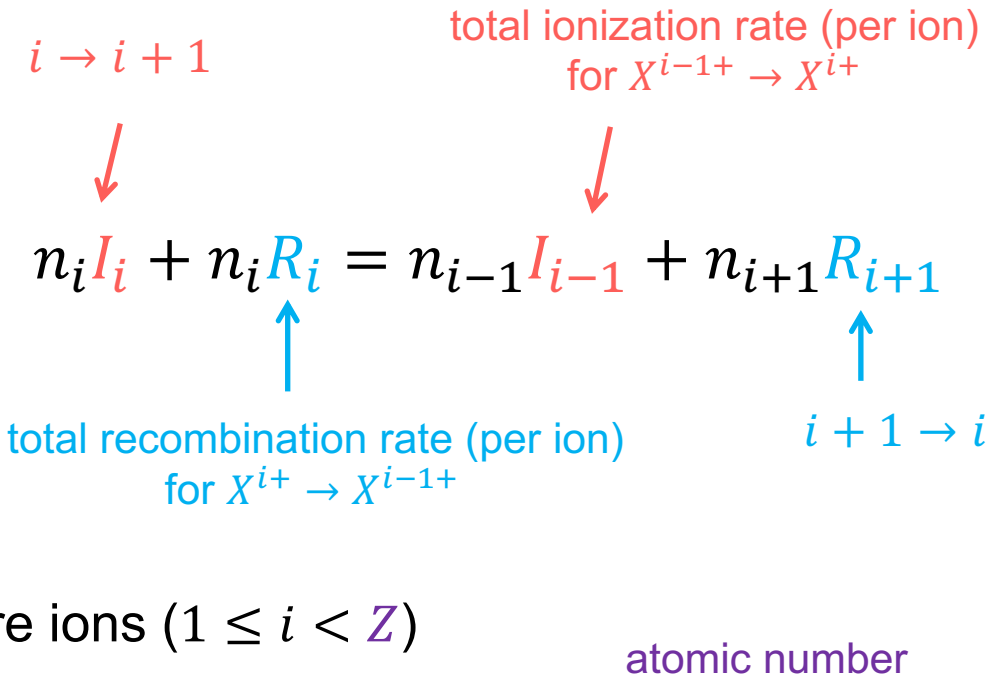
Isoelectronic sequence: Ne-like (i.e., ten bounded electrons)

Ionic charge (used by the atomic physics community): 16

I_i and R_i in cm⁻³ s

CIE: ionization balance (cont.)

the net change of ion fraction X^{i+} is zero



for all but bare ions ($1 \leq i < Z$)

$$n_i = n_{i+1} \frac{R_{i+1}}{I_i}, 1 \leq i < Z$$

prev. sl.

$$n_0 I_0 = n_1 R_1$$

$$n_1 I_1 + n_1 R_1 = n_0 I_0 + n_2 R_2$$

$$n_1 I_1 = n_2 R_2$$

... = ...

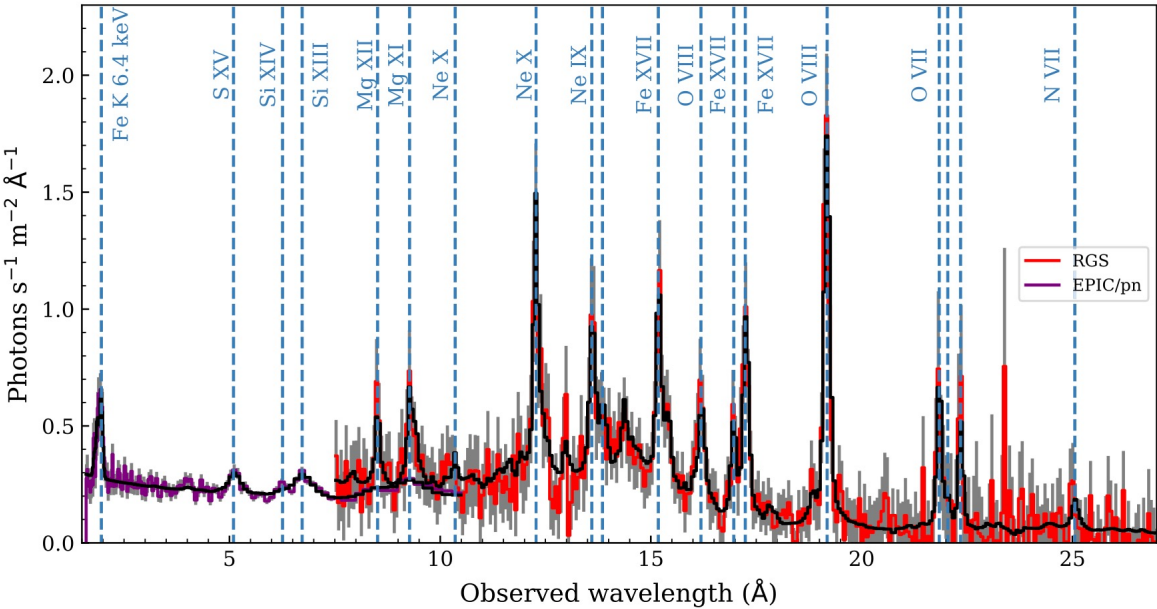
prev. sl.

$$n_{Z-1} I_{Z-1} = n_Z R_Z$$

$$\sum_{i=0}^Z n_i = n(Z) = n_H A(Z)$$

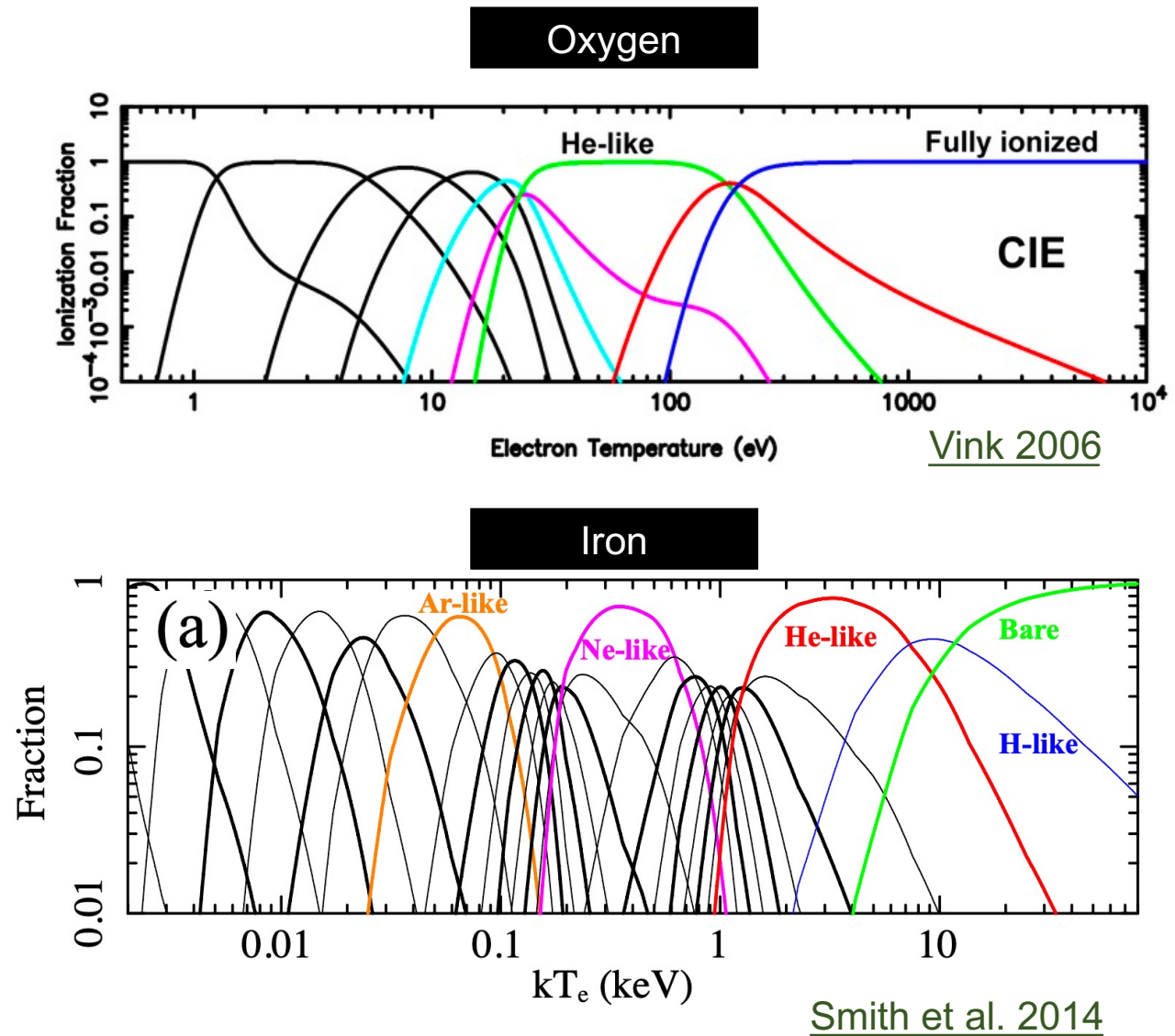
CIE: charge state distribution

aka. Ionization balance



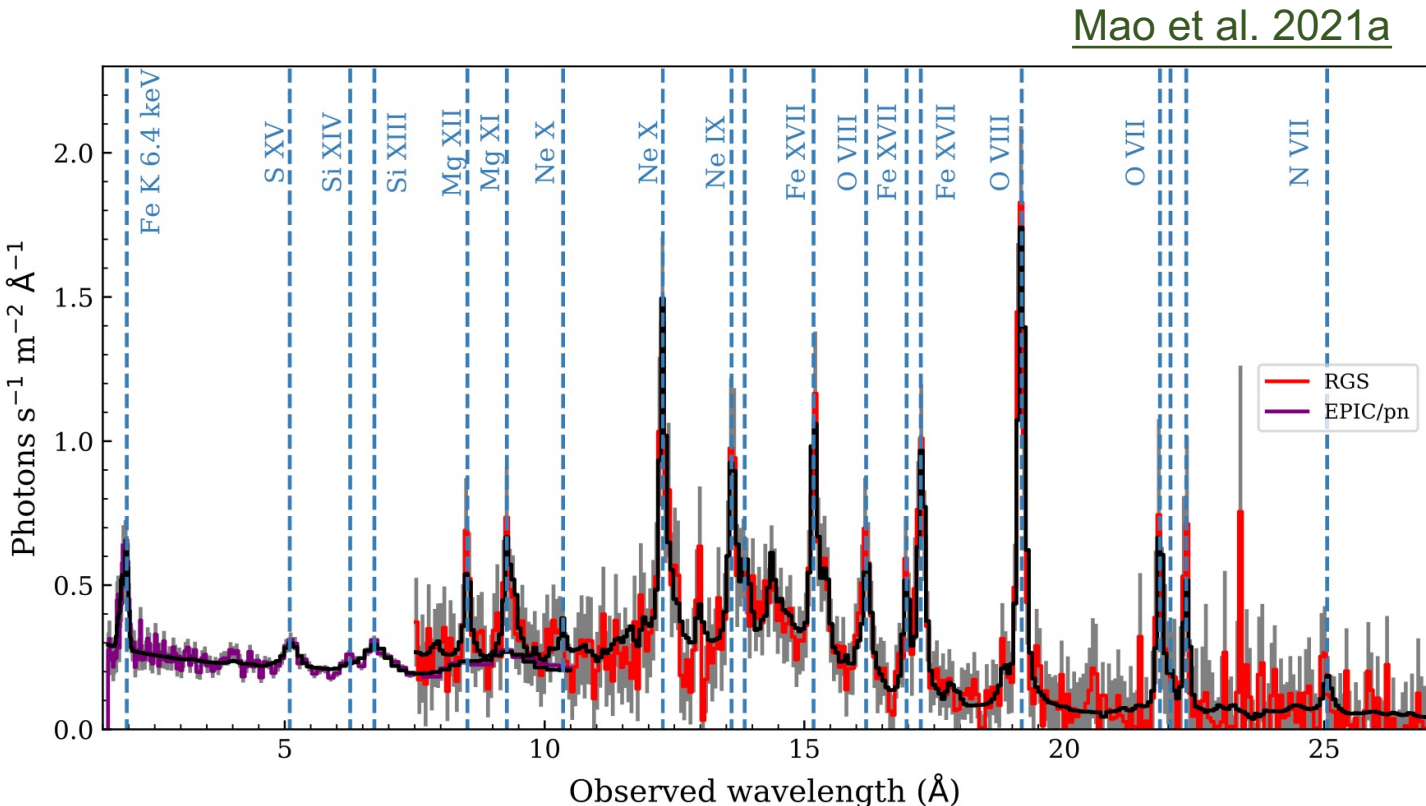
Mao et al. 2021a

CIE plasmas with $kT \gtrsim 10^6$ K usually have H- and He-like cosmic abundant ions, as well as other Fe XVII and neighboring ions



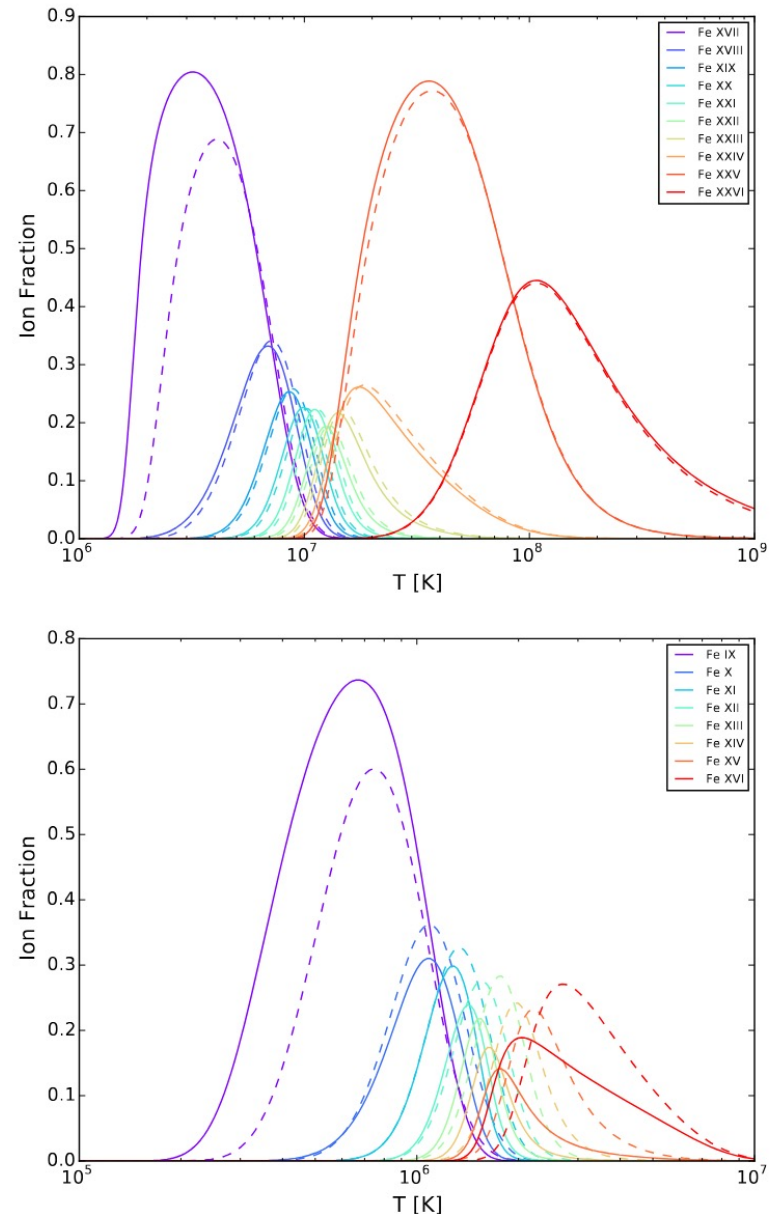
CIE: charge state distribution (high- T)

aka. Ionization balance

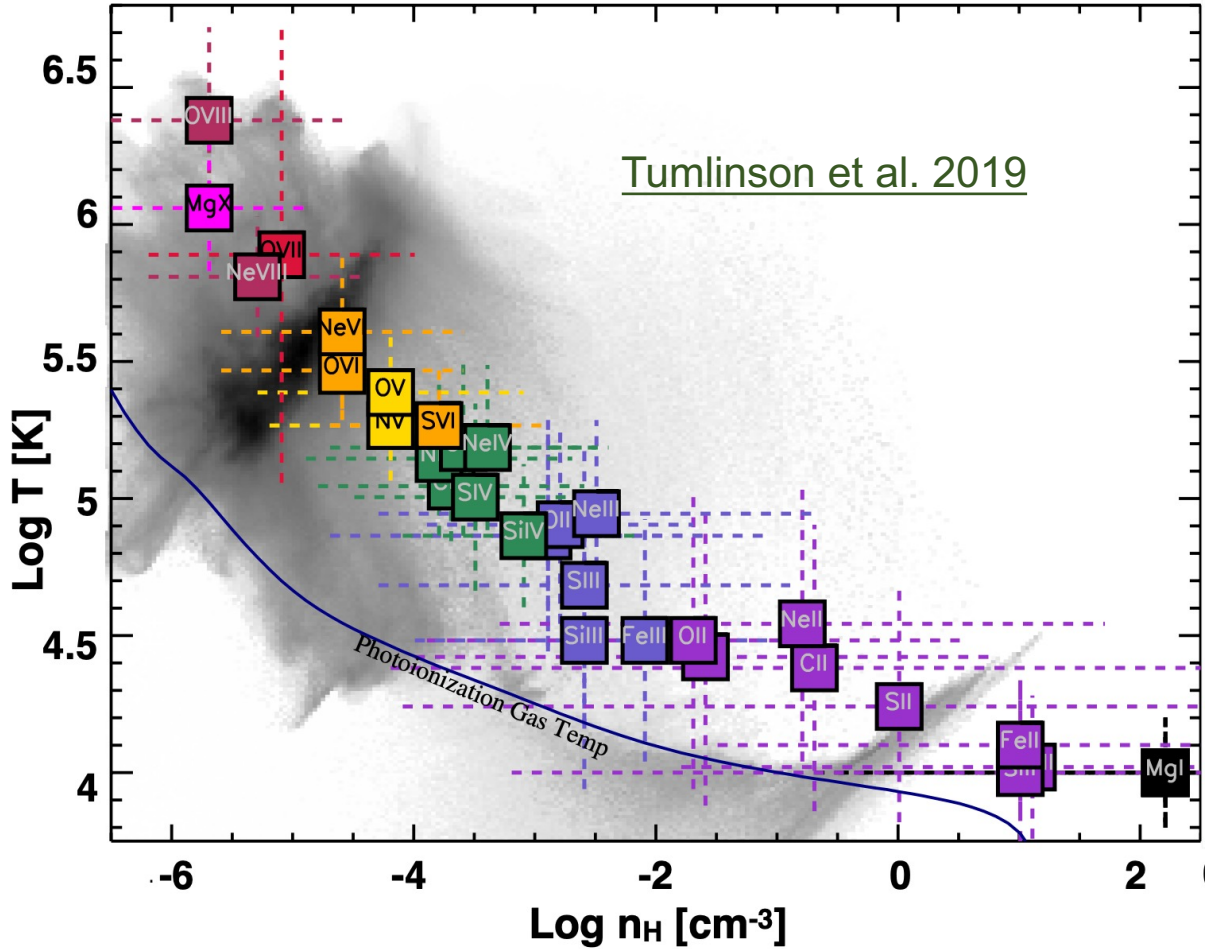


CIE plasmas with $kT \gtrsim 10^6$ K usually have H- and He-like cosmic abundant ions, as well as other Fe XVII and neighboring ions

Caution: Difference in atomic data and atomic processes can lead to different CSD (e.g., U17 vs. B09)

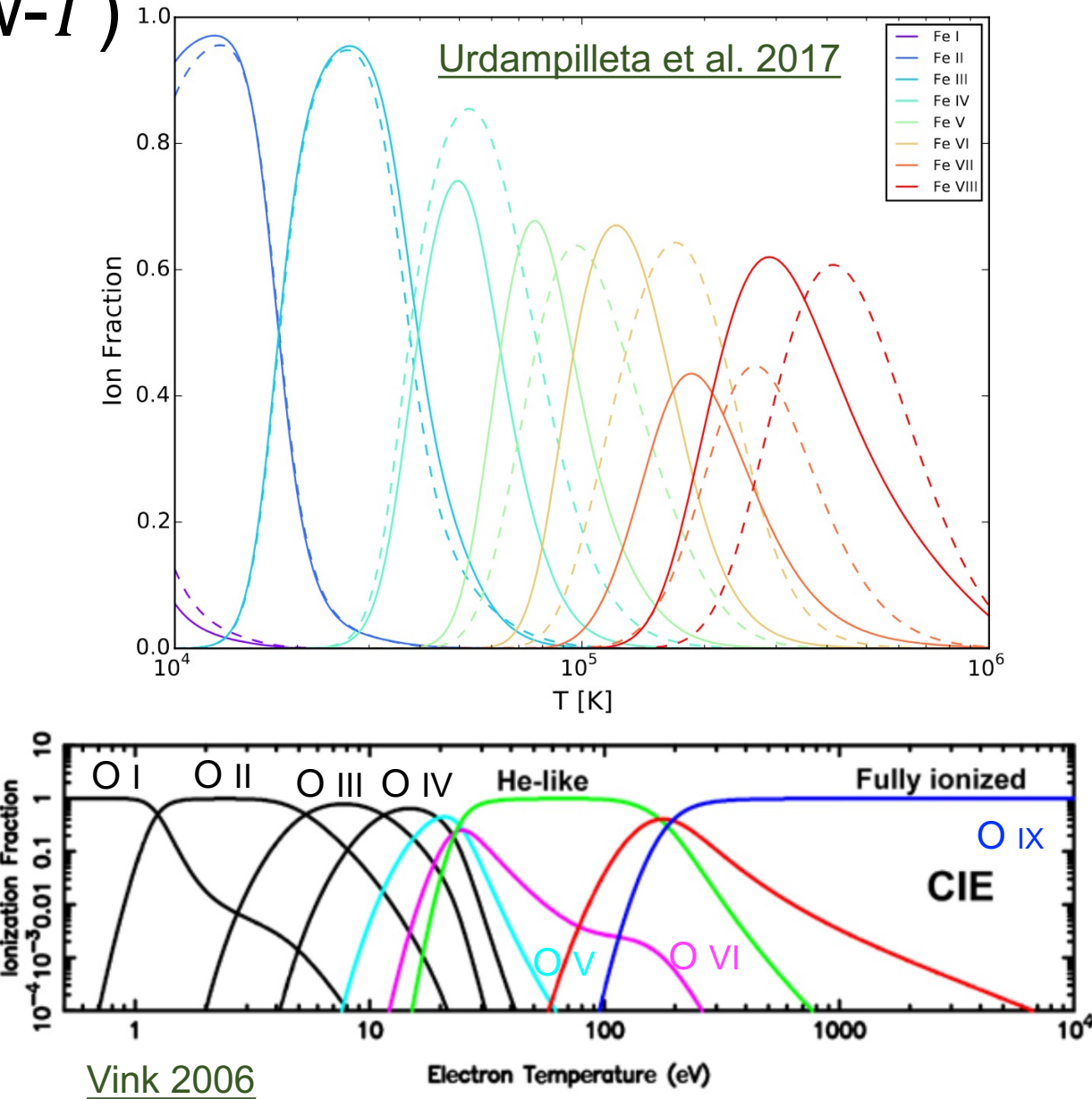


CIE: charge state distribution (low- T)



Tumlinson et al. 2019

CIE plasmas with $kT \lesssim 10^{5.5}$ K (~ 27 eV) but above the photoionization temperature (blue curve) have O VI, O V, O IV, ...



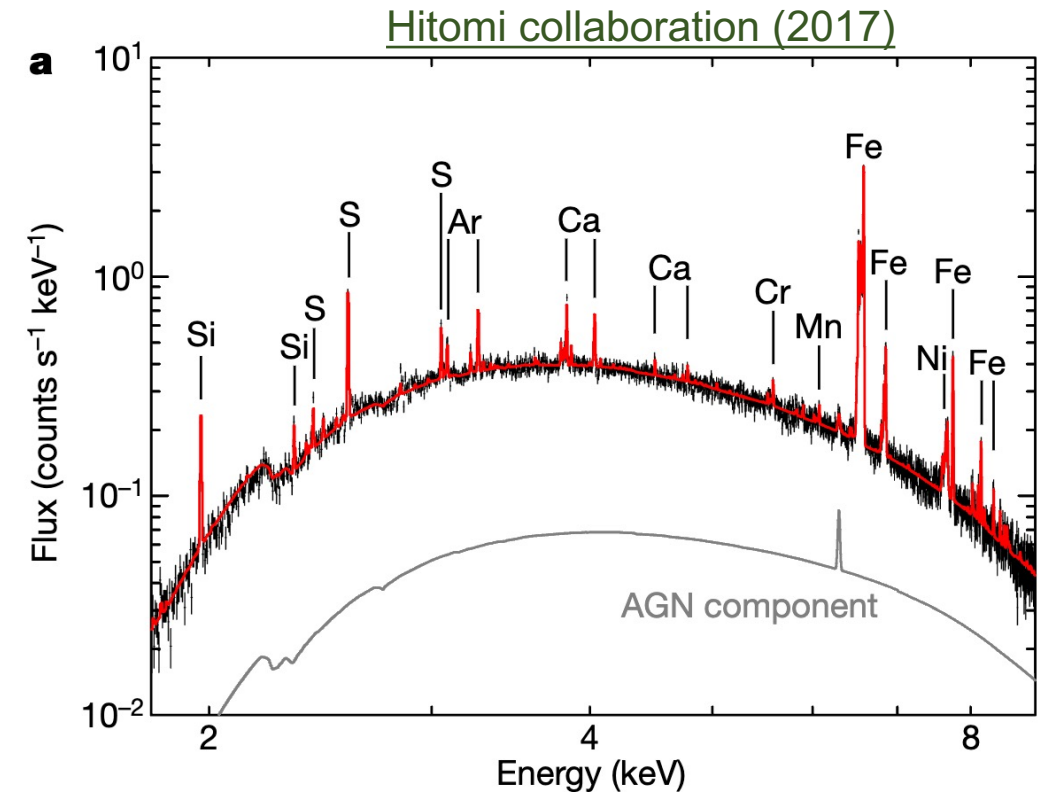
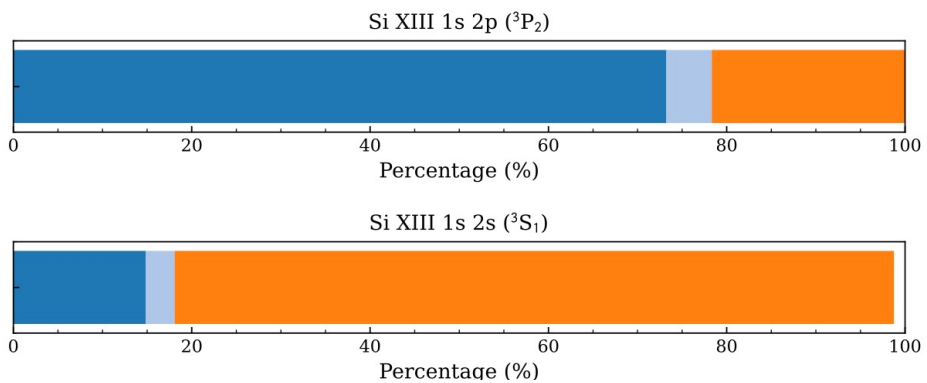
CIE line power

For an optically thin emission line from level $u \rightarrow l$ of ion X^{i+} with atomic number Z in CIE plasmas, the line power is

$$P_{ul}(T, n_H) = A_{ul} n_H A(Z) I_i(T, n_H) n_{i,u}(T, n_H)$$

↓ A-value ↓ ionic fraction
 ↓ abundance ↑ level population

Mao et al. 2022c



Non-equilibrium ionization

When a CIE plasma experience a sudden change of its physical condition (e.g., shock heating, rapid cooling, plasma instability), it takes time for the plasma to re-establish the equilibrium via collision. This transitional phase is referred to as NEI.

CIE $dn_i/dt = 0$

ionization = recombination

NEI $dn_i/dt \neq 0$

ionization \neq recombination

prev. sl.

total ionization rate (per ion)
for $X^{i-1+} \rightarrow X^{i+}$

$i + 1 \rightarrow i$

$$\frac{dn_i}{dt} = n_e(t)(n_{i-1} I_{i-1} - n_i I_i - n_i R_i + n_{i+1} R_{i+1})$$

$i \rightarrow i + 1$

total recombination rate (per ion)
for $X^{i+} \rightarrow X^{i-1+}$

NEI ionization imbalance

CIE $dn_i/dt = 0$

ionization = recombination

NEI $dn_i/dt \neq 0$

ionization \neq recombination

prev. sl.

total ionization rate (per ion)
for $X^{i-1+} \rightarrow X^{i+}$

$i + 1 \rightarrow i$

$$\frac{dn_i}{dt} = n_e(t)(n_{i-1}I_{i-1} - n_iI_i - n_iR_i + n_{i+1}R_{i+1})$$

$i \rightarrow i + 1$

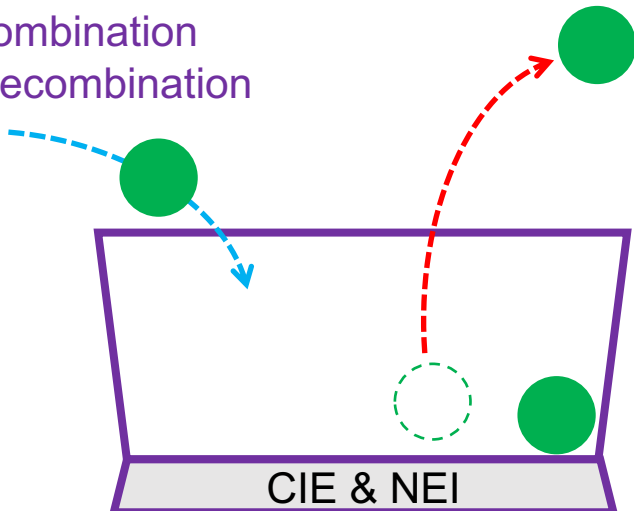
total recombination rate (per ion)
for $X^{i+} \rightarrow X^{i-1+}$

Recombination

- radiative recombination
- dielectronic recombination

Ionization

- collisional ionization
- (excitation-)autoionization



$$\frac{d\vec{n}(t)}{dt} = n_e(t) \vec{A}(T_e) \vec{n}(t)$$

$$\vec{A}(T_e) = \begin{pmatrix} -I_0 & R_1 & 0 & \dots & 0 \\ I_1 & -(I_1 + R_1) & R_2 & 0 & \dots \\ 0 & \dots & \dots & \dots & 0 \\ \dots & I_{i-1} & -(I_i + R_i) & R_{i+1} & \dots \\ 0 & \dots & \dots & \dots & 0 \\ \dots & 0 & I_{Z-2} & -(I_{Z-1} + R_{Z-1}) & R_Z \\ 0 & \dots & 0 & I_{Z-1} & -R_Z \end{pmatrix}$$

NEI ionization parameter

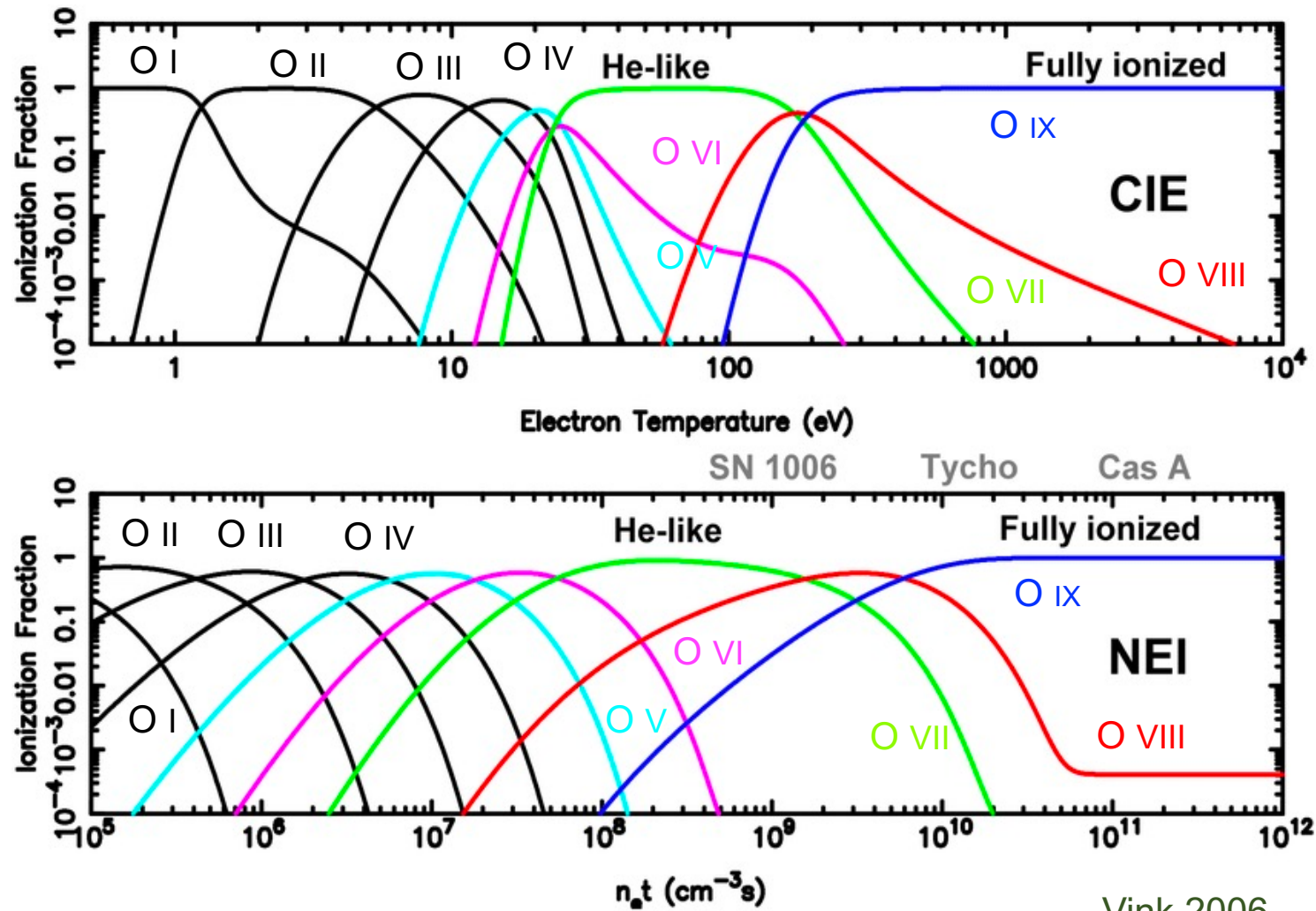
prev. sl.

$$\frac{d\vec{n}(t)}{dt} = n_e(t) \vec{A}(T_e) \vec{n}(t)$$

$$\int \frac{d\vec{n}(t)}{\vec{n}(t)} = \vec{A}(T_e) \int n_e(t) dt$$

NEI ionization parameter

$$U = \int n_e(t) dt$$



Vink 2006

NEI oxygen ionic fraction for $kT = 1.5$ keV

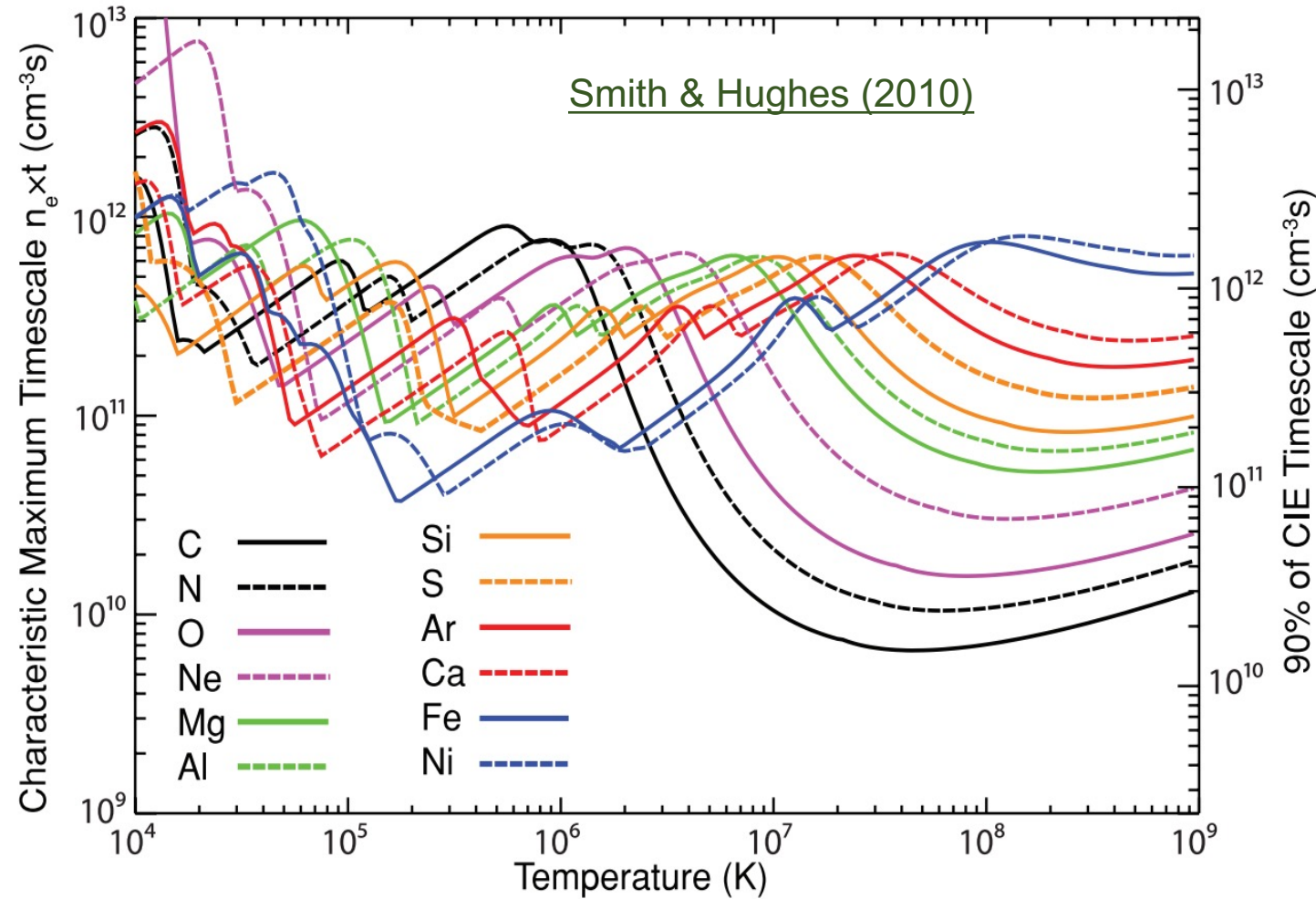
NEI ionization timescale

NEI ionization parameter

$$U = \int n_e(t) dt$$

In most cases, ionization equilibrium is reached for $U \sim 10^{12} \text{ cm}^{-3} \text{ s}$

$$\frac{t_{\text{CIE}}}{\text{yr}} \sim 3.17 \times 10^4 \left(\frac{n_e}{\text{cm}^{-3}} \right)^{-1}$$



Ionizing & recombining plasmas

balance temperature
(for ionization equilibrium)

CIE $dn_i/dt = 0$ ($kT_e = kT_b$)

ionization = recombination

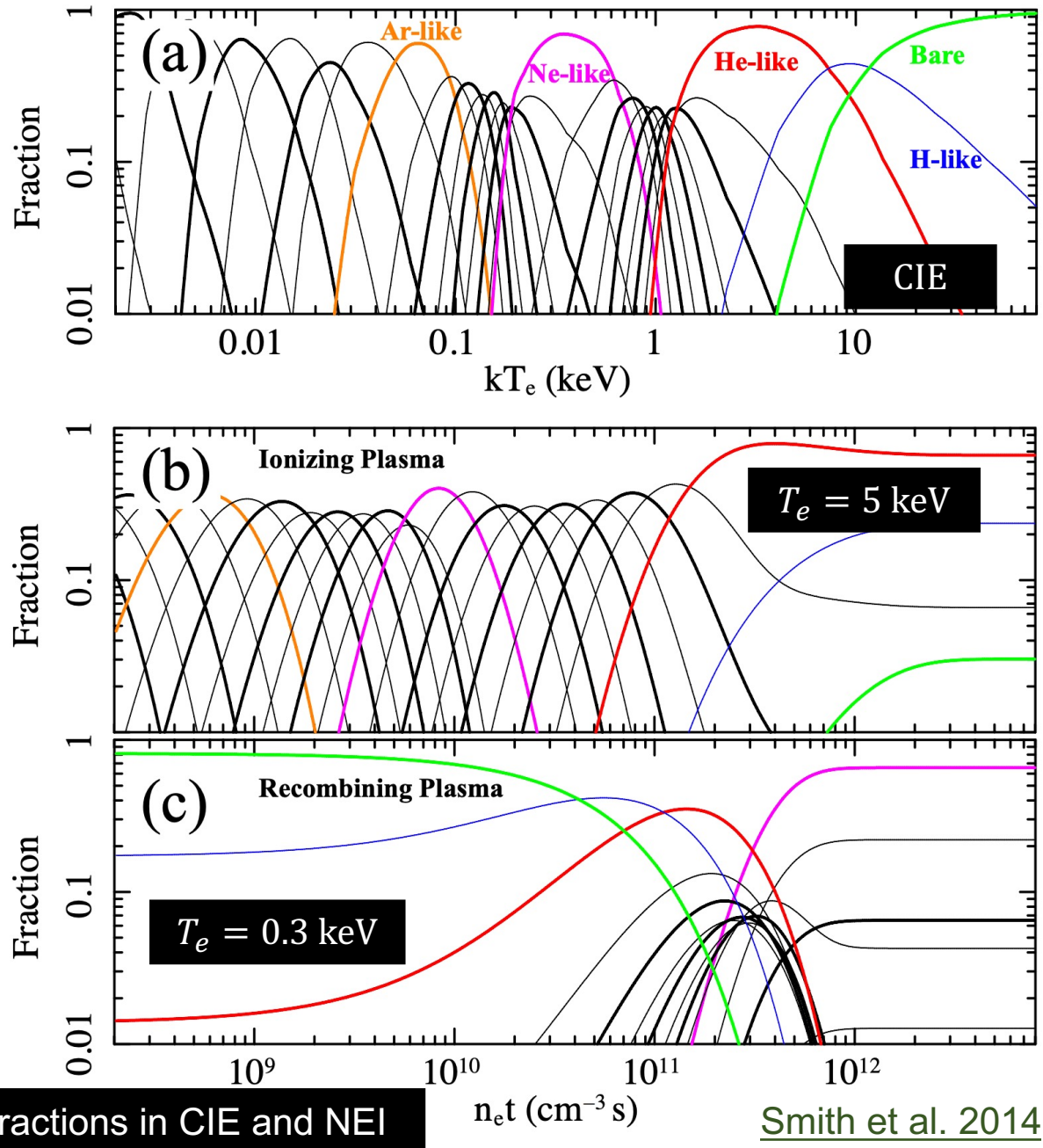
NEI $dn_i/dt \neq 0$

ionization > recombination ($kT_e > kT_b$)

- ionizing plasmas, aka under-ionized plasma
- Shock heating

recombination > ionization ($kT_e < kT_b$)

- recombining plasma, aka over-ionized plasma
- adiabatic expansion, thermal conduction



Ionizing plasmas

Image credit: NASA/CXC/SAO & ESA

2 – 6 keV
0.5 – 2 keV

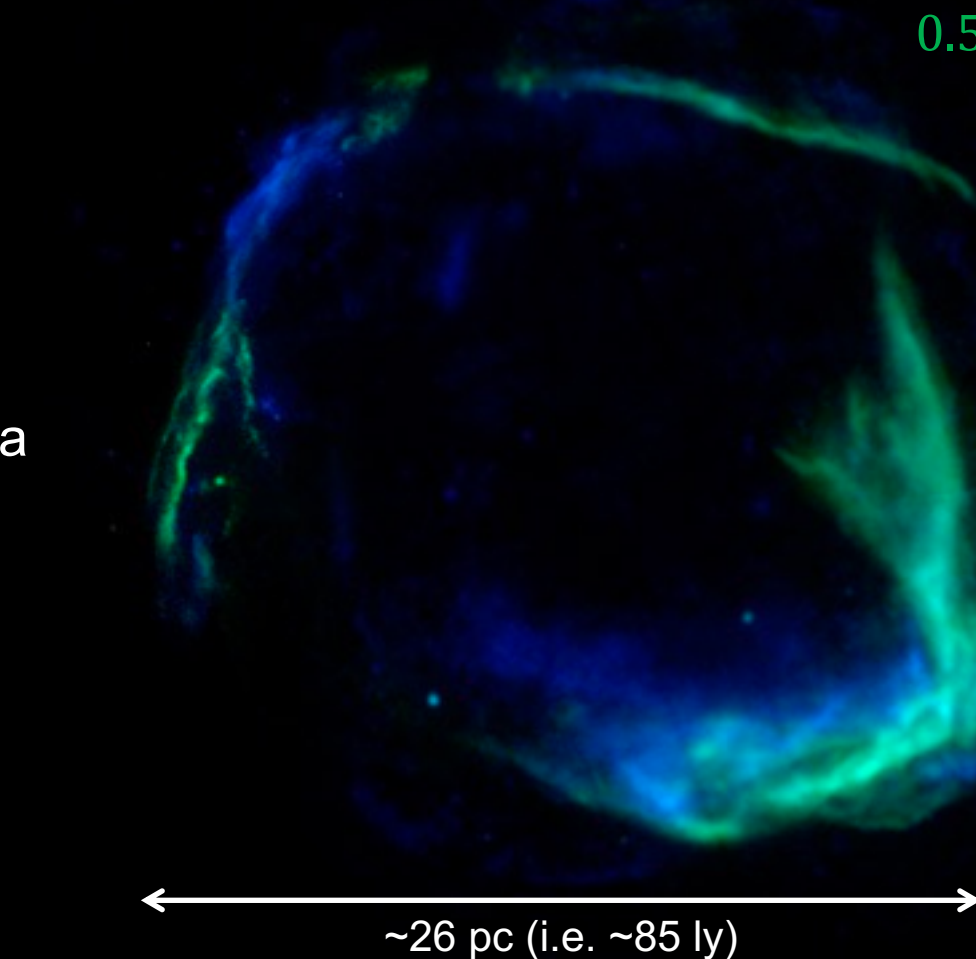
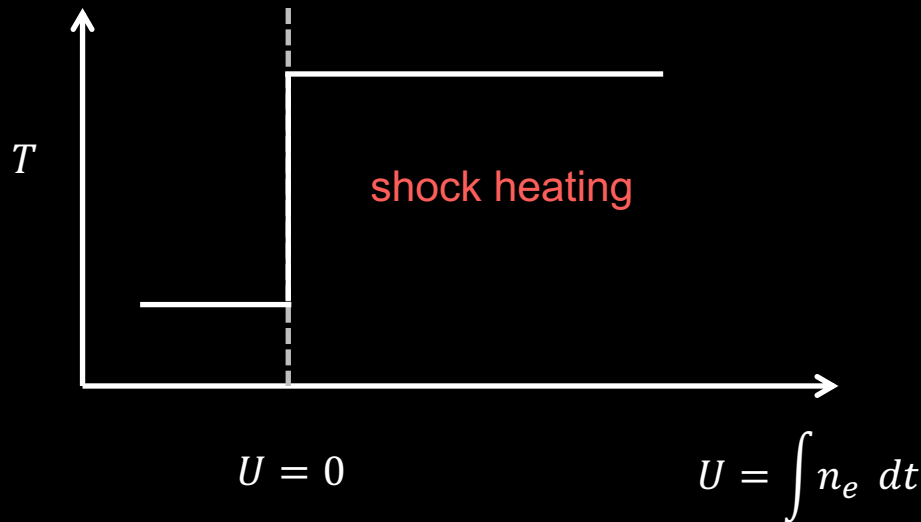
CIE $dn_i/dt = 0$ ($kT_e = kT_b$)

ionization = recombination

NEI $dn_i/dt \neq 0$

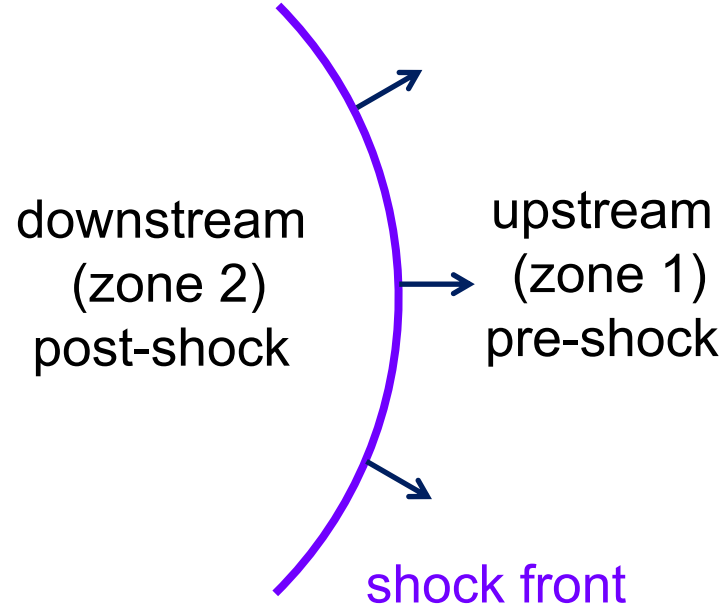
ionization > recombination ($kT_e > kT_b$)

- ionizing plasmas, aka under-ionized plasma
- shock heating



RCW 86, discovered by ancient Chinese astronomer in 185 AD (lasting for 8 months)

Ionizing plasma: shock transition region



(sonic) Mach number

$$M_{\text{sh}} \equiv \frac{v}{c_{\text{sh}}}$$

Sound speed

$$c_{\text{sh}} = \sqrt{\gamma \frac{P}{\rho}} = \sqrt{\frac{\gamma k T_e}{\mu m_p}}$$

adiabatic index:
5/3 for an ideal monoatomic gas

(e.g., [Vink 2020](#))

mean atomic weight:

0.6 for cosmic abundant ionized plasma

$$\frac{c_{\text{sh}}}{\text{km s}^{-1}} = 15.14 \sqrt{\frac{T_e}{10^4 \text{ K}}}$$

Ionizing plasma: shock temperature

Under the Rankine-Hugoniot jump conditions (conservation laws in the shock transition region) and $M_{\text{sh}} \gtrsim 5$ (e.g., young supernova remnants have $M_{\text{sh}} > 100$)

Downstream shock temperature

$$\langle kT_2 \rangle = \frac{3}{16} \mu_2 m_p v_{\text{sh}}^2$$

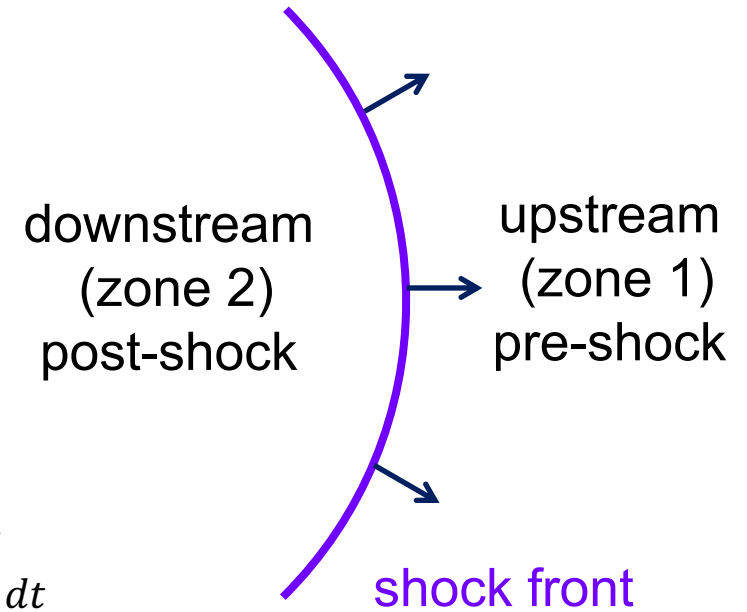
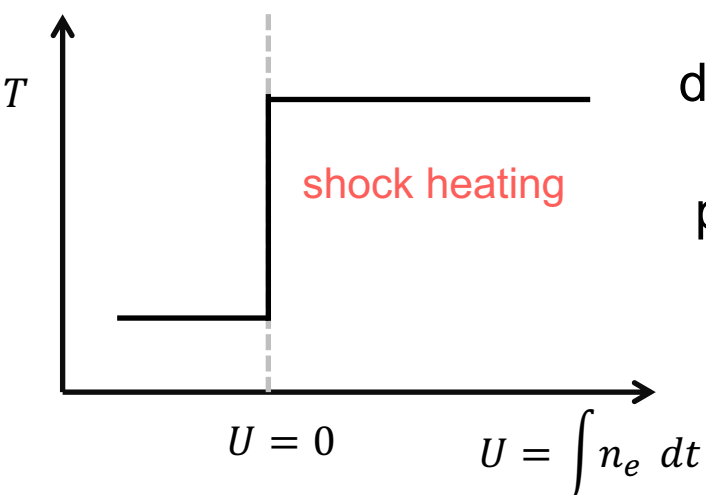
(e.g., [Vink 2020](#))

(sonic) Mach number

$$M_{\text{sh}} \equiv \frac{v}{c_{\text{sh}}}$$

That is to say, post-shock gas are heated to

$$\left\langle \frac{kT_2}{\text{keV}} \right\rangle \approx 1.17 \left(\frac{\mu_2}{0.6} \right) \left(\frac{v_{\text{sh}}}{10^3 \text{ km s}^{-1}} \right)^2$$



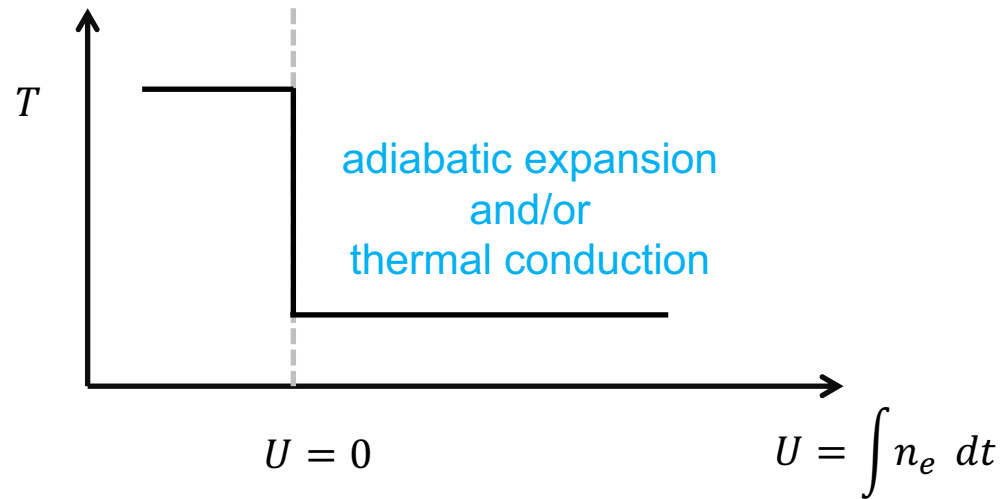
Recombining plasmas

CIE $dn_i/dt = 0$ ($kT_e = kT_b$)

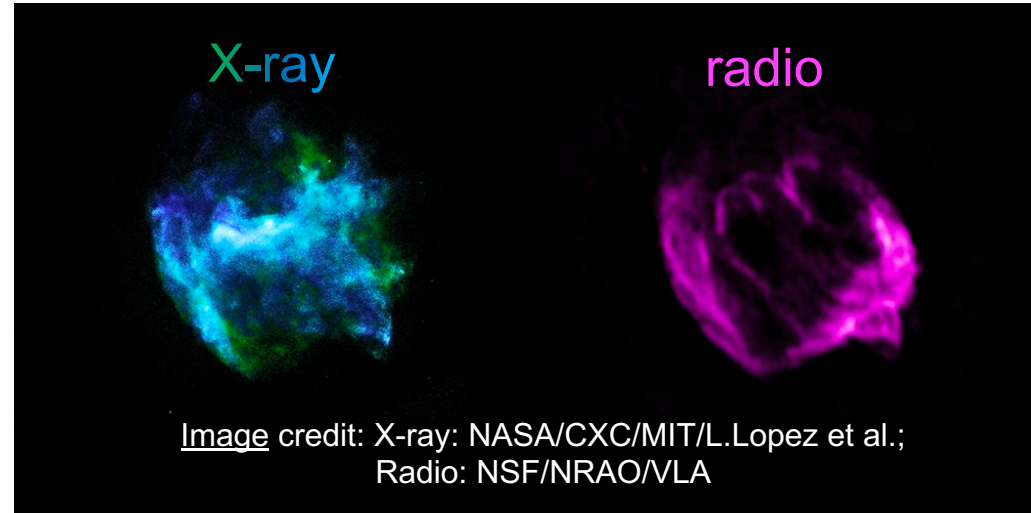
- ionization = recombination

NEI $dn_i/dt \neq 0$

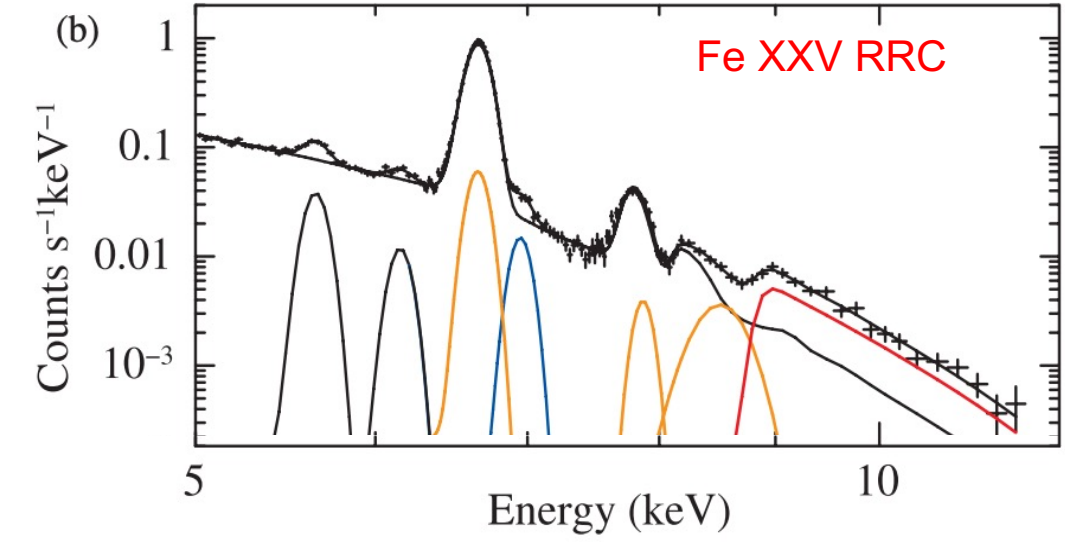
- recombination > ionization ($kT_e < kT_b$)
 - **recombining plasma**, aka over-ionized plasma
 - adiabatic expansion and/or thermal conduction



W49B: exemplary mixed morphology SNR

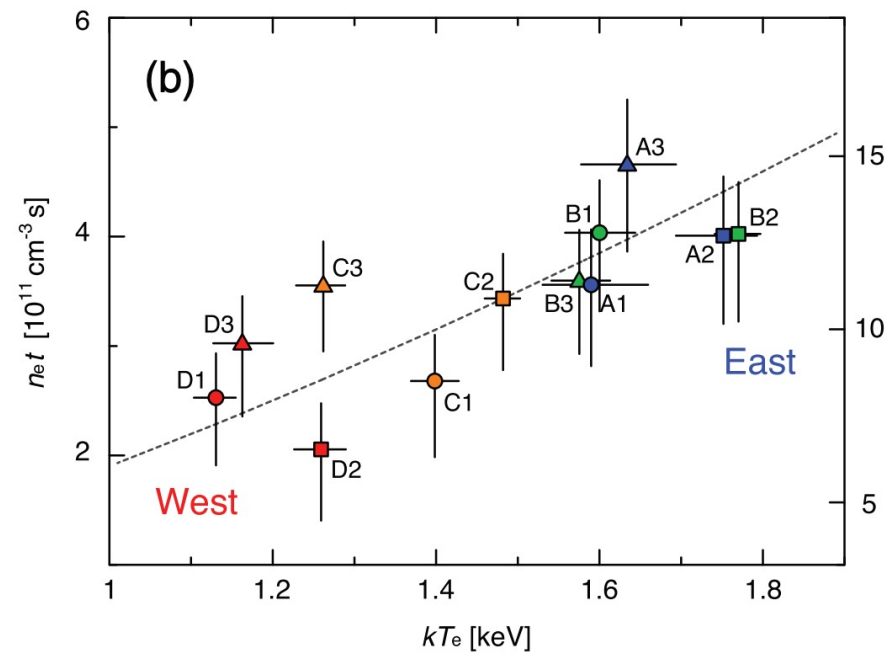
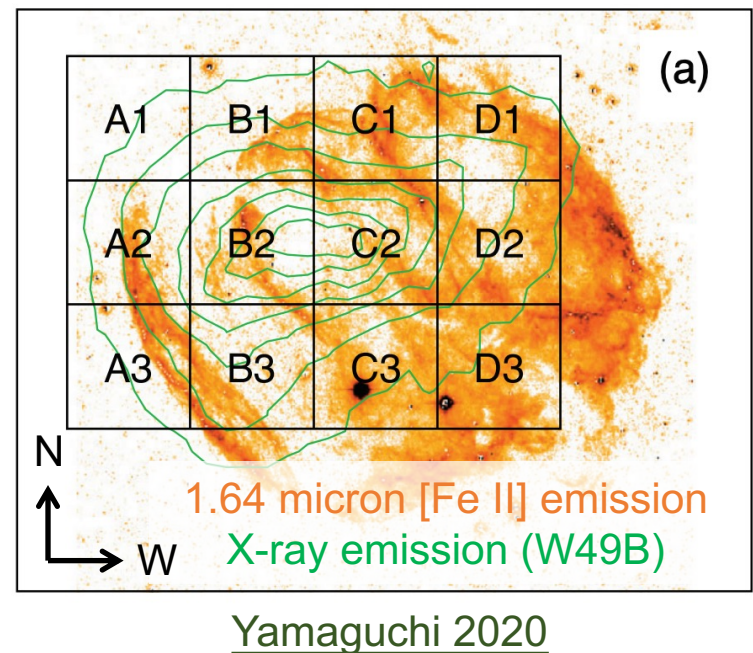
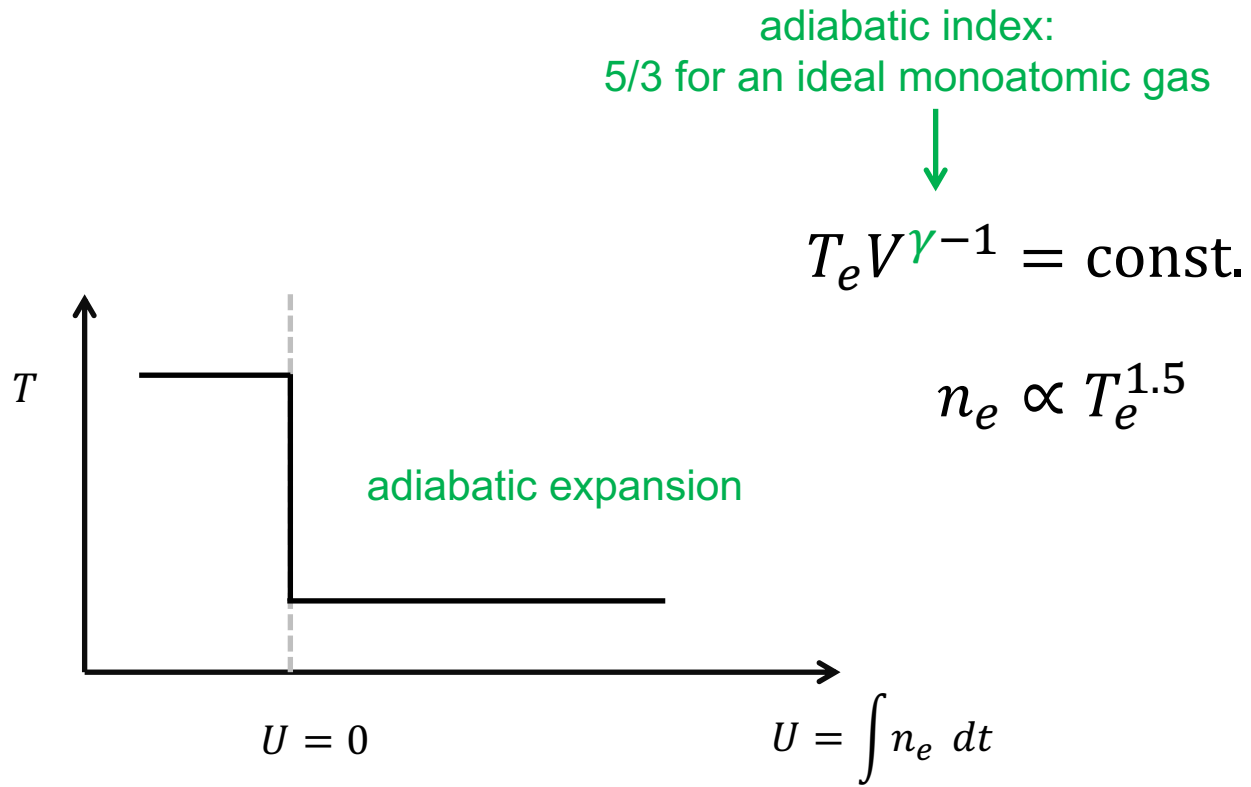


Ozawa et al. 2009
W49B (SNR, $kT_e = 1.52$ keV)



Recombining plasmas: adiabatic expansion

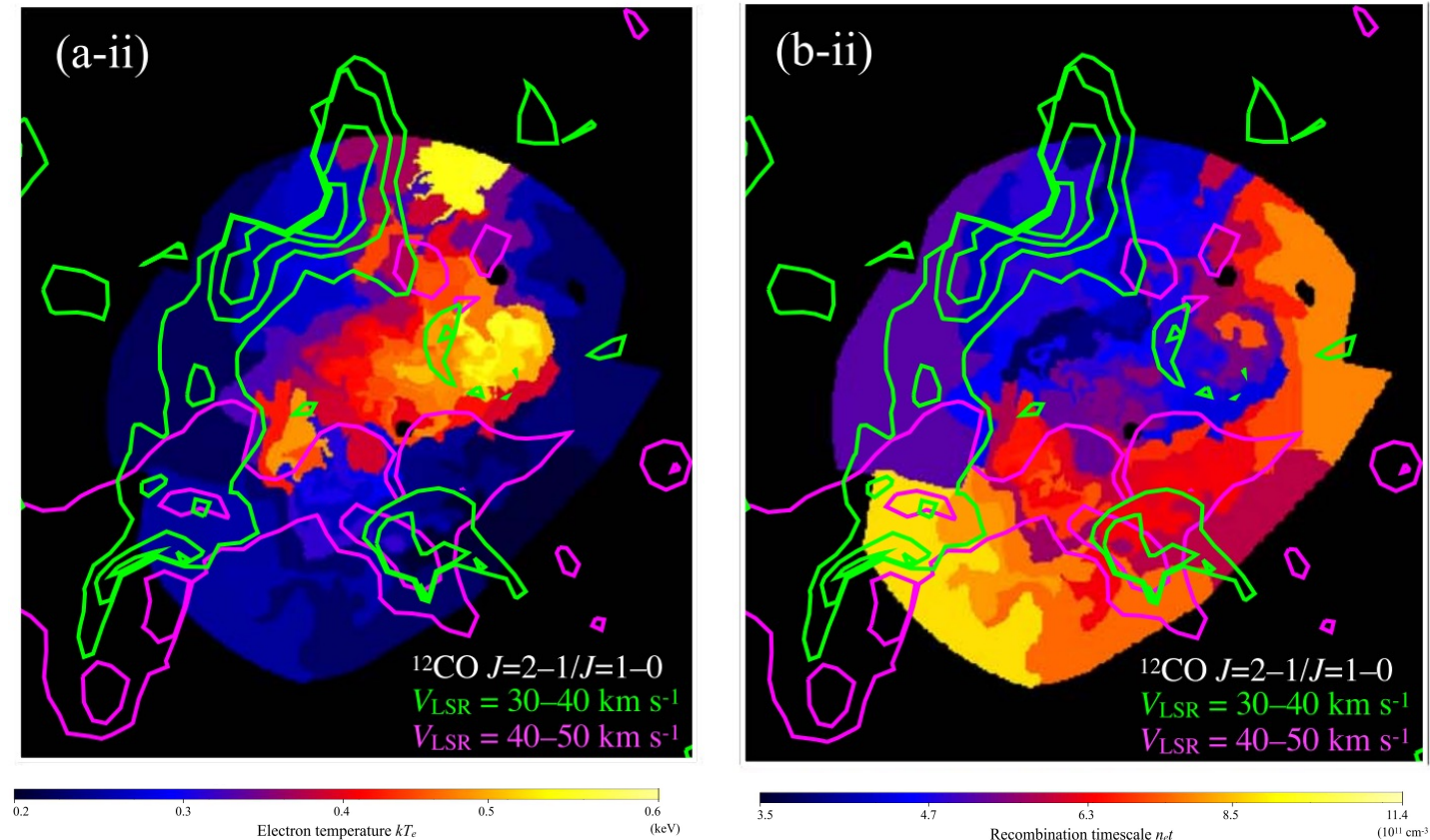
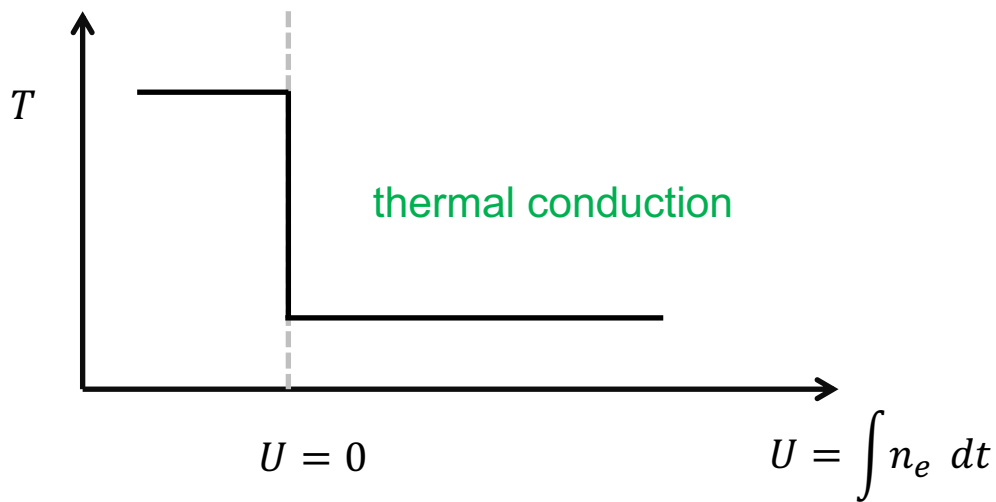
If SN explodes in a dense circumstellar environment, the circumstellar medium is shock-heated to high temperatures. Subsequently, the break out of the blast wave into the low-density interstellar medium. The drastic adiabatic expansion leads to the rapid cooling of electrons ([Itoh & Masai 1989](#)).



Recombining plasmas: thermal conduction

After the SN explosion, when the shock encounters a dense cloud region, the plasma cool down rapidly via thermal conduction.

No positive relation between $n_e t$ and T_e

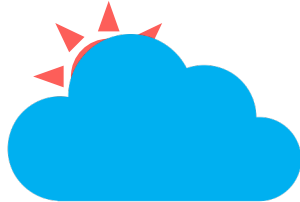


Okon et al. 2020
W44 (SNR)

Photoionized medium

When a medium is illuminated by a photoionizing source (nearby, behind, within),

- ✓ external radiation field
- ☐ photoionization and recombination processes dominates the **charge state distribution (CSD)**
- ☐ photoexcitation plays an important role in the level population balance
- ☐ examples: planetary nebulae, X-ray nebulae around X-ray binaries, AGN, etc.

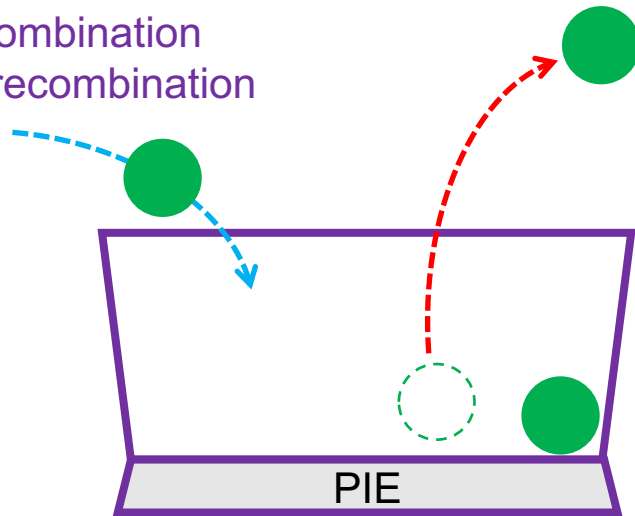


Recombination

- radiative recombination
- dielectronic recombination

Ionization

- photoionization ionization
- electron-impact ionization
- excitation-autoionization



Photoionization equilibrium (PIE)

Photoionization equilibrium is established if

- ✓ (time-independent) thermal equilibrium is reached
- ✓ ionization balance is reached (also required by CIE)

Examples of ionizing spectral energy distribution
[\(Mehdipour et al. 2016\)](#)

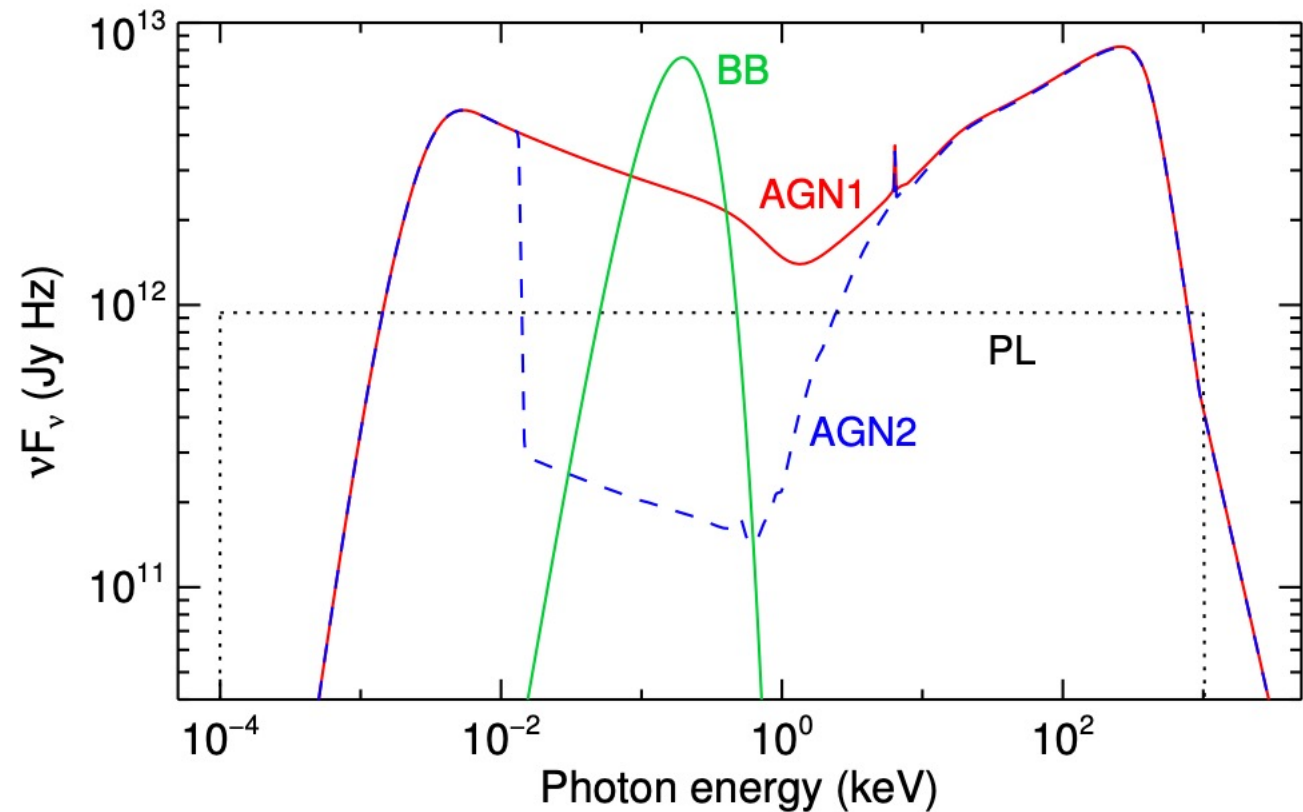
Ionization parameter

Tarter et al. 1969

$$\xi = \frac{L_{1-1000 \text{ Ry}}}{n_{\text{H}} r^2}$$

(cgs units): $\text{erg s}^{-1} \text{ cm}$

observable



Thermal stability curve

Photoionization equilibrium is established if

- ✓ (time-independent) thermal equilibrium is reached
- ✓ ionization balance reached (also required by CIE)

The equilibrium temperature (T_e) depends on the pressure form of the ionization parameter Ξ .

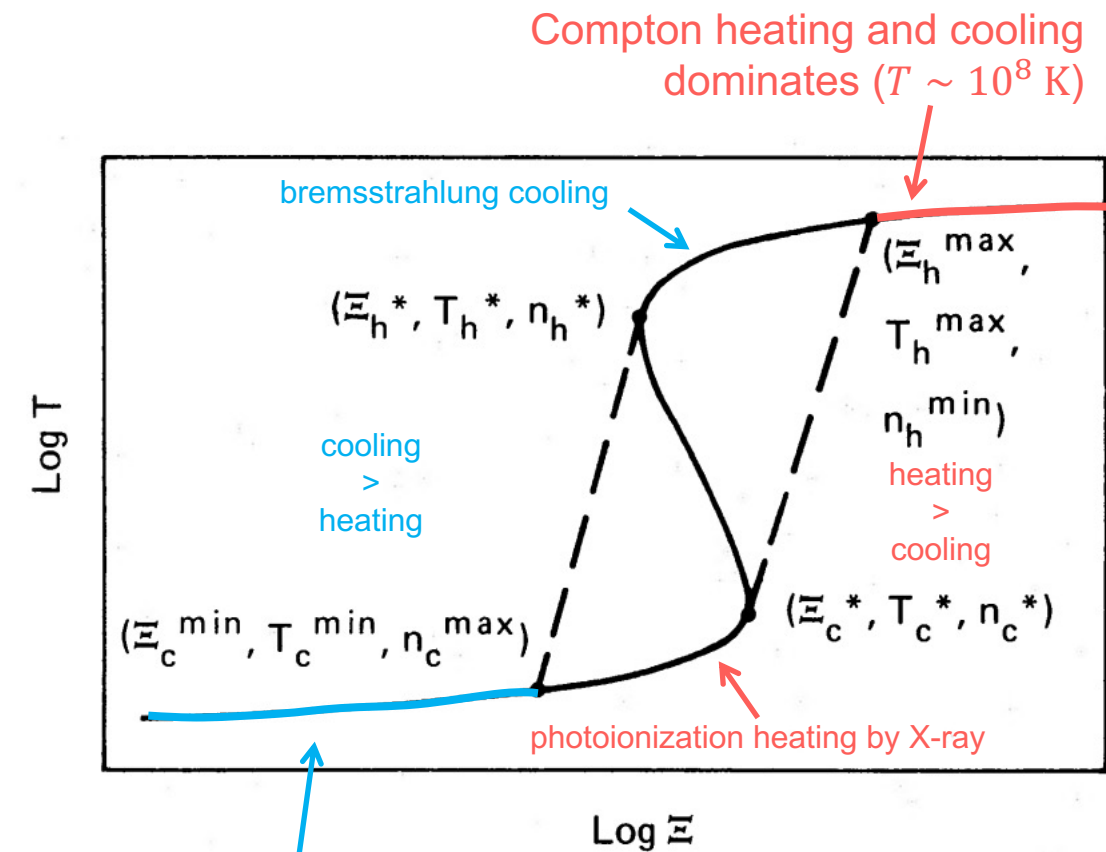
On the S-curve, heating and cooling are balanced.

Ionization parameter
(pressure form)

$$\Xi = \frac{F_{1-1000 \text{ Ryd}}}{c n_H kT} = \frac{L_{1-1000 \text{ Ryd}}}{4\pi r^2 c} \frac{1}{kT_e}$$

Krolik et al. 1981

$$\frac{\Xi}{\text{cm}^{-3}} \approx 1.92 \left(\frac{\xi}{\text{erg s}^{-1} \text{ cm}} \right) \left(\frac{10^4 \text{ K}}{T_e} \right)$$



Photoionization heating by UV radiation
balances collisional cooling ($T \sim 10^4 \text{ K}$)

thermal stability curve (i.e. S-curve)
(Krolik et al. 1981)

S-curve: stable branches

Photoionization equilibrium is established if

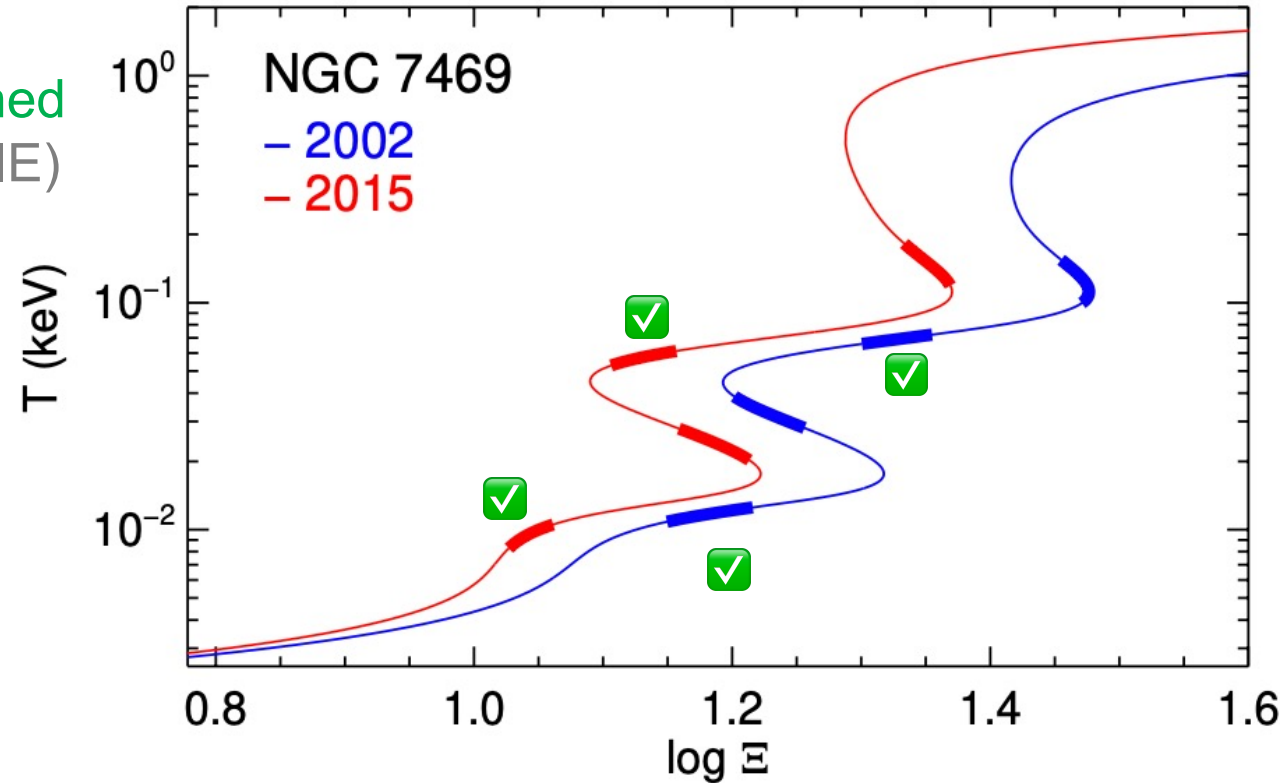
- ✓ (time-independent) thermal equilibrium is reached
- ✓ ionization balance reached (also required by CIE)

To the left of the S-curve, **cooling > heating**

To the right of the S-curve, **heating > cooling**

On the **stable** branch ($dT/d\Xi > 0$) of the S-curve, a small perturbation of upward (downward) temperature increase (decrease) will lead to more cooling (heating) and return to the stable branch

Depending on the details of the ionizing SED, there might be several small stable branches ($dT/d\Xi > 0$).



Mehdipour et al. 2018

S-curve: unstable branches

Photoionization equilibrium is established if

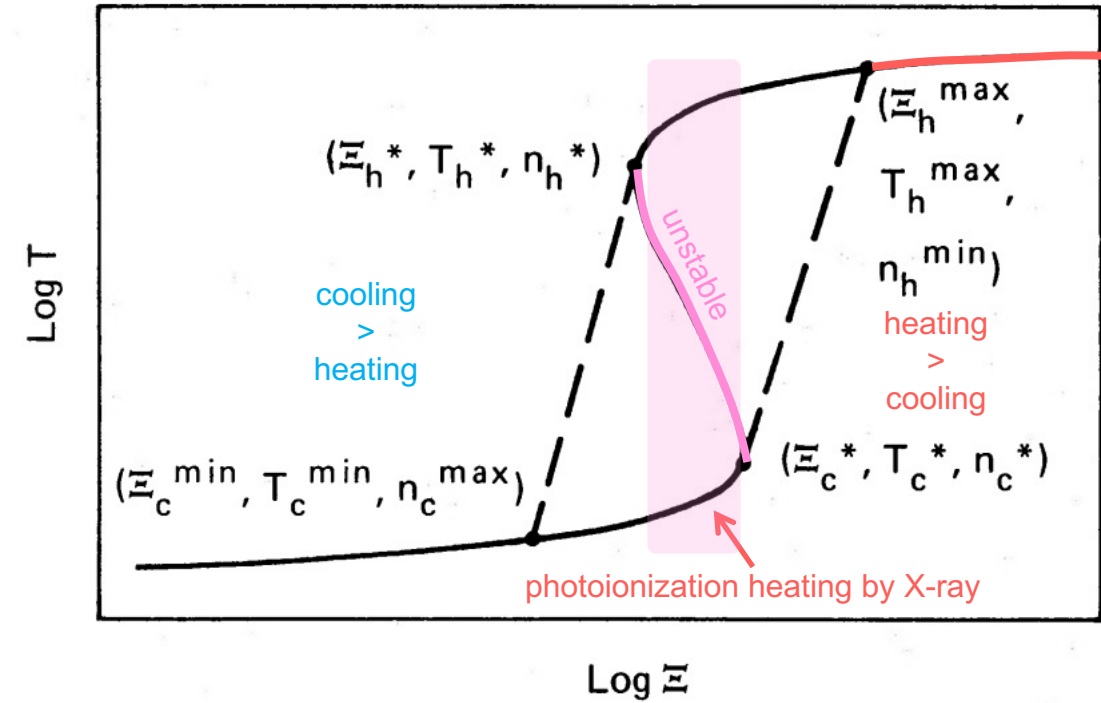
- ✓ (time-independent) thermal equilibrium is reached
 - ❖ heating by ionization and Compton scattering
 - ❖ cooling by recombination and radiation, as well as inverse Compton scattering
- ✓ ionization balance reached (also required by CIE)

To the left of the S-curve, **cooling > heating**

To the right of the S-curve, **heating > cooling**

On the **unstable** branch ($dT/d\Xi < 0$) of the S-curve, a small perturbation of upward (downward) temperature increase (decrease) will lead to more heating (cooling) and drive the medium all the way to the high-temperature (low-temperature) stable branch.

Cold dense matter can co-exist in pressure equilibrium with hot sporadic matter

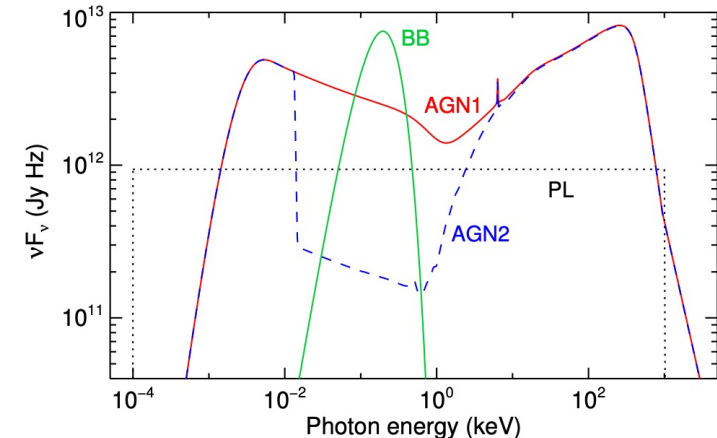


thermal stability curve (i.e. S-curve)
[\(Krolik et al. 1981\)](#)

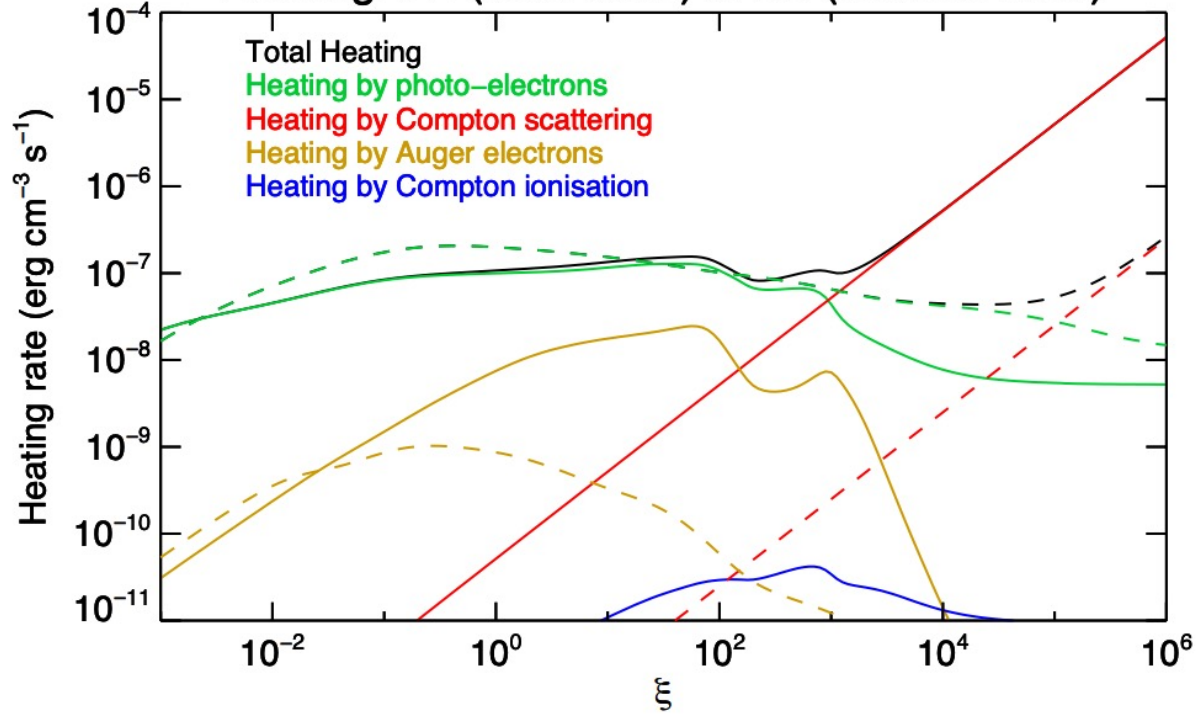
Heating and cooling processes

The input ionizing SED matters for PIE

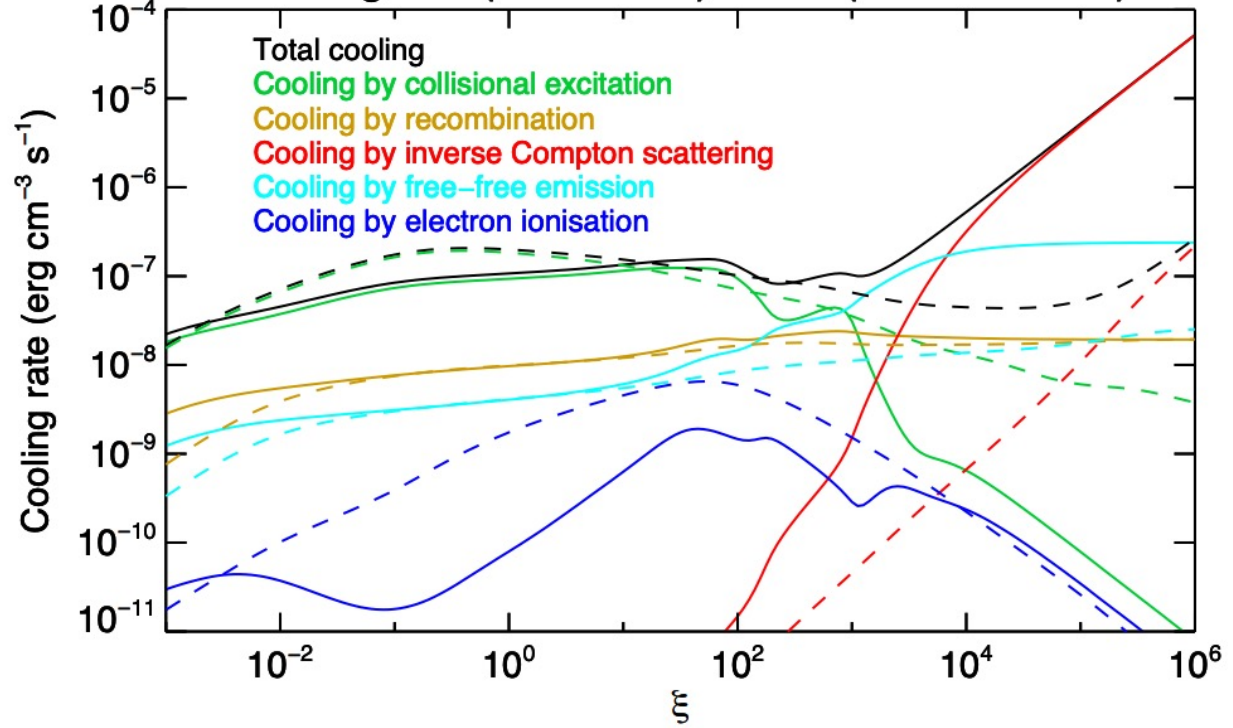
- PL = power law
- BB = blackbody



Heating: PL (solid lines) & BB (dashed lines)

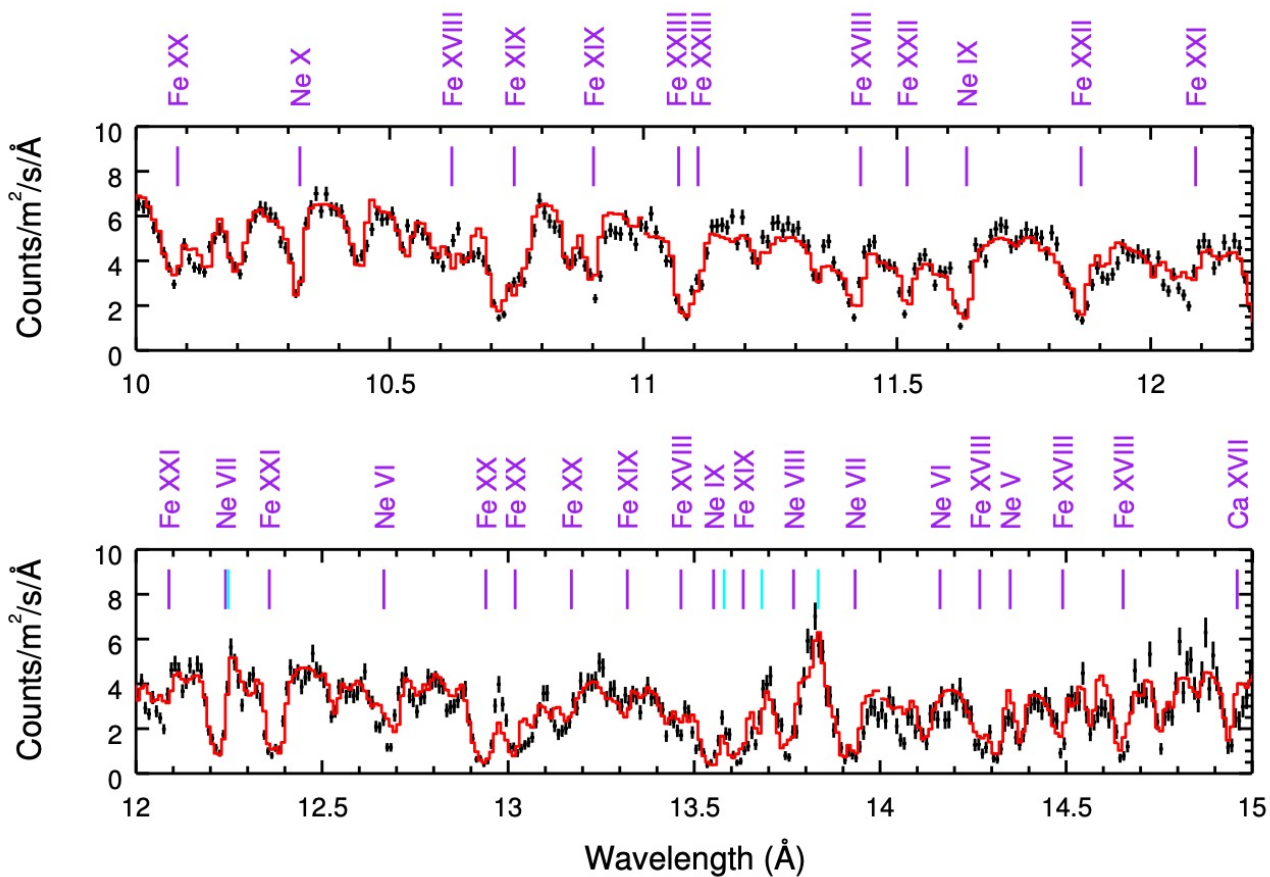


Cooling: PL (solid lines) & BB (dashed lines)

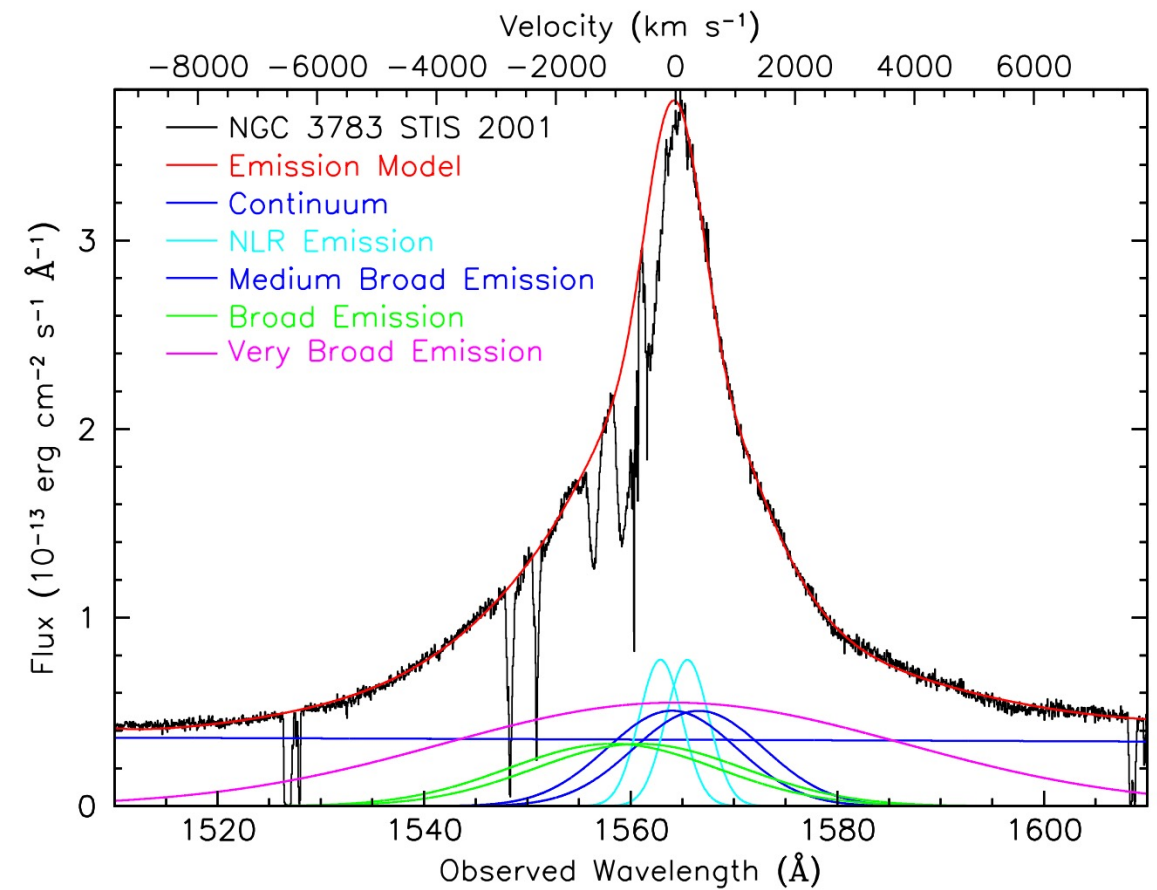


Mehdipour et al. 2016

PIE in absorption

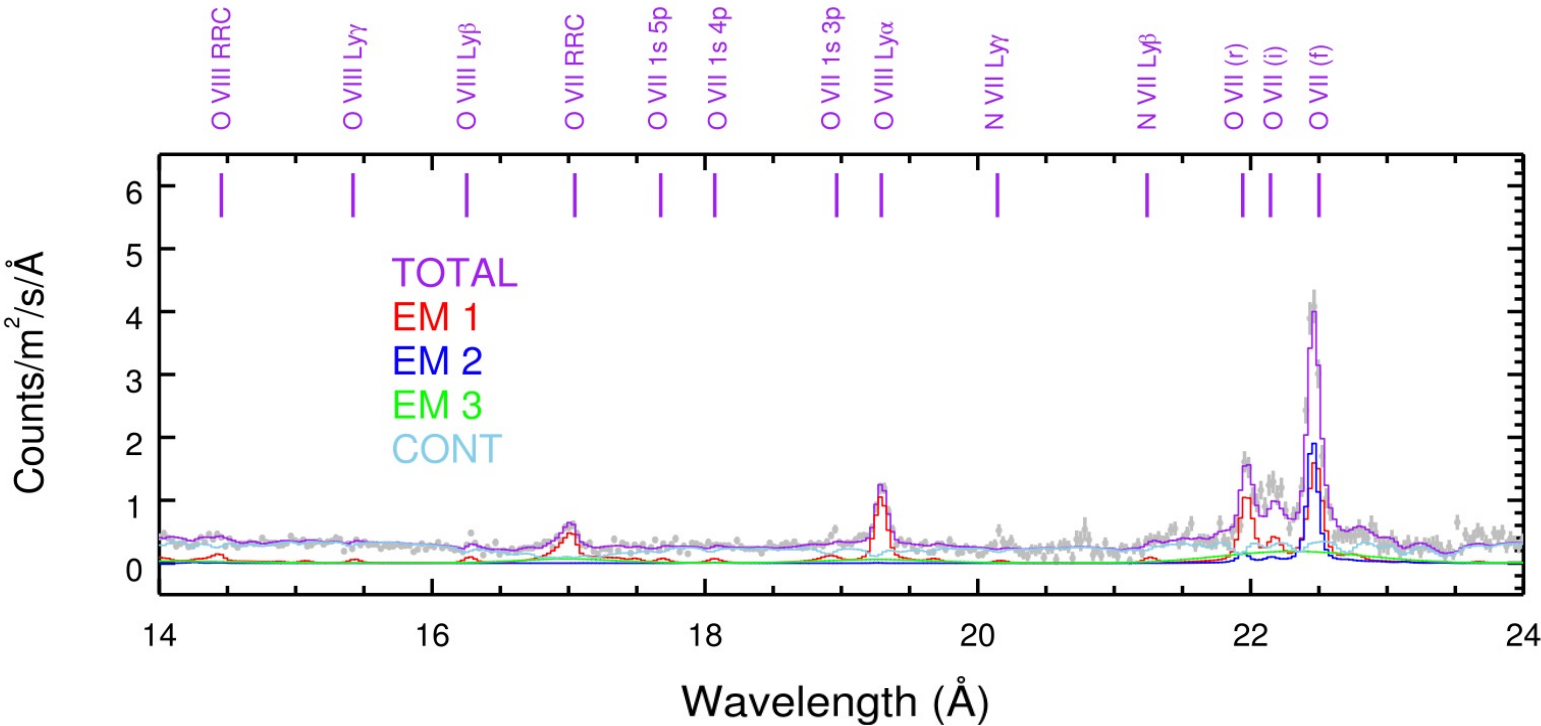


X-ray absorption features in NGC 3783 (Mao et al. 2019b)

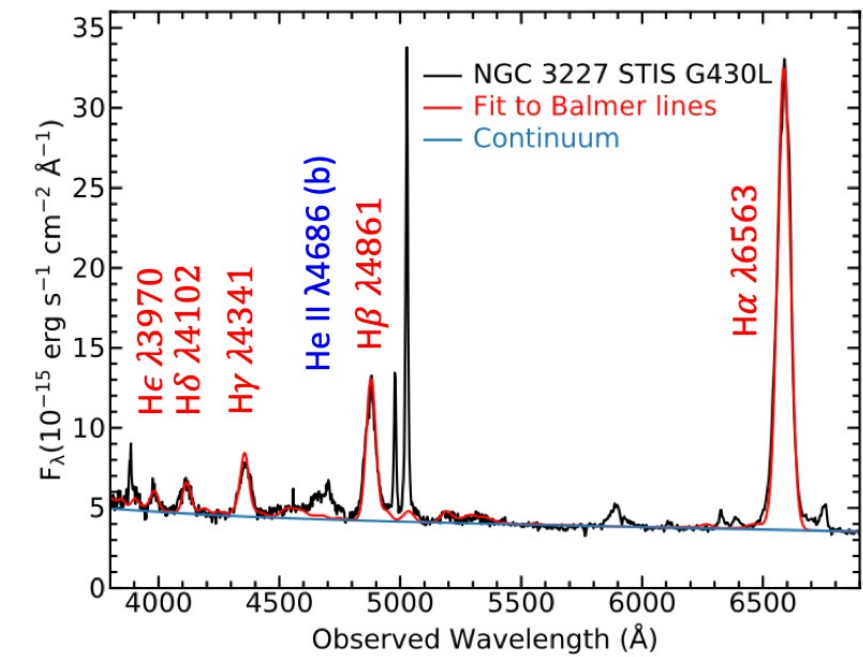


UV absorption features in NGC 3783 (Kriss et al. 2019)

PIE in emission



X-ray emission features in
NGC 5548 ([Mao et al. 2018](#))



Optical emission features in NGC
3227 ([Mehdipour et al. 2021](#))

- Recombination (Balmer) lines
- Radiative recombinant favors the population of $1s\ 2p\ ^3P_{2,1}$ and $1s\ 2s\ ^3S_1$, leading to stronger $z + x + y$ (or $F + I$) line and $G \sim 4$
- Radiative recombination continuum (RRC)

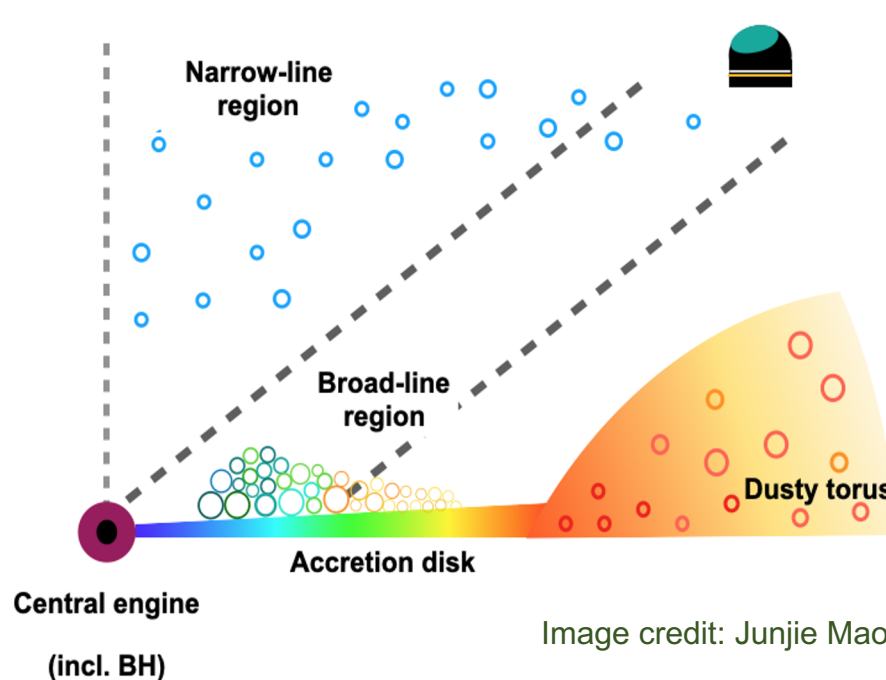
Reverberation mapping

□ Textbook anatomy of AGN

- Urry & Padovani (1995)

□ Broad-Line Region (BLR)

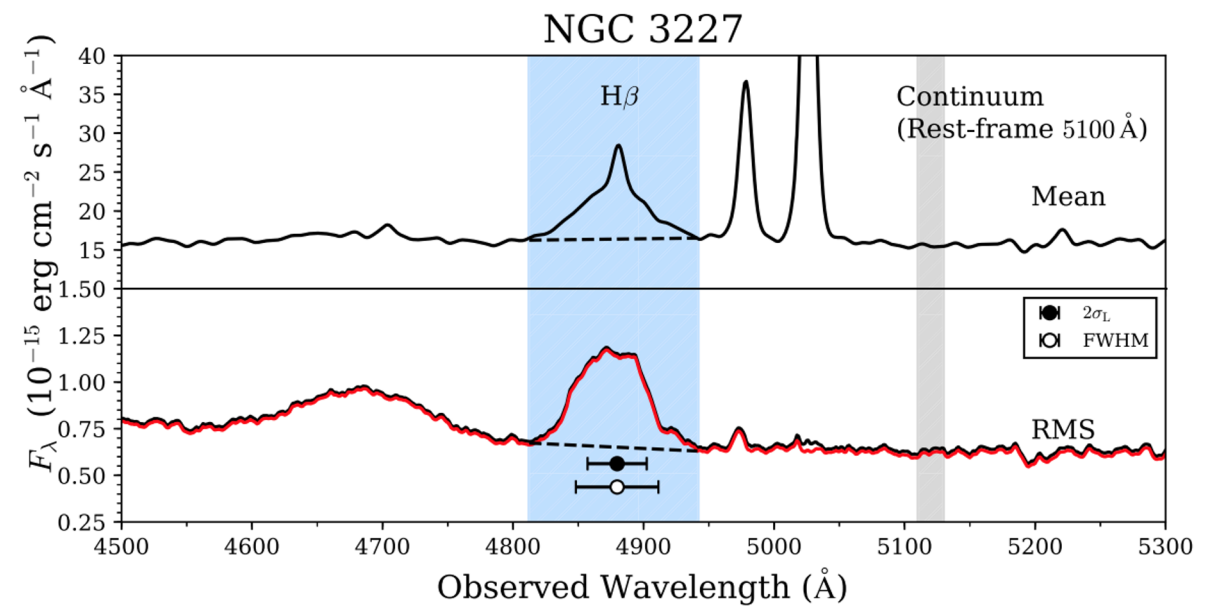
- **Reverberation mapping → MSMBH**
- Blandford & McKee (1982), Peterson (1993)



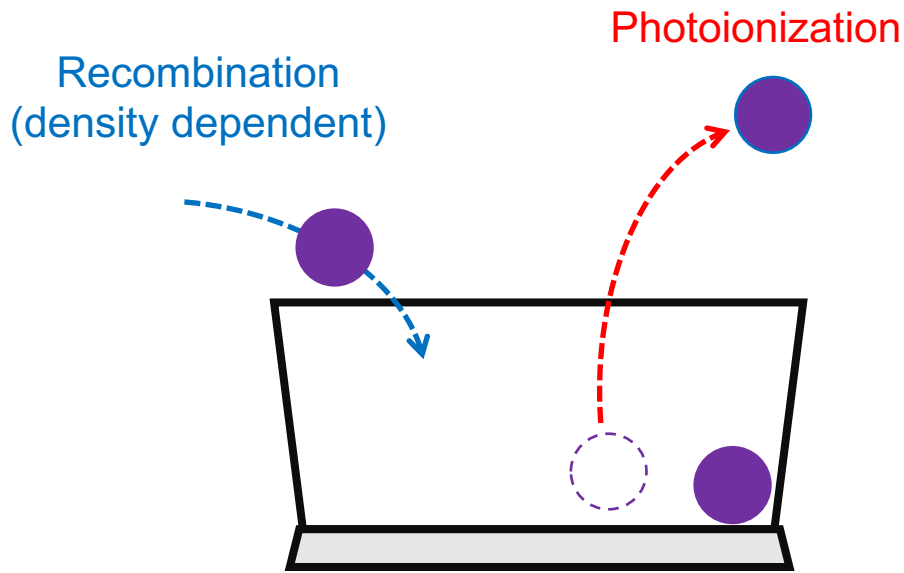
$$M_{\text{BH}} = f \left(\frac{c \tau \Delta V^2}{G} \right)$$

↑
geometry factor
↓
time delay

De Rosa et al. 2017



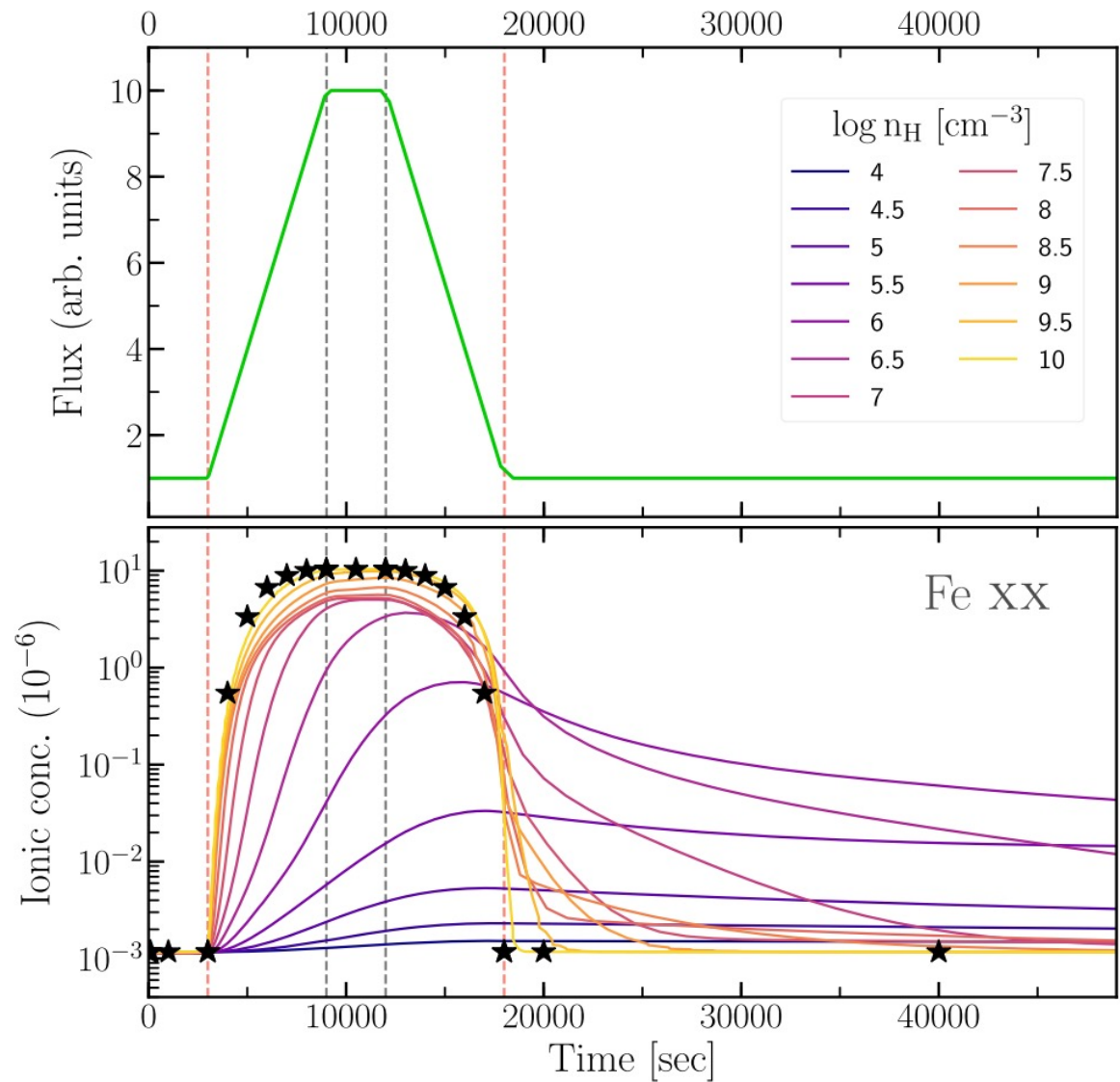
Time-dependent photoionization



The higher the number density, the faster it recombines.

$$t_{\text{rec}} \propto (n_e \alpha_{\text{RR}})^{-1}$$

α_{RR} : [Badnell \(2006\)](#), [Mao & Kaastra \(2016\)](#)



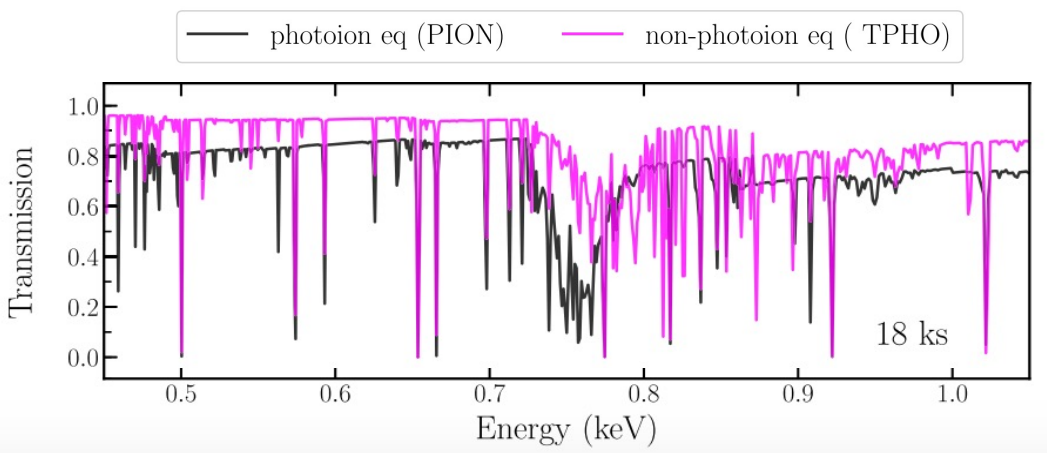
[Rogantini et al. 2022](#)

Spectral-timing analysis

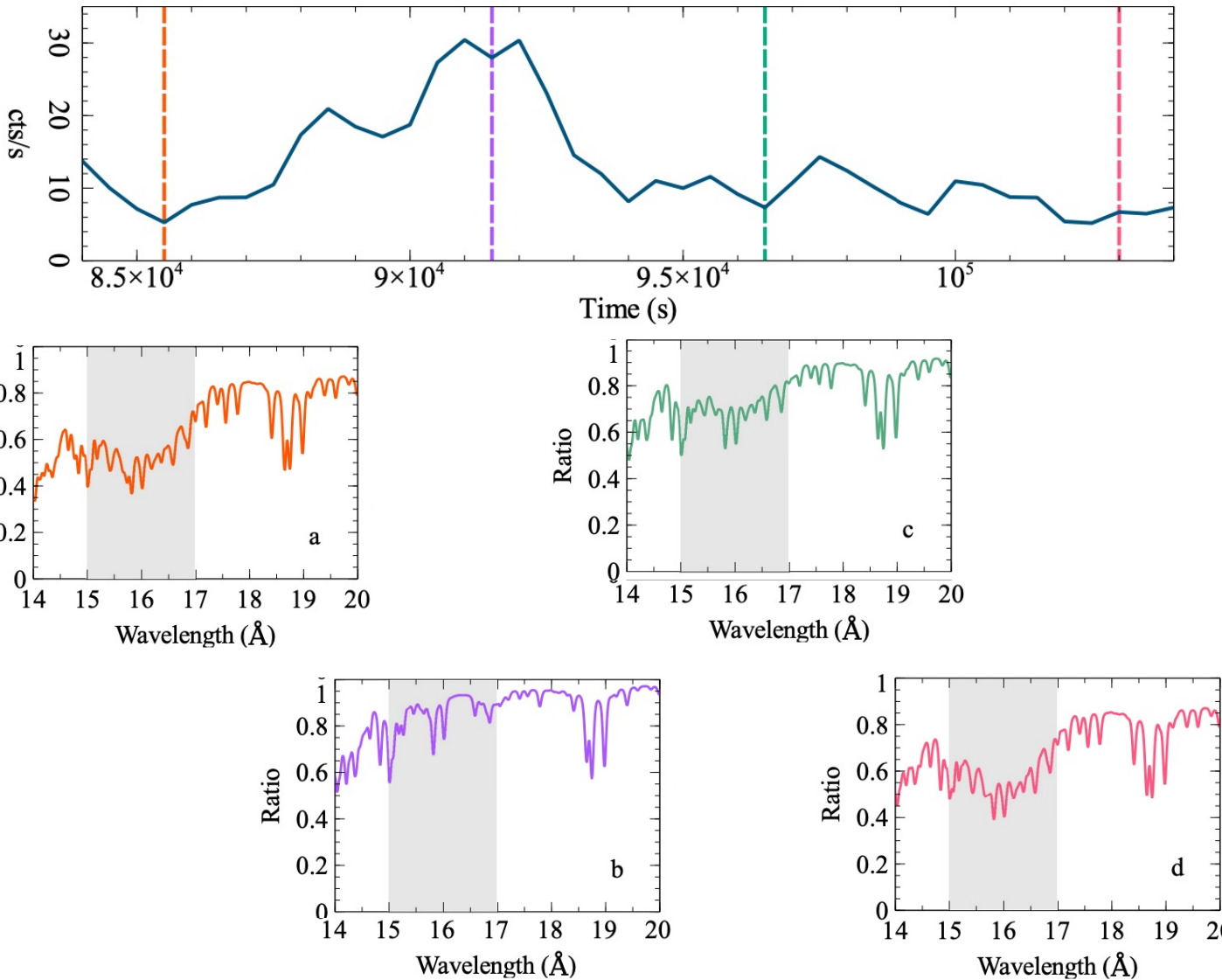
$$t_{\text{rec}} \propto n_e^{-1}$$
$$t_{\text{bin}} \lesssim t_{\text{var}} \lesssim t_{\text{rec}} \lesssim t_{\text{obs}}$$

Requirements to the observation:

- ✓ prominent variability
- ✓ Long term monitoring of X-ray + UV
- ✓ High-resolution X-ray/UV spectroscopy
- ✓ Deep exposure
- ✓ Not too low number density



[Rogantini et al. 2022](#)



[Silva et al. 2016](#)